Image Processing Techniques for Automated Diagnosis of Wall Motion Abnormality in Echocardiography Sequences

By

Vijayalakshmi Ahanathapillai

In the fulfilment of the requirement for the degree of

Doctor of Philosophy

Centre for excellence in Signal and Image Processing,
Department of Electronic and Electrical Engineering,
University of Strathclyde

Declaration

I declare that this Thesis embodies my own research work and that it is composed by myself. Where appropriate, I have made acknowledgments to the work of others.

Vijayalakshmi Ahanathapillai

Acknowledgment

First, I would like to express my deepest gratitude to my PhD supervisor, Prof. John J. Soraghan. Throughout my PhD, he provided encouragement, guidance, and valuable input to my research. He has provided unlimited mental and practical support to numerous personal concerns which includes allowing me to take a break during my PhD.

I would like to thank my previous supervisor, Dr. David Hamilton, who believed in my potential and provided an opportunity to work within the Centre for excellence in Signal and Image Processing (CeSIP). I would like to thank Dr. P. Sonecki, Cardiologist at Glasgow Western Infirmary, who provided technical support. I would like to thank Dr. Alagesan, Radiologist at Chennai for his valuable discussions and technical input on Echocardiography. I would like to thank Dr. George Corner for helping me with the ethical approval of the data that was obtained from Ninewells hospital in Dundee. I would like to thank Mr. Joe Divine, Siemens, for providing me with the Cypress software to visualise the raw echo data. I also wish to thank all my colleagues and my friends, for creating an enjoyable working atmosphere and a pleasant experience in Glasgow.

I would like to thank my parents and family, for their moral support throughout my education. I owe my deepest gratitude to my husband, Nishal, for his never ending support and encouragement, without which, this PhD and writing of this thesis would not have been possible. Last but not the least; I am indebted to my little son, Ram, who has been a lovely kid making this thesis writing experience achievable for me.

This research was supported by Overseas Research Scholarship Awards Scheme (ORSAS) and the University of Strathclyde.

Abstract

Myocardial Ischemia or heart muscle damage is a heart condition which leads to complications such as heart failure or heart attack. This damaged heart muscle does not contract as much as the healthy heart muscle leading to abnormal heart wall movement. Echocardiography (Echo) is widely used to identify such wall motion abnormality and help diagnose the possible presence of damaged tissue in the heart wall. The Myocardial Ischemia Detection Algorithm (MIDA) is developed to analyze echocardiography sequences automatically to detect the presence of heart muscle damage and locate abnormal segments in the heart chamber. Specifically, the proposed software algorithm involves a wavelet transform based speckle noise reduction followed by a Delaunay triangulation based contrast enhancement technique to enhance the heart wall boundary. The heart wall contour is obtained by performing fuzzy multi resolution edge detection. The heart wall boundaries obtained from the frames of an Echo scan are used to determine global features such as ejection fraction and cavity area to describe the heart function. Statistical pattern recognition techniques such as Principal Component Analysis (PCA) and Independent Component Analysis (ICA) are applied to extract features which are then classified to identify the abnormal heart wall movement. Segmental wall analysis is also performed by extracting segmental features based on cavity area, wall thickness, and radial wall displacement to locate the damaged wall segment. A selection of examples is provided to illustrate the usefulness of the proposed algorithm. The results to date indicate that such a feature extraction technique can be effective in diagnosing Myocardial Ischemia, at an early stage. The clinical data for this research are obtained from Ninewells Hospital, Dundee and Glasgow Western Infirmary Hospital.

Table of Contents

Image Processing Techniques for Automated Diagnosis of Wall Motion Abnormality in Echocardiography Sequences 1

CHAPTER 1 1

INTRODUCTION 1

1.1 Introduction 1

1.2 Motivation for this research 2

1.3 Contribution of the Thesis 3

1.4 Organisation of thesis 5

1.5 List of author's publications 6

CHAPTER 2 8

CARDIOVASCULAR SYSTEM, HEART ABNORMALITIES AND ECHOCARDIOGRAPHY 8

2.1 Introduction 8

2.2 Cardiovascular system 9

2.2.1. Anatomy of Human Heart 9

2.2.2. Physiology of the Human Heart 12

2.3. Common heart pathologic conditions 14

2.3.1 Coronary Artery Disease 14

2.3.2 Myocardial Ischemia 14

2.3.3 Myocardial Infarction 14

2.3.4 Congestive Heart Failure (CHF) 15

2.3.5 Regional Wall Motion Abnormality 16

2.4 Fundamentals of Echocardiography 18

2.4.1 Overview of Medical Ultrasound 18

2.4.1.1 Ultrasonic Diagnostic Imaging Technique 19

2.4.2. Ultrasound Tissue Interaction 19

2.4.3 Medical Ultrasonic Instrumentation 23

2.4.4 Operational modes or ultrasound imaging modes in Echocardiography 27

2.4.5 Artifacts present in 2D real time B-scans 30

2.5 Conclusion 32

CHAPTER 3 33

A REVIEW OF DIGITAL IMAGE PROCESSING IN ECHOCARDIOGRAPHY 33

3.1 Introduction 33

3.2 Image processing of Echocardiography images 34

3.2.1 Recognition of cardiac views in echocardiography 35

3.2.2 Image pre-processing stage (speckle noise reduction or image enhancement) 36

3.2.3 Segmentation or border detection (detecting both the inner and outer heart wall edges) and motion tracking 36

3.2.4 Cardiac parameter extraction for Automated/ Semi automated analysis 36

3.2.5 Echocardiography Data Storage 37

3.3 Image data 37

3.4 Image enhancement techniques for echocardiography images 38

3.4.1 Speckle noise reduction techniques 39

3.4.2 Image contrast enhancement techniques 40

3.5 Segmentation techniques used in echocardiography images 43

3.5.1 Radial search based approach 44

3.5.2 Snakes based approach 44

3.5.3 Shape based approaches 45

3.5.4 Local image phase based approach 47

3.5.5 Level set based approaches 47

3.5.6 Other approaches 48

3.6 Cardiac parameters extracted for automated or semi-automated analysis of echocardiography 49

3.7 Feature Extraction Techniques 55

3.7.1 Principal component Analysis (PCA) 55
3.7.2 Independent Component Analysis (ICA) 56
3.8 Delaunay triangulation 56
3.9 Conclusion 58
CHAPTER 4 60
ECHOCARDIOGRAPHY IMAGE ENHANCEMENT TECHNIQUES 60
4.1 Introduction 60
4.2 Echo Enhancement Algorithm 61
4.3 Speckle noise reduction 63
4.4 Edge detection 66
4.4.1 Left Ventricle Centre Point (LVCP) detection 66
4.4.2 Improved fuzzy LVCP detection: 70
4.4.3 Left ventricle boundary detection 75
4.4.4 Improved LV boundary detection: 76
4.5 Delaunay triangulation based enhancement 82
4.5.1 Delaunay triangulation 82
4.5.2 Processing tissue or wall region 83
4.5.3 Processing LV cavity or blood region 84
4.6 Experimental Results 85
4.7 Conclusion 92
CHAPTER 5 93
AUTOMATED DIAGNOSIS SYSTEM TO DETECT ABNORMAL WALL MOTION 93
5.1 Introduction 93
5.2 Overview of Automated Abnormal Wall Motion Diagnosis Algorithm 94
5.3 Composite motion (CM) image creation 96
5.3.1 LV boundary detection 97
5.3.2 Composite motion image using LV boundaries 98

5.4 Principal component analysis (PCA) approach..... 99
5.5 Independent Component Analysis (ICA) approach..... 100
5.6 Radon transform approach..... 102
5.7 Results and discussion..... 104
5.7.1 Heart Abnormality Diagnosis Result 1 - PCA approach..... 104
5.7.2 Heart Abnormality Diagnosis Result 2 - ICA approach..... 114
5.7.3 Heart Abnormality Diagnosis Result 3 - Radon Transform approach..... 116
5.7.4 Comparison between PCA, ICA and Radon approach..... 118
5.8 Conclusion..... 120
CHAPTER 6..... 121
MYOCARDIAL ISCHEMIA DETECTION ALGORITHM: MIDA..... 121
6.1 Introduction..... 121
6.2 Myocardial Ischemia Detection Algorithm (MIDA) overview..... 122
6.3 Features extracted from the LV boundary..... 125
6.3.1 Global features..... 125
6.3.2 Local or Segmental features..... 128
6.4 Regional wall motion synchrony analysis..... 133
6.5 Results and discussion..... 135
6.5.1 Regional features to identify segmental damage..... 135
6.5.2 Heart function classification using global and regional features..... 138
6.6 Conclusion..... 139
CHAPTER 7..... 140
CONCLUSION AND FURTHER DEVELOPMENTS..... 140
7.1 Concluding Remarks..... 140
7.2 Suggestion for Further developments..... 142
7.2.1 Improvements to MIDA algorithm..... 142
7.2.2 Extend to other views of Echocardiography..... 143

7.2.3 Radon Analysis of the composite motion image 144
References 165
APPENDIX A 1655
FRACTIONAL MYOCARDIAL WALL THICKENING 1655
APPENDIX B 1666
LEFT VENTRICLE FEATURES (GLOBAL AND SEGMENTAL) 166

List of Figures

Fig. 2.1 Sectional view of Heart [LYN2006] 10
Fig. 2.2: Coronary heart arteries [KANG2006] 12
Fig. 2.3: Conduction System [LYN2006] 13
Fig. 2.4: Coronary Artery Disease leading to Myocardial Ischemia (tissue damage) or Myocardial Infarction (tissue death) [KANG2006] 15
Fig. 2.5 Assignment of the 17 myocardial segments to the territories of the left anterior descending (LAD), right coronary artery (RCA), and the left circumflex coronary artery (LCX) [CER2002] 17
Fig. 2.6 Ultrasound reflection and refraction at tissue interface 21
Fig. 2.7 (a) Ultrasound Scattering (b) Ultrasound Diffraction at tissue aperture 22
Fig. 2.8 Principal electronic components in a medical ultrasound imager 23
Fig. 2.9 Transducer structure 24
Fig. 2.10. Receiver functions: amplification, compensation, compression, demodulation and rejection [BUSH1999] 26
Fig. 2.11 Different operational modes (a) A – mode (b) B – mode and (c) M – mode 27
Fig. 2.12 (a) Echo windows of the heart, (b) Parasternal short axis view and (c) Apical 4 Chamber view 29
Fig. 2.13 Standard echocardiograph views of the heart (a) Parasternal Short Axis view, (b) Apical 2 Chamber view and (c) Apical 4 Chamber view 29
Fig 3.1 Image processing stages in automated analysis of Echocardiography 35
Fig 3.2 Training data set for Short axis echocardiogram model [COOT1994] 46
Fig 3.3 Computing myocardial area by taking the difference between the area enclosed by the epicardial boundary and the area enclosed by the endocardial boundary 51
Fig. 3.4 Shows triangulation of the 4 points satisfying Delaunay in (a) and a triangulation which does not satisfy the Delaunay in (b) 57
Fig. 4. 1 Enhancement Algorithm Overview 62

Fig. 4.2 (a) Flow diagram for speckle noise reduction, (b) sample Echo image and (c) speckle noise reduced image and (d) vertical line profile (column 200) before and after speckle noise reduction 64

Fig. 4.3 Schematic diagram of a SA view showing the LVCP position and its relation to the VCL and HCL (indirectly to posterior wall and anterior wall) 68

Fig. 4.4 (a) extracted anterior and posterior epicardial boundary and the corresponding fuzzy vertical and horizontal membership functions are shown in (b) and (c). 71

Fig. 4.5 (a) Original low contrast image, (b) FDARK membership function obtained by setting the standard values of a=10 and b=30, (c) FDARK membership function obtained by determining the automatically (a=32; b=45). (d) Original good quality image, (e) FDARK membership function obtained by setting the standard values of a=10 and b=30, (f) FDARK membership function obtained by determining the automatically (a=21; b=43). 72

Fig. 4.6 (a) SA mid cavity level with papillary muscles in the LV cavity area, (b) SA basal level with mitral valve in the LV cavity area, (c) Data driven template to describe the LV cavity area 73

Fig. 4.7 Stages in the left ventricle centre point detection 74

Fig.4.8 Stages in the left ventricle inner and outer wall boundary detection 78

Fig.4.9 (a) Detection of the Endocardium (inner wall) along the radial line, (b) the signal along the radial line, the wavelet details at different scales are shown from (c) to (h). (i) the edge obtained by choosing the maximum of the edge fuzzy subset, and (j) the edge obtained by choosing the second highest peak when the edge fuzzy subset has more than one peak. 80

Fig.4.10 Edge detection results for echo image in SA mid cavity view (a) and SA basal view (e) using level sets with active contours, FMED and modified FMED 81

Fig. 4. 11 Shows the different stages in enhancement step for the synthetic Short Axis heart image. (a) Original image (b) image with extracted LVCP and wall boundary (c) triangulation for the blood region region (using the extracted inner wall and center) , (d) Delaunay triangulation for only the wall

region (using the extracted wall boundaries) and (e) Processed image for contrast enhancement. A Delaunay triangle is showed in (f) 84
Fig. 4.12 Enhancement result for synthetic Short Axis images, (a) Synthetic image 1(CR =0.5147), (b) Enhanced image 1 (CR=0.5732), (c) Synthetic image 2(CR == 0.4166) and (d) Enhanced image 2 (CR=0.4433) 86
Fig. 4.13. (a) Good quality SA basal view showing the mitral valve in the LV cavity area obtained from a Phillips machine, (b) enhanced image 89
Fig. 4.14. (a) Poor quality SA mid cavity view showing the papillary muscle in the LV cavity area from a Siemens machine, (b) enhanced image 90
Fig. 4.15. (a) Poor quality SA mid cavity view without papillary muscle in the LV cavity area from a Phillips machine, (b) enhanced image 91
Fig. 5.1 Automated Diagnosis of abnormal wall motion 95
Fig. 5.2 Block diagram to show the stages in creating composite motion image 97
Fig. 5.3 Process of creating the difference image 98
Fig 5.4. Integration of an object along the line $y = \tau + px$ 102
Fig. 5.5. (a) Concept of line integrals and Radon transform and (b) Radon transform of the Composite Motion (CM) image 103
Fig 5.6. Simulated database (28 image) 105
Fig 5.7.Variance plot showing the variance of the images in the simulated dataset (28 image dataset) 105
Fig. 5.8. Top 12 eigen vectors used for recognition 106
Fig. 5.9. Original image (left), modified image (right). The arrows in the figure show the contraction failure in the segment. 107
Fig. 5.10. Echo frame showing SA echo view where a section of the LV epicardium falls outside the imaging plane(a) The top right section of the LV epicardium falls outside the image plane(b) The top left section of the LV falls outside the image plane 109
Fig. 5.11. Composite motion images (constructed using the inner wall motion) in the real heart image database. (a)Sample images showing normal heart wall motion (b) Sample images showing abnormal heart wall motion 111
Fig. 5.12. Sample PC vectors obtained from the real dataset (Top 6) 111

Fig. 5.13 Combining the classifier output 112
Fig. 5.14. Top 12 ICA basis vectors used for recognition 114
Fig. 5.15. ICA basis vectors obtained from the real dataset (Top 6) 115
Fig. 5.16 Composite motion images (a, d, g), its corresponding Radon transform in (b, e, f) and the sum of the projections in (c, f, i) 117
Fig. 6.1 Myocardial Ischemia Detection Algorithm(MIDA) overview 124
Fig. 6.2 Extraction of global features from the LV inner wall and outer wall edges 126
Fig. 6.3 Global features extracted from the LV boundary showing the normalized radius, cavity area and myocardial area for the entire Echo scan 127
Fig 6.4 (a) Standard segmentation for mid cavity and basal SA view
(b) Dividing the LV into 6 segments with each segment angle of 60 128
Fig. 6.5 Normalised segmental cavity area for the entire scan 130
Fig 6.6 Normalised segmental wall thickness for the entire scan 131
Fig 6.7 Displacement Graph showing the wall displacement from the systole to the end diastole 132
Fig 6.8 Wall Displacement graphs showing (a) synchrony in normal heart motion (b) asynchrony in normal heart motion, (c) asynchrony in abnormal heart motion 134
Fig 6.9 Voting scheme combination of classifier output 137
Fig. 7.1 (a) 2 chamber view and (b) 4-chamber view Echocardiography 143
Fig. 7.2 Radon transform of a composite motion image of a normal healthy heart and an abnormal heart with 7th and 8th segment abnormality 144

List of Tables

Table 3.1 Overview of Automated / semi automated analysis of Echocardiography for heart function and wall motion abnormality 52
Table 3.2 Overview of Automated / semi automated analysis of Echocardiography for segmental wall motion abnormality 53
Table 4.1: Comparison of Contrast Resolution measures 88
Table 4.2 Contrast Resolution measure in 6 regions for image in Fig 4.13 89
Table 4.3 Contrast Resolution measure in 6 regions for image in Fig 4.14 90
Table 4.4 Contrast Resolution measure in 6 regions for image in Fig 4.15 91
Table 5.1 Performance of PCA approach using k-NN classifiers 113
Table 5.2: Performance of PCA approach using different classifiers 113
Table 5.3 Performance of ICA approach using k-NN classifiers 115
Table 5.4: Confusion matrix for the heart wall motion abnormality classification (Tested images= 62, Normal hearts= 27, Abnormal hearts= 35) 119
Table 6.1 Classification result using the segmental features 136
Table 6.2 Classification results by combining the segmental features 138
Table 6.3: Comparison of the features used for classifying the heart abnormality 138

List of Acronyms

2C view	2 Chamber view
4C view	4 Chamber view
2D	Two Dimensional
3D	Three Dimensional
AAM	Active Appearance models
AAMM	Active Appearance Motion Models
ABTF	Adaptive Brightness Transfer Function
ACC	American College of Cardiology
AHA	American Heart Association
A-mode scan	Amplitude mode scan
ASM	Active Shape Models
AV	AtrioVentricular
AoM	Abnormality of Motion
AWF	Assimilated Wavelet-based Feature
B-mode scan	Brightness mode scan
CA	Cavity Area
CAD	Coronary Artery disease
CHF	Congestive Heart Failure
CM image	Composite Motion image
CRT	Cathode Ray Tube
CR	Contrast Resolution
CT	Computed tomography
DVD	Digital Versatile Disk
Echo	Echocardiography
ED	End-Diastole
ES	End-Systole
EEG	Electroencephalography

ECG	Electrocardiography
EDV	End-Diastolic volume
ESV	End-Systolic volume
FA	Feature Asymmetry
FCP	Fuzzy membership function for centre part of the image
FD	Fuzzy Darkness
FHL	Fuzzy Horizontal Line
FMED	Fuzzy Multi resolution Edge Detection
FMWT	Fractional Myocardial Wall Thickening
FN	False Negative
FP	False Positive
FVL	Fuzzy Vertical Line
GAG	Generalized Adaptive Gain
HE	Histogram Equalisation
IC	Independent Components
ICA	Independent Component Analysis
LHE	Local area Histogram Equalisation
LA view	Long Axis view
LVCP	Left Ventricle Centre Point
LVEF	Left Ventricle Ejection Fraction
LoG	Laplacian of Gaussian
LV	Left Ventricle
MIDA	Myocardial Ischemia Detection Algorithm
M-mode scan	Motion mode scan
MRI	Magnetic resonance imaging
MRF	Markov Random Field
MEG	Magnetoencephalography
MLP	Multilayer Perceptron
PACS	Picture Archiving Computer System
PC	Principal Components
PCA	Principal Component Analysis
PDM	Point Distribution Model

RAM	Random Access Memory
ROI	Region Of Interest
RBF	Radial Basis Function
RF	Radio-Frequency
RWMA	Regional Wall Motion Abnormality
SA view	Short Axis view
SSCA	Systolic Segmental Cavity Area
TGC	Time-Gain Compensation
TN	True Negative
TP	True Positive
WD	Wall Displacement
WT	Wavelet Transform

CHAPTER 1

INTRODUCTION

1.1 Introduction

Heart failure is a worldwide problem with high morbidity and mortality rates [JESS2009]. The heart is one of the most important organs in the human body, which is comparable to a mechanical pump which works continuously. The health of this pump (heart) has to be assessed after a certain age or when a heart related medical condition is known to be present that could lead to further complications such as heart failure. As the unhealthy life style of the present generation is a major cause for heart related medical conditions such as hypertension, the heart assessment is vital in identifying abnormalities at an early stage in order to prevent further complications. Echocardiography (Echo) is a widely used imaging modality at the initial stage of assessment to identify such abnormalities. The diagnosis of a heart abnormality from an Echo scan is time consuming and depends on the observer expertise and available facilities. Thus, the difficulty in manual interpretation of the Echo images has led to the need for development of automated analysis tools.

Applying a range of image processing techniques to assist in the interpretation of Echo images is considered in this project. In particular, this project aims to develop a system to perform the segmentation of Echo scans, extract features and apply pattern recognition techniques to help diagnose a heart wall motion abnormality and consecutively the tissue damage in the heart wall. Finally, a diagnosis report is generated based on the information from the scan images. Ultimately this could be used to improve the precise location of the cardiac problems using this economical method of ultrasound scans. This system is not a replacement for the expert, but

would provide a reliable assistance to the cardiologists and help to prioritize the patient list for treatment.

1.2 Motivation for this research

Heart abnormality identification is an area of interest, as heart diseases are more prevalent especially among the Scottish population [MITC2005, BURNS2006, ALLE2008]. Cardiovascular disease such as myocardial ischemia is the leading cause of death worldwide [ALLE2008]. The rate of ischemic heart disease of Scotland is higher than for comparable nations [BURNS2006]. The main motivation of this work is to research into the problem of automatic identification of myocardial wall damage and abnormal wall motion from 2D Echo scan images.

Echocardiography is one of the widely used cardiac imaging modalities to visualise and assess the heart anatomy and function. When compared to the other modalities, an Echo scan is considered to be a safe imaging tool, with no known negative effects for patients. It is low-cost, non-invasive, real-time, portable, versatile and flexible to use.

According to European Society of Cardiology [ESC2007] and American College of Cardiology/ American Heart Association (ACC/AHA) guidelines [JESS2009], the initial assessment in cardiac patients involves history and physical examination, laboratory evaluation of blood, twelve-lead electrocardiogram and two-dimensional echocardiography with Doppler. Echocardiography imaging remains a standard technique in diagnosing left ventricular (LV) dysfunction (or abnormality) [BHF2010], myocardial infarction [ESC2007], myocardial ischemia in patients with heart failure and to define the likelihood of coronary artery disease (block in the artery that supplies blood to the heart muscle) in patients with heart failure and LV dysfunction [JESS2009, HUNT2005] .

Most of the commercially available echo scanning equipments such as Philips, GE and Siemens have dedicated software associated with their system which can be used for computer assisted manual interpretation for heart wall analysis. This can be performed by placing a few manual pointers on the heart contour of the first frame in

the scan, which is then traced along the entire Echo movie to provide an analysis report on the heart function and the wall segments. The drawbacks of Echo images (such as speckle noise, artifacts due to gain setting problems during recording, dropouts, shadowing, scan sector limitations and limited echo windows) have hindering effects on many of the existing automated analysis of heart and analysis of heart wall motion. The results are inconsistent and not reproducible as there is significant inter and intra-observer variability in placing the manual markers for the initial contour. As there is scope for significant improvements in the automated analysis tools with many issues remaining unsolved, continuous research is being performed within the manufacturing companies to advance their existing features, and develop additional features, in their tools. Therefore, there is a great need for automated image analysis tools which can overcome most of the Echo drawbacks.

This thesis looks into the problem of enhancing poor quality echocardiography images, visualisation of the features describing the heart function and performing automated image analysis which can overcome some of the drawbacks present in Echo images. The automatic identification of the wall motion abnormality and heart wall damage is considered as a feature recognition problem, as human decision making is related to recognizing features which represent abnormality in heart.

1.3 Contribution of the Thesis

In this work, the main research contributions are described below:

- Real data was used to extend and enhance the fuzzy logic based centre detection and fuzzy multi resolution edge detection (FMED) algorithms for heart wall boundary segmentation. A radial line search process is utilised to obtain the epicardial and endocardial edges. As the quality of the Echo images vary in different regions in a single frame, the region of interest and the criteria for selection of the edges is critical

- A novel echocardiography image enhancement method which combines undecimated wavelet based speckle noise reduction and edge detection, followed by a regional enhancement process that employs Delaunay

triangulation based thresholding is presented. The results to date are encouraging and suggest that this region based enhancement improves contrast near the edges, which are of diagnostic importance. The contrast improvement between the tissue and the blood region in echo images is performed based on local information so that the weak regions of the image are enhanced more than the strong regions.

- Eigenhearts, a Principal Component Analysis (PCA) technique based system for automated diagnosis of abnormality in the heart wall is developed. The feature extraction process uses principal component analysis and independent component analysis on the composite motion image which is created using the heart wall boundaries obtained from all the frames of an echo movie. These features provide information on the wall motion of the entire heart, which is subsequently used to identify abnormal hearts.

- The Radon transform is applied to the composite motion image to determine the symmetry in the wall motion. The characteristic of a normal wall motion is related to the sum of the projection of the image intensity in all angles. This feature is used to identify the abnormality in the heart wall motion.

- Development of the Myocardial Ischemia Detection Algorithm (MIDA) system which incorporates image pre-processing, heart wall boundary detection, heart classification based on principal component based feature extraction, and segmental wall analysis. The segmental wall analysis is carried out by extracting features that determine the health of the heart segment.

1.4 Organisation of thesis

The organisation of the thesis is as follows:

Chapter 2 provides fundamental information about the anatomy, physiology, and common pathologic conditions of human heart, followed by background information on medical diagnostic ultrasound techniques including ultrasound interaction with tissue, medical ultrasound instrumentation, different operating modes, image resolutions and common artifacts present in 2D real-time ultrasound imaging.

Chapter 3 presents a review of image processing techniques used in various stages of the automated wall motion analysis used in this research. A background review is presented on segmentation techniques to identify the endocardial and epicardial borders, Echo image speckle noise reduction and contrast enhancement techniques, and features used for identifying wall motion abnormality. This chapter also reviews some of the basic signal/image processing techniques which form a preliminary platform for subsequent research. A basic introduction to topics such as the Delaunay triangulation technique (which is used in the region based echo image enhancement of the algorithm described in Chapter 4), and pattern recognition techniques such as principal component analysis and independent component analysis and classification techniques (which is used in Chapter 5) are also presented in this chapter.

Chapter 4 presents the novel Delaunay triangulation based image enhancement algorithm to reduce the noise and enhance the contrast between the tissue and the blood region in echo images. It discusses an overview of an algorithm detailing the different stages such as speckle noise reduction, the Fuzzy-multi resolution edge detection technique in order to identify the heart wall boundaries. The local and global knowledge on the tissue and blood regions in the echo images is introduced and the region based processing for the tissue and the blood region based on Delaunay triangulation for contrast enhancement is explained in this chapter. The

results obtained for average and poor quality images are presented and the performance of the algorithm is discussed.

Chapter 5 introduces Eigenhearts, a novel Principal Component Analysis (PCA) technique based system for automated diagnosis of abnormality in the heart wall. It describes the process of creating the composite motion image from the heart wall boundaries obtained from all the frames of the echo movie. This chapter explains the feature extraction from the composite motion image using the Radon transform, ICA and PCA. These features provide information on the abnormality in the wall motion of the entire heart, which is then, used in subsequent identification of abnormal hearts. The experimental result with 62 patient data is presented. The performance of the three features for classification is also discussed in this chapter.

Chapter 6 presents the overall framework of Myocardial Ischemia Detection Algorithm (MIDA) which incorporates the heart classification, followed by the segmental analysis. The global and segmental features that are extracted from the inner and outer wall boundaries of the heart determined are described here. The classification of the extracted features obtained for the real patient echo images are presented.

Chapter 7 presents the summary of the research carried out so far and suggestions for future work.

1.5 List of author's publications

(1) V. Ahanathapillai, J. J. Soraghan, "Myocardial Ischemia Detection Algorithm (MIDA) for automated diagnosis of heart wall damage and abnormal wall motion", IEEE Transactions on Biomedical Engineering (submitted for publication in 2010)

(2) V. Ahanathapillai , J. J. Soraghan, P. Sonecki, "Region based image enhancement algorithm using delaunay triangulation to improve echocardiography image contrast", Digital Signal Processing Journal – Elsevier Publication, (submitted for publication in 2009)

(3) V. Ahanathapillai, J. J. Soraghan, "Myocardial Ischemia Detection Algorithm (MIDA): automated echocardiography sequence analysis for diagnosis of heart muscle damage", CinC2010, Computing in Cardiology Conference, Belfast, UK (2010)

(4) V. Ahanathapillai , J. J. Soraghan, P. Sonecki, "Delaunay triangulation based image enhancement for Echocardiography images", EUSIPCO 2009, 17th European Signal Processing Conference, Glasgow, UK (2009)

(5) V. Ahanathapillai , J. J. Soraghan, D. J. Hamilton, G. Morison, "Echocardiographical sequence analysis for the diagnosis of heart wall damage", DSP 2007, 15th International Conference on Digital Signal Processing, Cardiff, Wales, UK (2007)

(6) V. Ahanathapillai , D. J. Hamilton, " Eigenhearts for diagnosis of congestive heart failure (CHF)", MEDSIP 2006, 3rd International Conference on Advances in Medical, Signal and Information Processing, Glasgow, Scotland, UK (2006)

CHAPTER 2

CARDIOVASCULAR SYSTEM, HEART ABNORMALITIES AND ECHOCARDIOGRAPHY

2.1 Introduction

The heart, an important organ in the human body is a part of the cardiovascular system. Heart disease is a worldwide problem with high morbidity and mortality rates [PPSR2005]. Consequently, monitoring both structure and function of the heart is essential for the wellbeing of a person.

Ultrasound (Sound waves with frequency > 20 kHz) is routinely used in imaging the heart and other organs within the human body, because of its various advantages discussed later in this chapter. The field of Echocardiography (i.e. imaging heart using ultrasound) began in 1950, when Inge Edler, a cardiologist and Hellmuth Hertz, a physicist from Sweden modified a sonar device to record echoes from the heart [MEY2004] and acknowledged the relation between the received echoes, and the heart structure and function [EH1954]. Since then, there have been remarkable advancements in the field including wall motion studies, real-time imaging, Doppler and duplex techniques, and colour coded Doppler imaging [WEL1989, WEL1993].

This chapter provides the fundamental information about the anatomy and physiology of human heart in Section 2.2, followed by describing the common heart pathologic conditions in Section 2.3. Background information on medical diagnostic ultrasound techniques including ultrasound interaction with tissue, medical ultrasound instrumentation, different operating modes, image resolutions and

artifacts in 2D real-time are also discussed in Section 2.4. The chapter is concluded with Section 2.5.

2.2 Cardiovascular system

The cardiovascular system includes the heart (a pumping device), a closed network of blood vessels (the conducting pipes) and the blood (the fluid component). The heart pumps the blood to all organs through two circuits of blood vessels that begin and end at the heart. The blood vessels which carry blood to and from the lungs constitute the pulmonary circuit and the ones which carry blood to and from the rest of the body constitute systemic circuit. The blood vessels that carry blood away from the heart are arteries and the veins are those which carry blood back to the heart. The blood circulating through the body has various responsibilities including stabilizing body temperature, defending the body against toxins and pathogens, and transporting oxygen, nutrients, hormones and metabolic wastes between different parts of the body [MART2004]. The anatomy and physiology of the heart is discussed here.

2.2.1. Anatomy of Human Heart

The heart is a muscular organ located between the lungs near the chest wall, posterior to sternum. It is accountable for pumping about 2000 gallons of blood in a day. A normal adult heart weighs between 300g to 350g [RAN1998]. The heart is surrounded by a sac called the pericardial cavity. This cavity is lined by the pericardium and contains the pericardial fluid. This helps in reducing friction between the pericardium surfaces when the heart beats. The heart wall has three distinct layers:

- Epicardium, a thin membrane covering the outer surface of the heart.
- Myocardium, the muscular wall containing the cardiac muscle tissue, blood vessels and nerves.
- Endocardium, a membranous tissue covering the inner surface of heart.

The heart consists of four chambers, two atria and two ventricles.

2.2.1.1. Right Atrium

The right atrium receives impure deoxygenated blood from different parts of the body through superior vena cava, inferior vena cava and coronary sinus. The right atrium has a smooth posterior wall and inter-atrial septum. The anterior wall of atrium has muscular ridges (also called pectinate muscles).

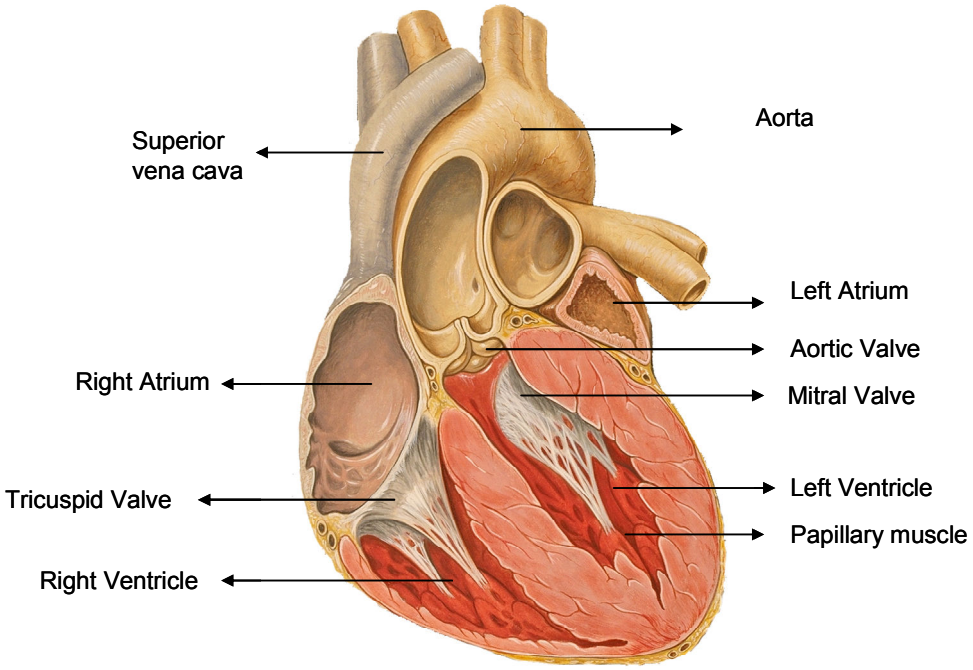

Fig. 2.1 Sectional view of Heart [LYN2006]

2.2.1.2. Right Ventricle

The right ventricle receives blood from the right atrium through an opening guarded by right atrioventricular (AV) valve or tricuspid valve. Valves are structures that ensure unidirectional blood flow during the cardiac cycle. The valves can be seen in the sectional view of the heart, Fig. 2.1. The inner surface of the ventricle has conical muscular projections called the papillary muscles. Chordae tendineae (a tendinous connective tissue fiber which originate at these papillary muscles) are connected to the valves to keep the valves in the required position. When the right ventricle contracts, the tricuspid valves close, preventing the blood flow back into the atrium.

The pulmonary valve or semi lunar valve is present at the end of conus arteriosus, where the pulmonary trunk starts from the right ventricle. The contraction of the right ventricle pumps blood to the lungs for purification.

2.2.1.3. Left Atrium

The left atrium receives pure oxygenated blood from the lungs through the four pulmonary veins (two left and two right). It opens at the posterior of the left artium. The blood is passed to the left ventricle through an opening guarded by the left atrioventricular valve or bicuspid valve or mitral valve.

2.2.1.4. Left Ventricle

The left ventricle (LV) receives blood from the left atrium and pumps the blood into the aorta through the aortic valve. The left ventricle has a thick, muscular wall, which enables it to develop the pressure required to pump the pure blood to the rest of the body. At the base of the ascending aorta, there are sac like dilations called aortic sinuses. The right and left coronary arteries originate at the aortic sinuses. These arteries supply blood to the cardiac muscles. The left ventricle is considered the most important chamber in the heart and is assessed mainly during the assessment of the heart.

2.2.1.5. Blood supply to heart

Similar to all the other tissue of the body, the heart also needs oxygen and nutrients, in order to function properly. As the blood flowing throughout the heart is too fast for it to absorb oxygen and nutrients, the heart has its own set of blood vessels (constituting coronary circulation) that supply it with blood. The coronary circulation is made possible through a network of two types of coronary blood vessels (as shown in Fig. 2.2):

- Coronary arteries including the right coronary artery, the left anterior descending and the left circumflex coronary artery.
- Cardiac veins including the posterior cardiac vein, the middle cardiac vein and the anterior cardiac vein.

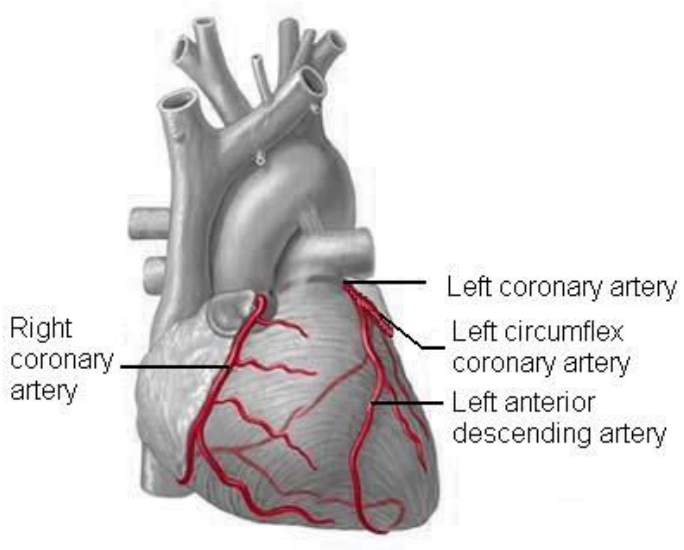

Fig. 2.2: Coronary heart arteries [KANG2006]

2.2.2. Physiology of the Human Heart

The cardiac cycle includes alternating periods of contraction and relaxation (atria contraction followed by the ventricular contraction). The contraction phase of the heart is called the systolic phase (or systole) and the relaxation phase of the heart is called the diastolic phase (or diastole). During a normal heart beat, two types of cells are involved:

- Conducting cells of the conducting system specialised to control and coordinate the heart beat
- Contractile cells to contract powerfully to force blood

2.2.2.1. Cardiac Conducting System

The heart muscles contracts automatically without neural or hormonal stimulation. The conducting system (as seen in Fig. 2.3) consists of cells responsible for initiating and distributing the stimulus to contract. The elements included in this cardiac conducting system are the Sinoatrial node, Atrioventricular node and conducting cells.

The Sinoatrial (SA) node is located in the posterior wall of the right atrium. The SA node is also called the cardiac pacemaker or natural pacemaker. It contains

pacemaker cells, which establish the heart rate. The SA node is connected to the larger atrioventricular node by the internodal pathways. The stimulus travels from the SA node to the conducting cells, which pass the stimuli to the contractile cells of both atria. The Atrioventricular (AV) node is located at the junction of the right atrium and the right ventricle, near the opening of the coronary sinus. The AV node receives the stimuli from the SA node. Then the impulse enters the AV bundle, also called the `Bundle of His'. The stimulus received by the AV bundle is passed to the interventricular septum and then to the right and left bundle branches. The impulse is conducted to the purkinje fiber, and then to the papillary muscles through the moderator band. The ventricular contraction starts at the apex and moves toward the base, as the purkinje fibers spread out from the apex to the base of the heart. The conducting cells interconnect two nodes and distribute the impulse through the myocardium. These cells are present in the internodal pathways, AV bundle, the bundle branches and the purkinje fibers are conducting cells.

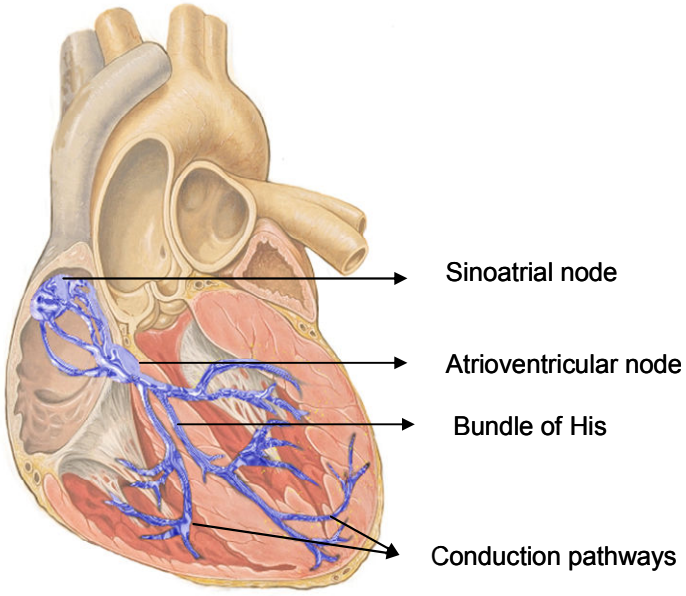

Fig. 2.3: Conduction System [LYN2006]

2.3. Common heart pathologic conditions

Some common heart pathologic conditions are introduced briefly in this section. Special emphasis is given to the heart conditions that will be diagnosed using the image processing techniques discussed in this thesis.

2.3.1 Coronary Artery Disease

Coronary Artery Disease (CAD) or Coronary artery atherosclerosis is a condition in which the coronary artery is partly or completely blocked by fatty deposits (plaque) or a blood clot. The coronary artery hardens and narrows because of the deposit of plaque in its inner wall, which is illustrated in Fig. 2.4. As the size of the deposit increases, the artery narrows, allowing less blood to flow through them. This affects the normal oxygen supply to heart muscles, causing damage to the muscles. CAD is usually a progressive disease [KANG2006, SDS2005].

2.3.2 Myocardial Ischemia

Myocardial ischemia, also called ischemic heart disease, is a condition in which the heart muscles are not supplied with sufficient blood, resulting in reduced supply of oxygen accompanied by inadequate removal of metabolic wastes. In other words, there is a blood supply and demand imbalance in the heart muscles. This damages the heart muscle leading to abnormal heart wall movement and gradually reduces the efficiency of the heart. This disease acts as a primary cause to other complications, eventually leading to acute coronary syndrome or myocardial infarction or heart attack or heart failure [ADSF2008, ZEV2006]. Consequently, diagnosing the presence of myocardial ischemia at an early stage is critical, as it is treatable helping to prevent further complications.

2.3.3 Myocardial Infarction

Myocardial infarction is a condition in which the heart muscle is irreversibly damaged (death of heart tissue) as a result of prolonged ischemia [SUT1993]. Approximately 90% of the myocardial infarction results from a severe blood clot in

the coronary artery. This condition is a secondary stage of myocardial ischemia and CAD [GZ2006, KANG2005].

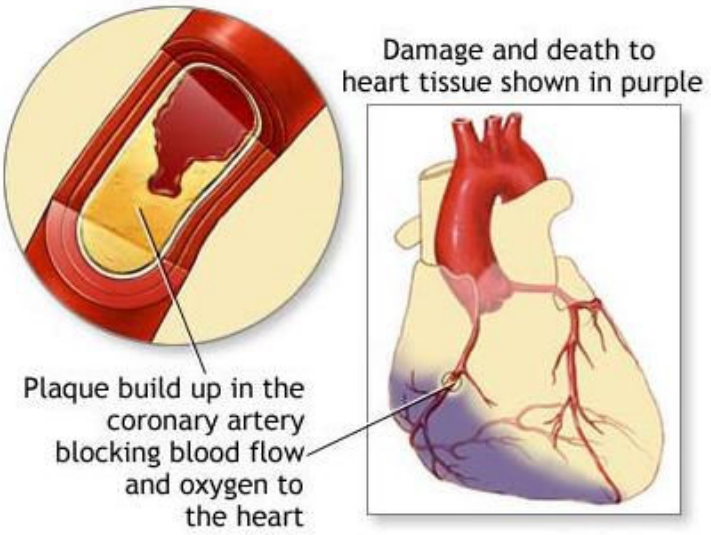

Fig. 2.4: Coronary Artery Disease leading to Myocardial Ischemia (tissue damage) or Myocardial Infarction (tissue death) [KANG2006]

2.3.4 Congestive Heart Failure (CHF)

Heart failure is the end stage of many different forms of heart diseases including common diseases like cardiomyopathy, myocardial ischemia, myocardial infarction, coronary artery and valve diseases. Congestive heart failure (CHF) is a state in which the heart becomes less efficient to pump blood. So, it has to work harder to compensate, which could ultimately lead to fatal damage [ZEV2005, GAND2006]. There are different types of CHF [BALES1997]:

- Systolic heart failure is the most common type. It occurs when the heart muscle does not contract with enough force, so there is not enough oxygen-rich blood to be pumped throughout the body.
- Diastolic heart failure occurs when the heart contracts normally, but the ventricle does not relax properly. So, less blood can enter the heart.

2.3.5 Regional Wall Motion Abnormality

The regional wall motion abnormality (RWMA) refers to abnormal movement in a section of the heart muscle. RWMA occur in heart conditions including ischemic heart disease, and CAD. The location of the RWMA could possibly identify the coronary artery that is responsible for the abnormality. The types of wall motion abnormalities are: hypokinesis (reduced inward motion); akinesis (absence of systolic inward motion); dyskinesis (outward wall motion during systole) and aneurismal (a blood filled sac formed by localized dilatation of the weakened wall). The segmental wall motion abnormalities may indicate ischemia or prior infarction [MPT2008]. During the assessment, a scoring is given to the heart wall segments. The myocardial segments are considered based on the standards [CER2002], which suggest that the LV should be divided into 17 segments. These 17 segments can be assigned to one of the three major coronary arteries, as shown in Fig 2.5.

Electrocardiography (ECG) is the first screening test that is often performed to identify the presence any abnormality in the heart's function. However, the ECG on its own is not sufficient to come to a conclusion on a case. It is used in parallel with one of the imaging techniques to study the health of the heart in order to derive a decision on the diagnosis. Though varies tests are useful in case of the diagnosis of these pathological conditions, a suitable test or mode of imaging is chosen based on the suitability of the technique for the patient. The benefits of a particular technique over the risks as a result of performing the test, is often the prime influential factor.

Echocardiography is chosen over other imaging techniques whenever possible as it is safe. There is no known risk associated with this imaging technique [DUN1991]. Most examinations are non-invasive [MCD1981], therefore examinations may be readily repeated, if necessary. Ultrasound is useful to image soft tissues, which are difficult to image using conventional X-ray techniques. Also, ultrasound machines are portable when compared to other imaging modalities such as the MRI and CT. Consequently, in certain medical conditions which can be identified using echocardiography, the test is performed as a first stage, just to check if the condition is present or not.

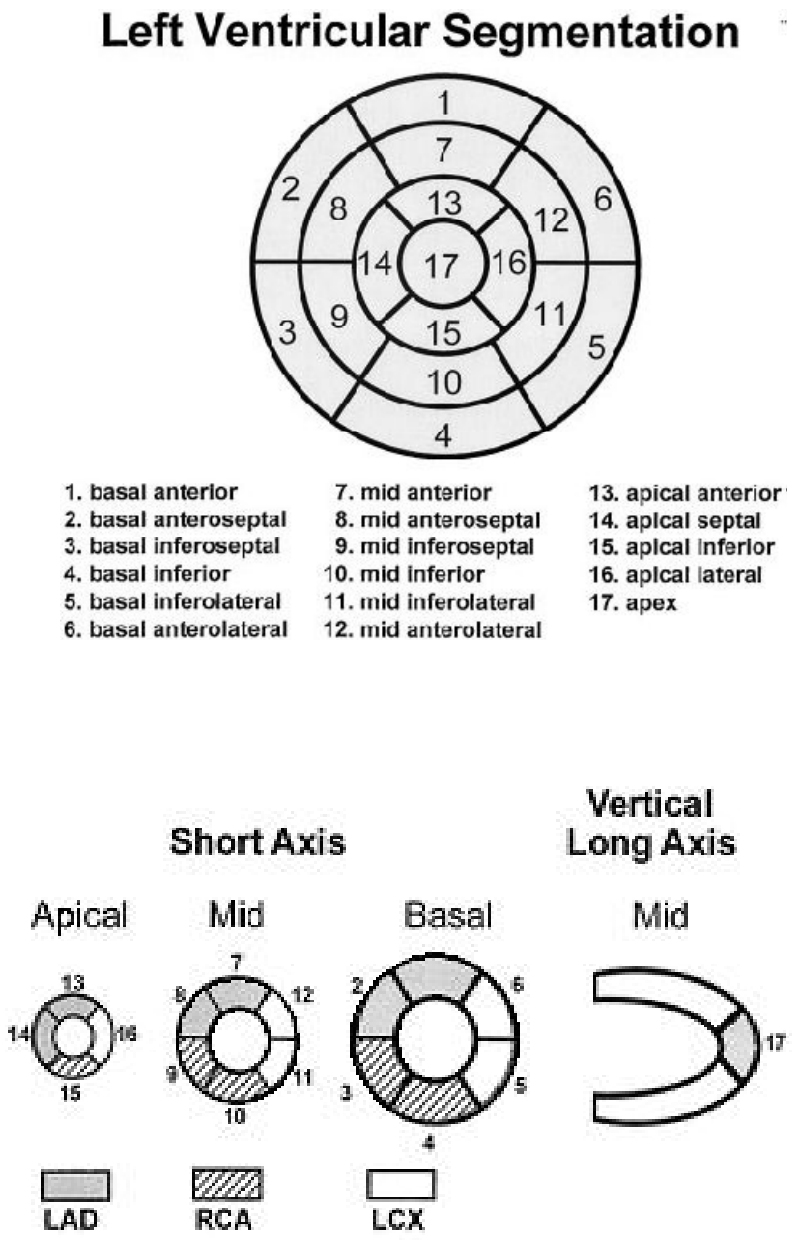

Fig. 2.5 Assignment of the 17 myocardial segments to the territories of the left anterior descending (LAD), right coronary artery (RCA), and the left circumflex coronary artery (LCX) [CER2002]

2.4 Fundamentals of Echocardiography

Ultrasound technology uses sound waves above human audible frequency (i.e. above 20 kHz). It is used routinely in wide range of applications including biomedical, SONAR, non-destructive testing or evaluation, and machine condition monitoring. This section provides the fundamentals of ultrasonic sensing technique, for medical imaging applications. The basic principle of generating the ultrasound, characteristics of ultrasonic waves propagating in tissue media, and interpretation of the received echoes and the display of the digital images are explained. The different mode of operation of the ultrasound scanner and the artifact in the Brightness-mode scan (also known as the B-scan), a common echocardiography imaging modality that is used within this PhD is also discussed.

2.4.1 Overview of Medical Ultrasound

Medical applications of ultrasound can be broadly categorised into surgical, therapeutic and diagnostic applications [RGR1987]. Surgical applications use highly focused ultrasound with high intensity that aims to destroy targeted tissue. An example application includes the treatment of Meniere's disease (a disorder of the inner ear), in emulsifying the diseased lens in cataract surgery, in breaking and removing the kidney stones and in removing warts.

Therapeutic applications use 0.8MHz to 4MHz transducers to generate heat and consequently relieve pain, reduce the stiffness of soft tissues and speed up the healing process. It is often used in physical therapy along with exercise in treating the joint and soft tissue ailments.

Diagnostic applications employ 1MHz to 40MHz signals to image various parts of the body for identifying different pathological conditions. This includes quantitatively measuring the heart chambers, studying the health of the heart valves and detecting wall motion abnormalities (Cardiology), locating lesions and tumors in brain (Neurology), monitoring the growth and development of the fetus (Obstetrics), detecting ovarian cysts, other pelvic masses and abscess (Gynecology), diagnosing detached retinas and retinal tumors in eye and also in measuring the thickness of the

cornea (Ophthalmology), detecting thyroid cysts, and identifying simple cysts from solid masses in breast, studying the health of liver, spleen, pancreas and kidneys, in diagnosing the presence of different types of cysts and cancers (Abdominal).

2.4.1.1 Ultrasonic Diagnostic Imaging Technique

Ultrasonography (or ultrasound) is a non-invasive medical imaging technique. This involves transmitting high-frequency acoustic energy into the human body using a set of transducers placed in direct contact with the skin. The ultrasound wave's reflections from boundaries between organs and surrounding fluid, and between regions of differing tissue density, are captured using the same transducer (using inverse piezoelectric property) and reconstructed to visualise the internal body structures for possible pathology.

Echocardiography (or Echo) is one of the most widely used medical imaging techniques for diagnosis of the heart. An Echo scan is a movie captured over a time period, to cover a complete cardiac cycle. Though echo scans are low quality images, they are chosen for this project over the other cardiac imaging techniques (such as the MRI and CT) as it has the following advantages:

1. The ultrasonic scanning equipment is transportable, and the images can be stored electronically
2. Reliable; harmless; painless; relatively inexpensive; noninvasive technique; and
3. Suitable for imaging soft tissues such as hearts to determine valve disease, left ventricle wall thickness, and the regional wall motion abnormalities [ZEV2005, KAD2001].

2.4.2. Ultrasound Tissue Interaction

When the ultrasound beam travels through tissue, some of its intensity or energy is lost due to its interaction with the tissue. This energy loss is known as attenuation. Some of the sources of attenuation are: absorption, scattering, reflection, refraction, diffraction, interference and beam divergence.

2.4.2.1. Absorption

Absorption of ultrasound is a direct process of energy loss, in which the tissue molecules suffers random mechanical motion which produces heat energy. Energy transferred into internal molecular energy and back is known as thermal relaxation. If transfer of energy takes the form of heat flowing from one region to another and back, it is called conductional relaxation. If the transfer of energy is between two states of different physical structure, it is called structural relaxation [MCD1981]. Absorption increases with increase in operating frequency, and depends on the elasticity and density of the medium.

2.4.2.2. Reflection

Reflectivity depends on the acoustic impedance or characteristic impedance of the tissue and the angle of incidence. Fig. 2.6 illustrates the reflection of ultrasound wave at an interface with an angle of incidence (θ_i) and the angle of reflection (θ_r). The intensity of the reflected wave (I_r) is given by

$$I_r = I_i \left(\frac{Z_2 - Z_1}{Z_2 + Z_1} \right)^2 \tag{2.1}$$

where Z_1 and Z_2 are the acoustic impedance of the two tissue media and I_i is the intensity of the incident wave.

At the interface of tissues with similar acoustic impedance, little reflection takes place, allowing most of the ultrasound to be transmitted across the interface. More reflection takes place at the tissues interface with very different acoustic impedance. When the ultrasound beam is perpendicular to the tissue interface, reflections from smooth tissue interfaces produce specular reflections.

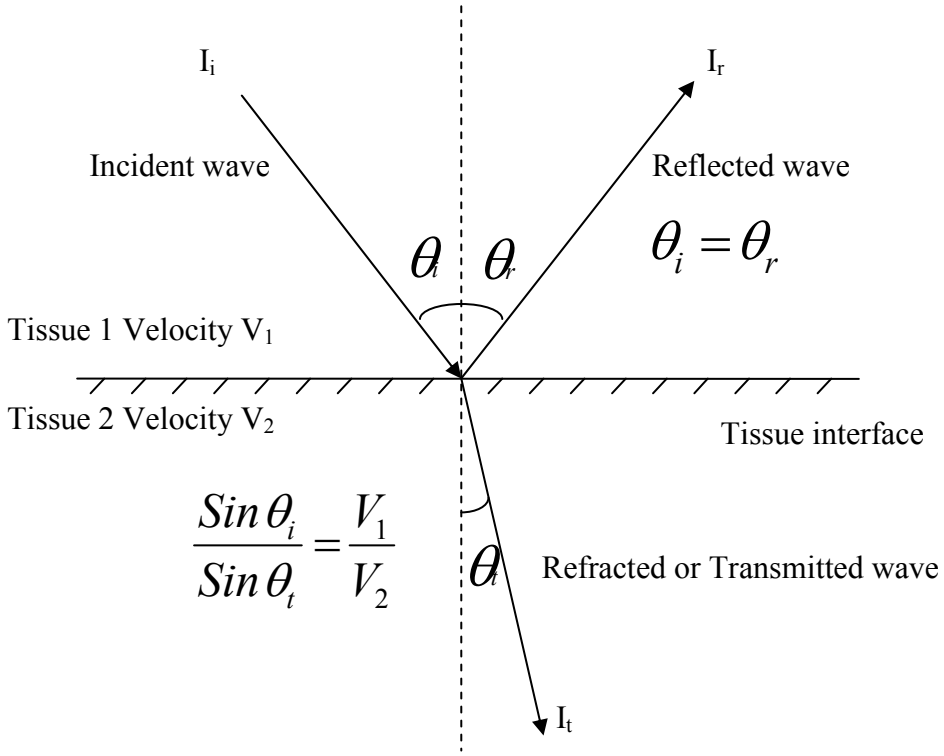

Fig. 2.6 Ultrasound reflection and refraction at tissue interface

2.4.2.3. Refraction

If energy incident to an interface is not perpendicular to the interface, refraction of the beam takes place. Fig. 2.6 illustrates the refraction of an ultrasound wave at a tissue interface. Effect of refraction is negligible when the beam is perpendicular to the reflecting surface. It depends on the angle of the incident beam to the interface (θ_i) and the change in velocity at the boundary between materials. The relationship between the angles and the velocities of the waves, is given by Snell's Law

$$\frac{Sin\ \theta_i}{Sin\ \theta_t} = \frac{V_1}{V_2} \tag{2.2}$$

where V_1 and V_2 are velocity at the two tissue media and θ_t is the angle of refracted wave.

2.4.2.4. Scattering

The incident ultrasound wave is reflected in many directions after interacting with an individual molecule in homogeneous tissue (as seen Fig. 2.7(a)). This phenomena known as the Rayleigh scattering (or beam spread) take place when the target dimension is much less than the incident wavelength. High frequency results in strong scattering, and offers the most diagnostic information for imaging application. Scattering at regular or smooth tissue interface produces specular reflections, while irregular tissue interface produces diffuse or non specular reflection.

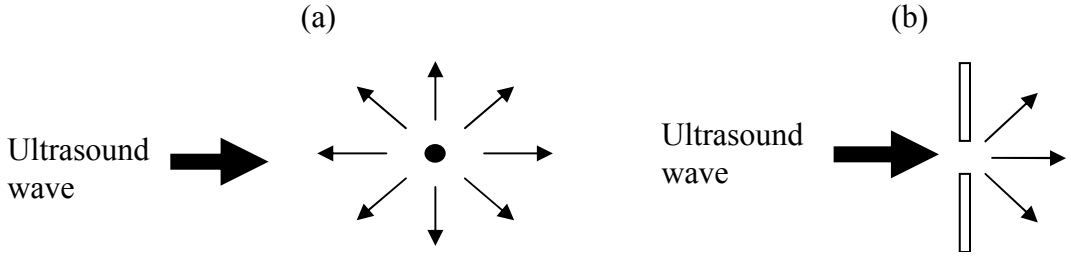

Fig. 2.7 (a) Ultrasound Scattering (b) Ultrasound Diffraction at tissue aperture

2.4.2.5. Diffraction

Diffraction is a type of scattering which results in uniform spreading of the beam as it propagates from the source. Diffraction is inversely proportional to size of the source. Ultrasound gets diffracted when passing through a tissue aperture as illustrated in Fig. 2.7(b). More diffraction results in more attenuation.

2.4.2.6. Interference

Interference refers to the interaction of two or more ultrasound beams having different frequency and/or phase. Interference strengthens or weakens the wave, depending on the phases of the interacting wave fronts. It can be classified as follows

- Constructive interference occurs when two or more waves of the same frequency are in phase, adding up to increase the intensity of an ultrasound beam.

- Destructive interference occurs when ultrasound waves which are out of phase, cancel out decreasing the intensity of an ultrasound beam.

The received echo train contains reflections from separate tissue boundaries and other small signals produced by overlapping echoes scattered at closely packed structures. The time and amplitude information in these echo trains are used to create images.

2.4.3 Medical Ultrasonic Instrumentation

The instrumentation involved in a medical ultrasonic imaging system is discussed in this section. A schematic overview of a typical medical ultrasonic instrument is shown in the Fig. 2.8. The system consists of an ultrasonic transducer, pulser, receiver, scan converter and a display device. These principal components are described below.

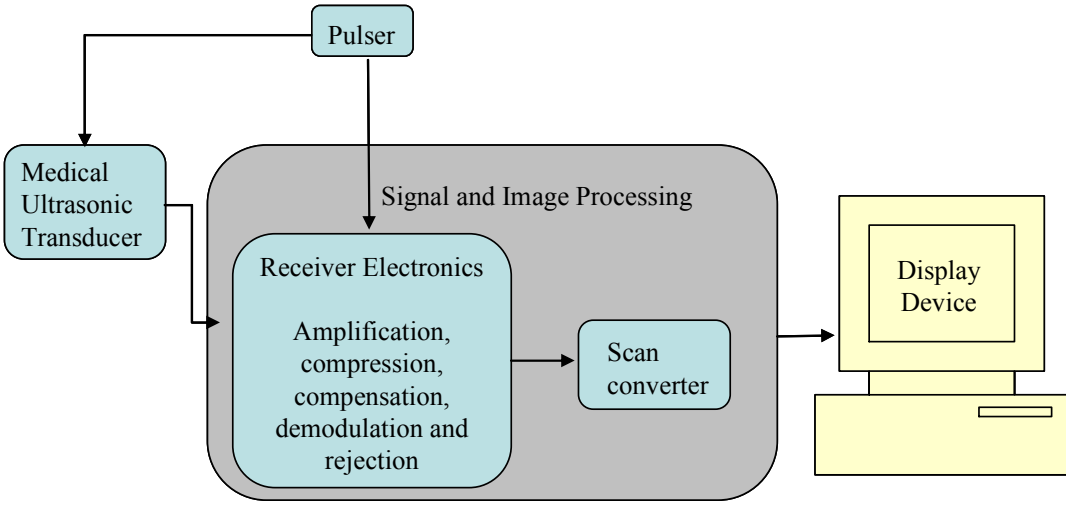

Fig. 2.8 Principal electronic components in a medical ultrasound imager

2.4.3.1. Medical ultrasonic transducers and associated electronics

At the heart of the instrument is the transducer, which converts electrical signal into pressure waves and vice versa. The structure of an ultrasonic transducer consists of ceramic crystal, matching layer, backing medium, and electrodes (as seen in Fig. 2.9). Crystals with piezoelectric properties are used in such ultrasonic transducer assembly. Piezoelectric crystals are either naturally occurring (for example, quartz, lithium sulphate, and rochelle salt) or synthetic ceramic crystals (for example, some

transducer are made of lead zirconate titanate [MH2008] or polyvinylidine difluride). At the front face of the crystal, one or more matching layers are bonded to overcome/compensate the acoustic mismatch present between the piezoelectric element and the tissue. This increases the efficiency of energy transfer to the tissue. Aluminium powder in Araldite is commonly used as a matching layer material, as it doubles also as a front face electrode. For pulse echo imaging, a backing medium is placed at the back face of the crystal, to give mechanical support and quickly damp out the crystal vibrations immediately after excitation. In other words, the energy radiated into back face of the crystal is absorbed completely and not reflected back into the element. This damping layer helps in producing short pulses, and consequently improves imaging resolution. Epoxy resin (such as Araldite) loaded with heavy tungsten powder is an example of a typical damping material used as a backing block. Thin silver electrodes are placed in the front and back face of the crystal, and the active piezoelectric material is permanently polarised across its thickness. The operating frequency depends on the thickness, while the beam shape depends on the diameter of the crystal. Standard transducer is disc shaped crystal which is 2cm in diameter and varies from 1.8 mm (for 1MHz transducer) to 0.18mm (for 10 MHz transducer device) in thickness, approximately. The frequency range required for heart applications is approximately in the range 1 to 5MHz.

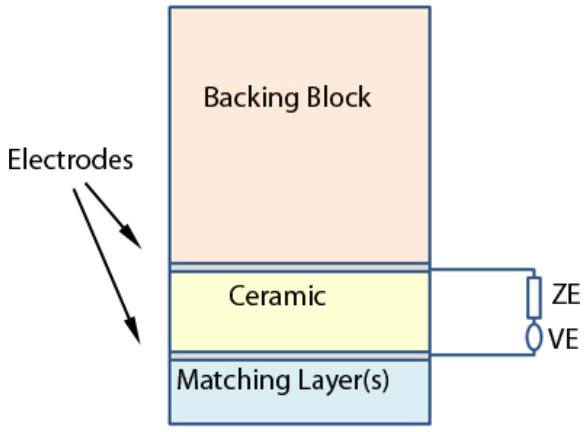

Fig. 2.9 Transducer structure

When a voltage is applied across the electrodes, proportional change in thickness is produced. When pressure is applied across the two faces a potential difference builds up between the electrodes. The generated ultrasound is focused by shaping the transducer crystal (internal focusing), phased array techniques (to electronically

change the focal depth and direction), zone plates or zone lenses (to produce high-intensity focus) or by using a lens or a mirror in front of the transducer. For imaging application, an array of ultrasonic sensor is driven by a pulser unit, with a pulse repetition frequency between 1 to 5 kHz (i.e. 1000-5000 pulses/second). The beam intensity depends on the amplitude of applied voltage. The transmitted beam interacts with the tissue (as discussed in section 2.2.2) and produces echoes, which are received by the same array. The receiver modifies these electric signals suitably so as to create an image, and typically consists of amplification, compensation, compression, demodulation and rejection stages, as illustrated in Fig 2.10.

- The amplification range or gain is up to 120 decibels. The sensitivity to weak echoes increases with increase in the amplifier gain.

- Time-gain compensation (TGC) is adjusted, so that the echoes from deeper structures are amplified more than the echoes from the closer structures, resulting in uniformly bright images.

- Compression (opposite of the TGC) reduces the amplitude of large echoes. Compression is also responsible for producing an image with uniform image intensity.

- Demodulation is performed to convert the received oscillating signal to a direct signal. It involves rectification and filtering.

- If the received echoes are below a threshold (very weak), they are rejected.

2.4.3.2. Digital Scan Converters

The electrical signals from the receiver travel to the ultrasonic scanner where they are processed and transformed into a digital image or movie. A scan converter consists of integrated microprocessor with a random access memory (RAM) to store the signals. The depth of the structure in the image depends on the time taken by the echo to be received and the intensity of a pixel depends on its strength. Conventionally, the resultant image is a pixel matrix in the grey scale format. The spatial resolution gets better as the image matrix size increases while the contrast resolution corresponds to the dynamic range. Contrast Resolution (CR) is the ability

to differentiate one tissue from the other. It is the smallest measurable difference in echo intensity. The dynamic range of echo is more than the dynamic range of human perception of gray levels (approximately 100 dB to 20 dB) [KRE2006]. The dynamic range of echo is compressed to be sensitive to the human eye. Post processing of these images after acquisition is also possible. A new contrast enhancement algorithm is developed within the scope of this thesis are presented in Chapter 4.

2.4.3.3. Image display device and storage

Storing images are important as they are valuable for teaching or training purpose, or to review study how the disease progresses or how the patient responds to a particular treatment by comparing with the previously recorded images. A Cathode ray tube (CRT) is normally used to display the ultrasound image. The ultrasonic images are archived by three main ways [TG2004]:

- Hard copy: This is the oldest type of storage, recorded on a paper or film.
- Analog video: Analog videos are recorded by connecting a video cassette tape or magnetic disk recorder to an ultrasound scanner.
- Digital storage: The digital or computer storage is also known as Picture Archiving Computer System (PACS). These digital data can be stored in Digital Versatile Disk (DVD).

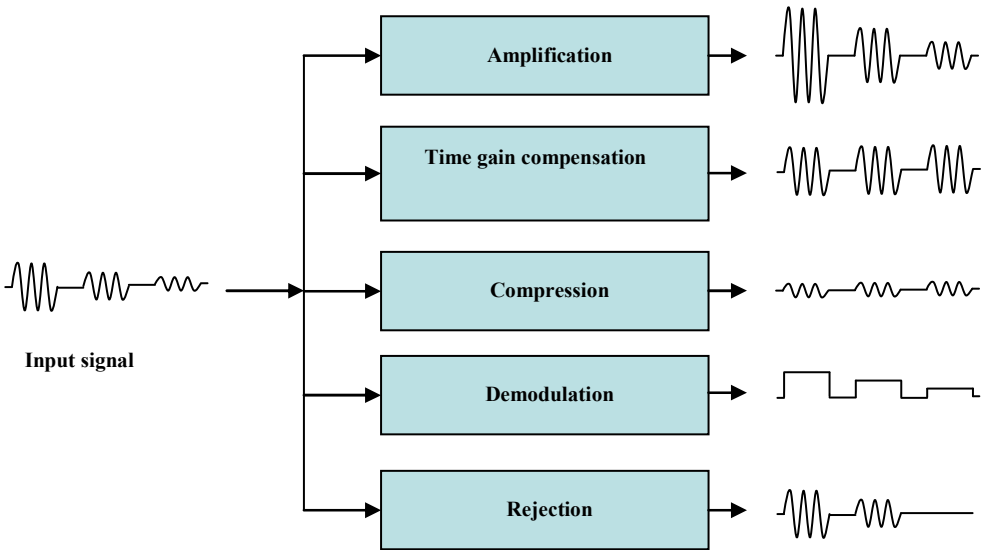

Fig. 2.10. Receiver functions: amplification, compensation, compression, demodulation and rejection [BUSH1999]

2.4.4 Operational modes or ultrasound imaging modes in Echocardiography

The pulse echo ultrasound instrument can be operated in a variety of ways. The main operational modes are as shown below

2.4.4.1. A-mode (Amplitude mode)

An A-mode scan produces chain of spikes which is displayed on a cathode ray tube (CRT) as shown in the Fig. 2.11(a). The distance between the spikes is proportional to the distance between the interfaces and the amplitude is proportional to the strength of the echo. The depth and separation of the interfaces is measured using this technique. The limitations of this operational technique are that the direction of the echo and the information on the reflecting surface is unknown.

2.4.4.2. B-mode (Brightness mode)

A B-mode scan produces composite images (as shown in the Fig. 2.11(b)) on the CRT, where the pixels are illuminated in proportion to the strength of the received echo. That is, the received echoes are plotted as lines with varied intensity along the ultrasound beam path. B-mode image views are rectangular or sector, depending on

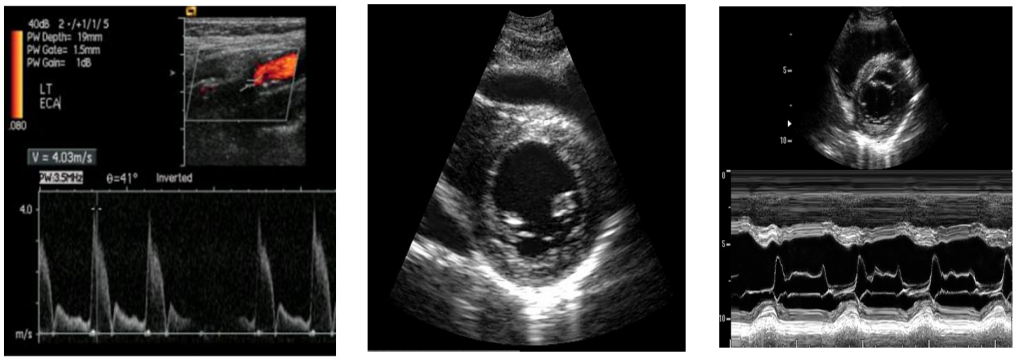

(a) (b) (c)

Fig. 2.11 Different operational modes (a) A – mode (b) B – mode and (c) M – mode.

the transducer design. 2D-real time imaging systems displays up to 100 images per second. B-scan movies are used within this thesis.

2.4.4.3. M-mode (Motion mode)

M-mode scan gives time axis information on the movement of tissue interfaces. The received echo from successive pulses are plotted side by side to show the interface movement with time. Fig. 2.11 (c) shows a sample M scan.

2.4.4.4. Standard 2D echocardiography views

The heart is examined by placing the ultrasonic transducer in standard positions, which allows good penetration of ultrasound. These positions are also referred as acoustic windows. Sections of heart are examined in these acoustic windows to avoid limitations due to anatomy of heart and surrounding structures like lungs and ribs, and to obtain standard images to be used for a comparative study. The main echo windows [KAD2001] are apical window, subcostal window, left parasternal, right parasternal view and suprasternal view as shown in the Fig. 2.12.

Among these, the left parasternal window provides the best access to the heart. It is located between the 2nd and 4th intercostal spaces in the left side edge of the sternum. Additional access can be obtained from the other windows. In theory, infinite cross sectional images of the heart can be obtained. The few standard echo views are used for diagnostic purposes are: parasternal short-axis(SA) view, parasternal long-axis view, apical long-axis two-chamber view, and apical long-axis four-chamber view. Fig. 2.13 shows few standard views of the heart. Short axis view is considered for processing in this thesis.

Also, the Left Ventricle (LV) is the most vital chamber of the heart as it pumps blood at high pressure. Its performance is generally studied to examine cardiac condition. These standard views mentioned above are used for assessing the heart structure and evaluating its function.

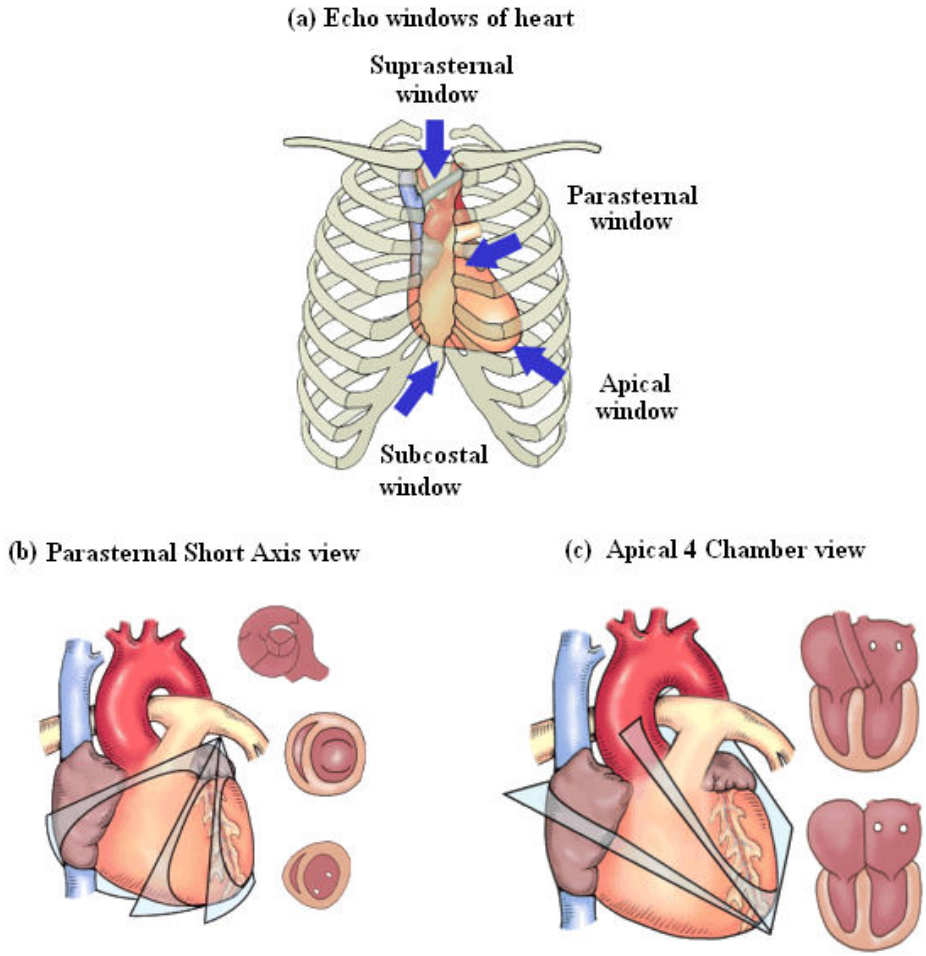

Fig. 2.12 (a) Echo windows of the heart, (b) Parasternal short axis view and (c) Apical 4 Chamber view

(a) (b) (c)

Fig. 2.13 Standard echocardiograph views of the heart (a) Parasternal Short Axis view, (b) Apical 2 Chamber view and (c) Apical 4 Chamber view

2.4.5 Artifacts present in 2D real time B-scans

The quality and accuracy of the 2D B-scan images is often greatly influenced by various imaging artifacts. An artifact is a signal or information that appears accidentally and does not represent any structure in an image. These artifacts could be the characteristic of pulse-echo imaging used or due to the imperfections in different stages of the imaging system. Image artifacts are false features of image which could be due to equipment deficiency, peculiar patient features, patient instability or image processing defects [BUSH1999]. Some of the common artifacts present in the B-scans are:

2.4.5.1. Reverberation

False representation of closely/equally spaced parallel interfaces is produced in an image due to reverberation. When the ultrasound beam is perpendicular to the reflecting tissue interfaces, reverberation artifact is produced. In the presence of strong reflectors, regularly repeated echoes of reverberations are observed as a set of parallel lines, spaced by the depth of the reflector [HUS1985]. Comet tail and ring-down artefact are characteristic reverberation artifacts [BUSH1999].

2.4.5.2. Displacement artifact

Displacement artifact occur when an image is formed with false structures. Some of the displacement artifacts observed is due to side lobes. Side lobes of the main ultrasound beam could produce structures in the image which lie outside the main beam, if the side lobe intensity is large. Multipath artifact [RWC1998] creates an image with ghost structure placed at the back of the true location of the structure. Refraction artifact results when refraction at one boundary directs the beam at right angles towards a reflector. This produces a ghost structure displaced from actual position of the reflector. Both Multipath artifact and Refraction artifact can be eliminated by compound scanning.

2.4.5.3. Shadowing

Shadowing is caused by strong reflections at tissue interface. Sometimes, in the presence of strong reflectors, blank regions without any features (shadow) are

formed behind or deeper than very bright regions. Due to the presence of strong reflectors in superficial tissue, the beam does not penetrate enough into the deeper structures to get significant echoes. Refraction at curved tissue interface, having different ultrasound velocities could produce something called edge shadows [GA1997]. Increasing the far field time gain compensation and repositioning the transducer could reduce shadowing.

2.4.5.4. Image enhancement or echo enhancement

Image enhancement is caused by false amplification. If there is a weak reflecting tissue interface, image enhancement occurs (opposite to shadowing). The region below this interface produces echoes which have amplitude greater than expected. This artifact can be reduced by changing the TGC setting [WEBB1988].

2.4.5.5. Speckle

Speckle is a characteristic of ultrasound images, which has a grainy appearance [FJ1980]. This is mainly caused by the constructive and destructive interference of back-scattered ultrasound. Speckle usually falls in the high sensitivity region of human vision to spatial frequency. The presence of speckle degrades the image information that is of clinical importance. So, speckle reduction is performed as a preprocessing of many ultrasonic image processing methods. In this thesis, a review of speckle reduction is also discussed.

2.4.5.6. Incomplete imaging

Other imaging artifacts include incomplete imaging, which is caused by moving the probe fast compared to the pulse repetition frequency. This results in image consisting of lines of information with blanks between them.

2.4.5.7. Patient movement

During image acquisition, patient movements like breathing change the probe's direction slightly causing structures to be formed in different locations during the image build-up.

2.5 Conclusion

The anatomy and physiology of the heart along with the common heart conditions were presented in this chapter. Also, the importance of locating RWMA to possibly identify some of heart conditions was illustrated. One significant problem is the time consuming and laborious procedure involved in identifying RWMA using Echocardiography. Consequently, automation of this diagnostic procedure will be a useful tool for the cardiologist.

This chapter also discussed the basics of the ultrasound imaging system including the ultrasound wave propagation in tissue, the ultrasound instrumentation, image formation, the views that are widely used, and the quality of 2D scan images. The short axis views are used in this research. The image contrast enhancement of this view is one of the research interests. The major disadvantage of ultrasound compared with other techniques is that the resolution of images is often limited. In the following chapter, various image processing techniques applied to ultrasound images to solve this problem of image enhancement and to developing a semi or fully automatic algorithm for RWMA identification.

CHAPTER 3

A REVIEW OF DIGITAL IMAGE PROCESSING IN ECHOCARDIOGRAPHY

3.1 Introduction

This chapter presents a background to the image processing techniques used in this research. It provides a review on the four main sections of the research: noise reduction, image enhancement, edge detection, and, pattern recognition and classification techniques. The quality of echo scan images depends on the subject and the operator to a great extent. Also, the image could contain various imaging artifacts such as a large amount of noise, missing structures (those parallel to the ultrasound beam), false echoes, shadowing, restricted echo windows etc [BOSCH2002]. Consequently, extracting accurate information from such echo scans is time consuming and clinician dependent. Over the past few decades, a great deal of research is constantly carried out in the field of 2 dimensional (2D) echocardiography images to extract information which are of diagnostic importance. Specifically, the research area includes detection of the outline of heart wall or chamber, heart wall segmentation and motion tracking, quantitative analysis of the LV wall and compression of echo scans. Recently, the research in echocardiography has extended from 2D to 3 dimensional (3D) imaging. As 3D Echo is in its early stages of research and not used widely in hospitals for diagnosis, this research aims at solving the problems faced by cardiologists in working with 2D Echo.

This thesis investigates a method to enhance contrast in Echo images and also the automatic identification of the abnormal heart wall motion, to help the cardiologists in diagnosing the heart condition. The Echo image enhancement aims at improving the image quality for manual interpretation and for machine analysis (to get better segmentation of the heart wall). Also, the manual interpretation of heart wall movement in the Echo is laborious with a significant inter-observer and intra-observer variability, encouraging researchers to explore the field of automatic and semi-automatic detection of abnormal wall motion.

This chapter is structured as follows. Section 3.2 presents a background of the image processing techniques on Echocardiograph images presenting the various areas of research in the field. The details on the image data that is used in this research is provided in Section 3.3. The image enhancement research techniques for Echo images is discussed in section 3.4, detailing the speckle noise reduction techniques in the subsection 3.4.1 and the other image contrast enhancement techniques in the subsection 3.4.2. Various segmentation techniques used in echocardiography images to identify the endocardial and epicardial borders in the Echo images are discussed in section 3.5. A brief overview of research in the automatic and semi automatic wall motion abnormality detection is discussed in section 3.6. Section 3.7 presents the feature extraction techniques used in the research. Section 3.8 details the basics of Delaunay triangulation technique which is used in this thesis and its applications. Section 3.9 contains the concluding remarks.

3.2 Image processing of Echocardiography images

Echocardiography is the commonly used imaging modality to study and assess the left ventricular function. It is used in the emergency rooms and intensive care units [KACH2006]. So the research in echo images has various directions, considering the manual interpretation and the automated analysis. Researchers work in image enhancement and computer aided diagnosis, considering the manual interpretation. When considering automated or semi-automated diagnosis, the basic block diagram in the automated analysis is given in the Fig 3.1. The research in automated analysis is performed in various modules as given below.

3.2.1 Recognition of cardiac views in echocardiography

Echo scan can be recorded in various views such as short axis views, long axis views, 2 chamber view, 4 chamber view, etc. When an Echo scan is obtained, the medical experts identify the cardiac view and then interpret the images to assess the health of the heart. Active research is performed by [OTEY2006], [PARK2007], [BEY2008] to automatically recognize the cardiac view in the echocardiography sequences, as this would significantly reduce the work load for clinicians.

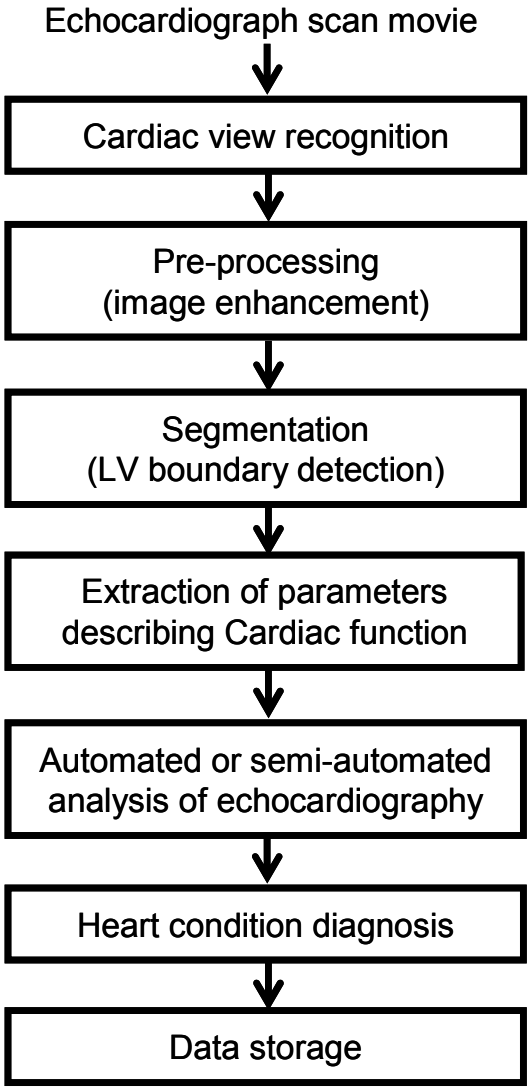

Fig 3.1 Image processing stages in automated analysis of Echocardiography

3.2.2 Image pre-processing stage (speckle noise reduction or image enhancement)

After identifying the Echo view, manual interpretation is performed. The manual interpretation or machine analysis is difficult in some cases with very poor quality of images due to high level of noise or poor contrast due to lots of tissue on the path of ultrasound. Being beneficial to both manual interpretation and automated analysis, research on enhancement of echo images is constantly encouraged. This will be discussed further in detail in Section 3.4.

3.2.3 Segmentation or border detection (detecting both the inner and outer heart wall edges) and motion tracking

The LV boundary detection is performed to differentiate the heart wall tissue from the LV blood cavity. Wall motion analysis is performed by machine by detecting the wall borders in consecutive frames. Research on the segmentation of heart wall is an important field as the identification of the heart wall manually has significant intra-observer and inter-observer variability. Image processing techniques may reduce variability due to human interventions in such border tracing operations, by providing automated or, at least, semi automated methods for tracing contours of relevant structures found in an image [NOBLE2006]. The section 3.5 provides details on different techniques that are used to identify the wall boundaries.

3.2.4 Cardiac parameter extraction for Automated/ Semi automated analysis

The heart function is mainly judged by the function of the LV, which is the largest chamber in the heart. Once the heart wall of the LV is identified, the cardiac parameters and wall movement are analyzed to determine if it is functioning normally or if there is an abnormality. The expert performs this by recognizing these features that correspond to the abnormality and categorizing the heart accordingly. Therefore, the extraction of parameters that describe cardiac function is another vital stage in the automated analysis of the Echo scans. Automated or semi-automated analysis of echocardiography has been performed to analyse LV function, to identify

abnormal wall motion in the heart wall. This is also applicable to identify the presence of ischemia or damaged tissue in the heart wall. Segmental wall analysis is also performed to score the heart wall automatically. The health of the LV can be measured by means of various features such as LV volume, ejection fraction, wall thickness and percent systolic wall thickening, radial movement in the wall, curvature function, timing based features, duration of systolic and diastolic phases, etc. Section 3.6 will present a background on the automated analysis of echocardiography in the context of identifying the wall motion abnormality. The section 3.6 also details different researchers have used different features to categorize the heart function.

3.2.5 Echocardiography Data Storage

Another important requirement is to store the images and results obtained from the echocardiography examination in a user friendly system, for future reference. [COL2004] developed a database for hospital to store the echocardiography examination, ECG evaluation and patient clinical history.

Though active research is performed in each of the general stages involved in the automated or semi-automated diagnosis, they can be adjusted to suit the need. Specifically the stages that are investigated in this research are the image enhancement, heart wall segmentation, automated analysis of LV wall motion and segmental wall analysis for identifying ischemia.

3.3 Image data

The Echo image data was obtained from Ninewells Hospital, Dundee and Glasgow Western Infirmary. Ethical approval was obtained for the Echo data from National Health Service. The image data used in this research is the standard short axis views (SA views), which shows a slice of the left ventricle covering the entire wall circumference. The views used in this research are the SA views, basal level and mid cavity level. One of the aims of this research is to enhance the ultrasound images. The image data obtained from the hospital for the image enhancement research was of poor quality as considered by the expert. The images were marked as poor quality

based on the poor contrast between tissue and blood region, or images with shadowing effect. In some regions of the LV wall segment. The images used for this purpose were acquired from Siemens and Philips Echo machines.

The other aim of this research is to automatically analyse SA view echo scans and provide an initial classification whether the heart is normal or abnormal. The heart image database consists of SA 27 normal hearts and 35 abnormal hearts, which are annotated by medical experts. The abnormal hearts used in the database had varied levels of wall damage. The types of wall motion abnormalities are: hypokinesis (reduced inward motion); akinesis (absence of systolic inward motion); dyskinesis (outward wall motion during systole) and aneurismal (a blood filled sac formed by localized dilatation of the weakened wall). The LV wall segments are assigned a score based on the type of abnormality present. The segments with normal contractions are assigned a score of 1; hypokinesis, 2; akinesis, 3; dyskinesis, 4; and aneurysmal, 5. The scoring of the abnormal segments in some cases was 2 (hypokinetic segments) and for others it was 3 (akinetic segments).

3.4 Image enhancement techniques for echocardiography images

In the process of ultrasound imaging, a random granular pattern is formed due to the constructive and destructive interference of backscattering. Speckle noise is a characteristic of coherent images such as ultrasound images. Speckle patterns depend on the frequency and geometry of an ultrasound transducer [ZYKK2007]. Though the texture of the observed speckle pattern does not correspond to the underlying anatomical structure of the heart, the mean speckle brightness at any region of the image corresponds to the tissue's capability to produce echoes. Hence, the presence of speckle is useful in some cases, such as speckle tracking to naturally tag the tissue.

From an engineering point of view, speckle is regarded as a main source of noise in ultrasonic images. Speckle noise is one of the causes for the low contrast in the images. In this application of finding the inner and outer wall boundaries of the heart in the echocardiography ultrasound images, the speckle noise prevents in getting a most favorable result. A pre-processing stage to perform speckle noise reduction

and/or contrast enhancement is required to get images which are more suitable for semi-automatic or automatic heart wall boundary detection. The techniques in the literature can be grouped as speckle noise reduction techniques and contrast enhancement techniques.

3.4.1 Speckle noise reduction techniques

Speckle noise can be reduced either before (that is, when the echo data is acquired) or after the image is formed. In [TAXT2004], the authors claim that super resolution can be obtained by using first and second harmonic signals. The separate deconvolution of first and second harmonic signals results in sharper images with distinctive speckle pattern than the original. Speckle is reduced by adding the envelopes of separately deconvolved first and second harmonic images, to remove ultrasound image distortion produced by a pulse. Speckle noise reduction can also be performed by different compounding techniques, where a series of ultrasound images of a tissue structure are captured using different transducer operating frequencies [ZHOU2008] or in different directions or strains [LI2000] and combined to form a composite image. The ultrasound imaging system hardware has to be modified to perform image compounding. Compounding techniques improves contrast resolution, but results in some loss of spatial resolution [WEBB1988].

The post acquisition image processing techniques is simpler in terms of system complexity. These image processing techniques can be categorized into single scale spatial filtering techniques and multi-scale techniques. The image processing techniques for speckle noise reduction are discussed in the following sections.

3.4.1.1 Spatial filtering techniques

Spatial filtering techniques include Frost filter [FRO1982, CHEN2007], Kaun filter [KAUN1987], Lee filter [LEE1986], Adaptive weighted median filter [LOUP1989], and Homomorphic Weiner filter [JAIN1989]. Speckle noise reduction is performed by 2D - weighted Savitzky-Golay filter, which is based on the least squares fitting of a polynomial function to image intensities. This filter is an extension of the 1D Savitzky-Golay filter. This filter reduces noise, preserves edges and is computationally efficient when compared to median filter. This filter is suitable for

filtering problems with large windows [CS2001]. [CHEN2007] modified the Frost filter for speckle reduction in Synthetic aperture radar images based on anisotropic diffusion for better edge preservation. [AKSEL2006] discusses the extensions to speckle reducing anisotropic diffusion (SRAD) applied to echocardiography images.

3.4.1.2 Multi-scale techniques

The multiscale approaches include discrete wavelet transform [LAINE1998] and undecimated wavelet transform [GS2005] with thresholding to reduce speckle noise. [HG1999] used multi scale nonlinear thresholding with adaptive non-linear filtering. Donoho's soft thresholding is used for speckle reduction. [TDB2009] used the Rayleigh distribution for modelling the speckle wavelet coefficients and Gaussian distribution for the signal wavelet coefficients. An adaptive shrinkage function was used to estimate the signal adaptively.

[YOO2008, YOO2009] applied adaptive speckle reducing anisotropic diffusion (SRAD) uses wavelet decomposition for speckle reduction and edge preservation in medical ultrasound images. The homogeneous region which operated as diffusion threshold in SRAD work is identified by modified coarse-to-fine classifier, followed by applying SRAD filters on each sub-bands with determined homogeneous regions.

3.4.2 Image contrast enhancement techniques

Image enhancement techniques for better resolution and contrast enhancement start with frequency-domain pre-processing of digitally acquired radio-frequency (RF) echo signals before image formation [LF2000]. Image enhancement is performed by various researchers to facilitate the processes of segmentation of regions in ultrasound images. An intravascular ultrasound image enhancement was proposed by [FIL2004], where a pre-processing based on morphological smoothing followed by a fuzzy enhancement based on the intensity and variance information of the input image.

The contrast enhancement technique proposed by [NOBLE2001-1] is based on a phase congruency. 2D Feature Asymmetry (FA) measure computed by equation 3.4 was used to detect features, followed by sparse surface interpolation to interpolate

sparse data at feature locations and subsequent nonlinear post-processing to enhance feature values. Phase congruency is highly sensitive to noise. The poor SNR of B-mode ultrasound, including heavy speckle, means that this is a problem that has particularly to be addressed when applying it to cardiac ultrasound [NOBLE2001-2].

A temporal compounding of the cardiac data was proposed by [PER2009], where an intensity averaging of temporally aligned frames from consecutive cardiac cycles is performed to enhance the appearance of anatomic structures.

3.4.2.1 Histogram based techniques

Contrast enhancement techniques based on histogram equalization (HE), in which the pixel values in the image are changed to make the gray level distribution as uniform as possible. The overall visibility of an image is enhanced, while the local contrast at some local positions in the image may be decreased. [PIZ1987] proposed local area histogram equalization (LHE), a variation of HE, which uses a sliding window to label an image region for each pixel. The histogram of a region is equalized to determine the new pixel value. As this procedure is computationally very intensive, [DALE1993] proposed a modified LHE, where varying window size was used over different regions of the image. Later [ZHANG2008] proposed an entropy-based LHE algorithm by using local entropy value of a sub-block to decide whether LHE is applied on the center pixel of this sub-block. A wavelet based histogram equalization enhancement was proposed by [FU2000] where a wavelet-based enhancement algorithm is used for post-processing to further enhance the image and compensate for the information loss during histogram equalization [FU2000].

[ZA2004] proposed a histogram based technique for image enhancement called Adaptive Brightness Transfer Function (ABTF) designed to optimally determine the gray levels used for each Echocardiograph cine loop. This method is based on fitting the cine-loop's gray-level histogram to a sum of three Gaussian functions, each of which relates to a different region within the image, the left ventricular cavity, the relatively dark regions within the cardiac muscle and the bright regions within the cardiac muscle.

3.4.2.2 Wavelet based techniques

Speckle Reduction and Contrast Enhancement using wavelet shrinkage and nonlinear adaptive gain was proposed by [LAINE1998] [LAINE1996] [LAINE1995]. A regularized soft thresholding (wavelet shrinkage or shrinking the transform coefficients) to remove noise energy within the finer scales was performed as soft thresholding results in smoothness. A nonlinear processing of feature energy was performed to enhance contrast. This was achieved by using a generalized adaptive gain (GAG) nonlinear operator through nonlinear stretching of wavelet coefficients [LAINE1998].

Contrast resolution enhancement technique proposed by [SAIM2000] was based on wavelet shrinkage to reduce speckle noise and gray level mapping to enhance ultrasound images in different contrast level, brightness and gamma control. On wavelet decomposition, [CHEN1997] integrated the tree-structured zero crossings of wavelet coefficients and low-pass-filtered subimage to enhance the desired image features. Recently, [TANG2009] proposed a contrast enhancement technique in the wavelet domain to enhance features present in different scales using a contrast measure. This technique was proposed for mammograms, which usually contains calcification in small scales and large objects with smooth borders in coarse scales [TANG2009].

3.4.2.3 Local information or Region based techniques

Contrast enhancement helps better edge/boundary detection by enhancing the structures in the ultrasound. A dynamic filtering based on speckle detection for ultrasound images was proposed by [XIA2007]. Regions in an image are identified as speckle regions or tissue structures based on a similarity value obtained from histogram matching between the histogram in the processing window and a reference speckle area. Low pass filtering is performed to smooth speckle pixels with big similarity values, and high pass filtering is performed to enhance the structure pixels with small values.

A region based image processing was performed by [TTI2000] for ultrasound image enhancement. In their research, an adaptive morphological operation is performed by using variable structuring element, which depend on the local region of the image. [LI2007] presented a segmentation method based on texture analysis of the spatial grey level co-occurrence matrix. The method identifies the regions whose edge needs to be enhanced and level out the error edges caused by speckle noise. A modified sigmoid function is used as the enhancement function. [KIM1997] proposed an adaptive image enhancement method for mammographic images, which is based on the first derivative and the local statistics. Once the film artifacts are removed, gradient images are computed by using the first derivative operators, followed by determining the adaptive gain for the gradient images based on local statistics. The enhancement is obtained by adding the adaptively weighted gradient images [KIM1997].

[GORD1984] [GORD1986] proposed a method where the gray-level of each pixel is modified to enhance the contrast between the pixel and its neighborhood. The boundary of the center area is adjusted to maximize the contrast between the pixel and its neighborhood. It is probably more suitable for static imagery (such as mammograms) than for dynamic imagery [FU2000]. [XIA2005] proposed an independent component analysis based method by considering image enhancement to be a "signal source separation and enhancement" problem. The basis images are classified into signal subspace and speckle subspace. Image sub blocks are separated into edge region to enhance image structure and noise region to suppress noise.

3.5 Segmentation techniques used in echocardiography images

Defining the LV boundary (or LV boundary detection) is an important step towards the automated analysis, as the features used depend greatly on the extracted wall boundary. The heart wall segmentation techniques include approaches which are radial search based, snakes based, shape based, local image phase based, and level set based. A critical evaluation of automated border detection system in determining the LV ejection fraction was presented in [SAPR1998], stating that the cavity clutter and endocardial drop outs results in incorrect endocardial contour estimate. In some

cases, LV volume is under estimated because of the presence of papillary muscles, and LV volume is over estimated when the borders are less distinct.

3.5.1 Radial search based approach

As the wall motion in echocardiography is along the radial line and the wall edge is perpendicular to the direction of the radial line, at any instant of the scan. This is the motivating factor for researchers [MON1988], [SS1999], [NAGY1999], [BAN2007], [LAC2008] to use the radial search based approach for LV border detection.

[SS1999] proposed fuzzy multiscale edge detection to detect edges along the radial line which is used in this thesis. [NAGY1999] proposed a method where the gradient of the pixels along the radial line is used for identifying the edge points, which are then modified using active contours or snakes. [YAO2004] determined four maximum gradient points on each radial line as candidates. A cost function based on mean neighborhood distance and mean gray level of boundary points, was used to identify the edge, which is smoothed to obtain the contour. [BAN2007] detected an approximate LV border along the radial line by a gradient search with magnitude as well as direction, followed by smoothing it locally and temporally. [LAC2008] proposed a radial search based algorithm which involves initial watershed segmentation, followed by merging the small regions to get initial contours. Then, the candidate points are searched along the radial lines originating from centre of the ventricle cavity. The final contour is obtained after interpolation followed by morphological closing.

3.5.2 Snakes based approach

The Snakes approach is a deformable model, which is also known as active contours model. A snake is an energy-minimizing spline guided by external constraint forces and influenced by image forces that pull it toward features such as lines and edges [KASS1988]. The energy function for snake position, V(s) = (x(s),y(s)) can be given by

$$E^*_{Snake} = \int_0^1 E_{Snake}(V(s))\, ds = \int_0^1 E_{\text{int}}(V(s)) + E_{image}(V(s)) + E_{con}(V(s))\, ds \tag{3.1}$$

where, E_{int} represents the internal spline energy due to bending, which is given by

$$E_{\text{int}} = \frac{(\alpha(s)|V_s(s)|^2 + \beta(s)|V_{ss}(s)|^2)}{2} \tag{3.2}$$

The first order term and the second order term of the spline energy is controlled by weights $\alpha(s)$ and $\beta(s)$ respectively.

E_{image} represents the image energy which is the weighted sum of three energy functionals which pull a snake towards line, edge and terminations,

$$E_{image} = W_{line}E_{line} + W_{edge}E_{edge} + W_{term}E_{term} \tag{3.3}$$

E_{con} represents the external constraints, which can be applied to smooth the edges and to limit the degree that it can be bent. The boundary detection is obtained as the curve evolves by minimizing the energy associated to the current contour.

[MALA1999] used a Hough transform technique to find the initial boundary and applied an active-contour model to estimate the LV boundary. [CHENG2006] located the LV region using the watershed transform and morphological operation, and performed snake deformation with a multiscale directional edge map for the detection of the endocardial boundary of the LV. In [FANG2008], they detected the heart wall boundary by incorporating temporal information into the active contour method. [MIK1998] proposed an active contour based technique that integrates the optical flow information to the estimate initial contour. [HOSS2003] proposed an adaptive snake initialisation method to identify the LV borders in the mouse heart ultrasound image.

3.5.3 Shape based approaches

Active Shape Models (ASM) [COOT1995] or Active Appearance models (AAM) [COOT1998] and Active Appearance Motion Models (AAMM) [BOSCH2006] are iterative shaped based image search models. [COOT1994] proposed a Point Distribution Model (PDM) to detect LV boundaries. A statistical model of the shape variability was created from a set of training images (see Fig 3.2), by performing Principal Component Analysis (PCA) on the positions of the aligned points. The

model derived from this analysis is called a Point Distribution Model. The search is initialised by placing the mean shape in the image and iteratively modified in line with the statistical model derived from training set, to better fit the data. The combination of a PDM and the iterative refinement procedure was called Active Shape Model. The difference between snakes and shape models is that the curve positions get modified in line with the statistical model derived from training data. AAM, an extension of ASM describes both image appearance and object shape over a training set to form a combined statistical shape–appearance model. [BOSCH2002] proposed an AAMM, an improvement to the AAM with temporal consistency over an image sequence. The whole image sequence was considered as a single shape or

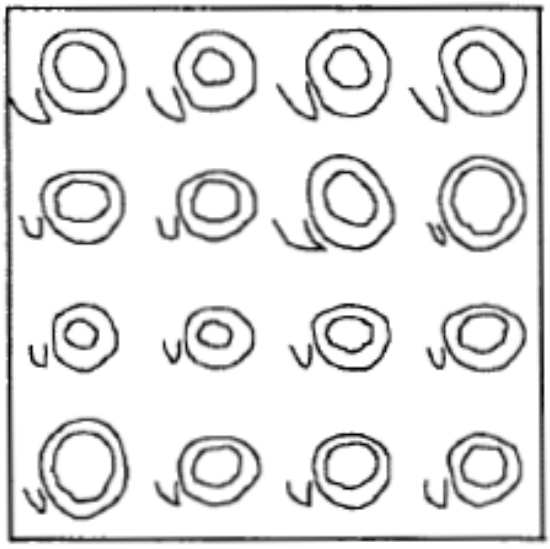

Fig 3.2 Training data set for Short axis echocardiogram model [COOT1994]

intensity sample to extend the AAM to a time sequence.

[COOT2006] observed the effect of using image texture representations to improve the accuracy of the AAM search. They concluded that normalising the gradient images by non-linear techniques can improve the search results. [PICK2006] used ASM to segment the contrast echocardiography and apply a specialized gradient vector flow field to move the contours to the myocardial borders. [NOBLE2002] proposed a spatio-temporal contour model, which has a shape-model to describe the deformation, and a motion-model to describe the temporal properties of the contour. [CZK2004]] proposed an information fusion approach for shape tracking, using sub-

space shape model information and spatially varying uncertainties. The uncertainties are estimated from the optical-flow during the shape model constraining process, that is flows from high confidence areas weighs more while flows estimated from uncertain areas weigh less. The initial contour is used to update a PCA model. This model is used to limit the border tracking of particular shape.

3.5.4 Local image phase based approach

[NOBLE1998] used a 2D Feature Asymmetry (FA) measure for detecting asymmetric features such as step edges. The 2D FA measure is given by a summation over m orientations of the normalised difference between the odd $o_m(x, y)$ and the even $e_m(x, y)$ filter responses,

$$FA_{2D}(x,y) = \sum_m \frac{\lfloor |o_m(x,y)| - |e_m(x,y)| - T_m \rfloor}{\sqrt{o_m(x,y)^2 + e_m(x,y)^2} + \varepsilon} \tag{3.4}$$

where $o_m(x, y)$ is the odd filter response

$e_m(x, y)$ is the even filter response

ε is a small positive number to avoid division by zero

$\lfloor \ \rfloor$ denotes zeroing of negative values, and

T_m is an orientation-dependent noise threshold, $T_m = k.\, std\{|o_m(x,y)| - |e_m(x,y)|\}$,

where k is a positive value to control the noise threshold.

[NOBLE2008-2] used a spatio-temporal boundary detection based on this phase-based method to identify the borders in echocardiography. [TIM2006] used this approach in contrast echocardiography.

3.5.5 Level set based approaches

A level set is a curve propagation technique which was initially proposed by Osher and Sethian [OSHER1988] to track moving interfaces. It represents a growing contour using a signed function, where its zero level corresponds to the actual

contour. [LIN2003] proposed a segmentation of echo images using multi-scale level set framework. The region homogeneity and edge-based level set method extracted boundary from the coarse scale was used as boundary initials at finer scales and also as an external shape constraint to evolution of active contours. [DYDEN2006] proposed use of image statistics, shape and motion a prior constrains for the evolution of the level sets. An improvement to the fast marching level set approach was proposed by [YAN2003], incorporating the contour energy of the active contour model into the speed term of fast marching model. The level set assumes a boundary to be a closed curve, which could be a limitation when applying to echo images with incomplete boundaries.

3.5.6 Other approaches

Other approaches include methods based on mathematical morphology [CHOY1998], watershed transform [AMOR2009], Laplacian of Gaussian (LoG) operator [LAMB1990], Spiral architecture [HE2006] and Markov random field (MRF) methods [XIAO2002].

[CHOY1998] also performed morphological filtering followed by identifying zero crossing points in Log filtered image, along with watershed segmentation. [RRV2008] proposed a method combining mathematical morphology, high-boost filtering and LoG operator and thresholding for image segmentation. [AMOR2009] applied image fusion to echo sequence of three cardiac cycles and performed watershed transform for segmentation. The authors claim that the similarity of corresponding frames from different cycles produces contrast enhancement in the left ventricular boundary. Only normal cardiac cycles were presented in that work. The problem in this method would be the registration of the frames as there might be motion artefacts.

[LAMB1990] applied low pass filtering, followed by Laplacian of Gaussian (LoG) operator. Then edge strength is detected by means of anisotropic diffusion technique, a binary image is created by thresholding and to create a binary image and LoG operator is applied to obtain a Laplacian image. The zero crossing points in this Laplacian image were considered to be the contours.

[XIAO2002] proposed a region segmentation method that combines the maximum a posteriori and Markov random field (MRF) methods. [HE2006] proposed a contour extraction method based on Spiral architecture, where an image is represented as a collection of hexagonal pixels. A pixel is decided as a contour pixel if there is at least two adjacent pixels and at least one non-object pixel next to it.

Most of the boundary segmentation techniques are applied on good quality data as the segmentation result depends on the quality of the data [NOBLE2010], leading to continued research in this field.

3.6 Cardiac parameters extracted for automated or semi-automated analysis of echocardiography

The automated analysis of echocardiography for the diagnosis of heart conditions is an important area of research as the echo images are difficult to interpret. Inter-observer and intra-observer variability in diagnosis using echo scans is as high as 20% [QAZI2005]. Research in computer aided analysis of biomedical images is performed constantly to make the lives of the physicians easier. In particular, the research in echocardiography for automated analysis is given in this section. An overview of the research in automated/semi-automated analysis of Echocardiography for heart function and wall motion abnormality is given in Table 3.1 and segmental wall motion abnormality is given in Table 3.2.

Assessment of heart function using Echocardiographic sequences is based on quantifying global function or regional contractility. The assessment of global LV function is based on ejection fraction, contractility, relaxation, filling and end – diastolic pressure [TP2006]. Researchers have used different features for determining the health of the heart and identifying abnormalities. [CHIA2008] proposed a system for general management of heart failure based on processing the Electrocardiogram (ECG) signals and Echo scans. The Left ventricle ejection fraction (LVEF) is extracted from the Echo, which is used for decision making. LVEF is defined by

$$LVEF = \frac{EDV - ESV}{EDV} \tag{3.5}$$

where EDV is the End-Diastolic Volume and ESV is the End-Systolic volume. The Volume of the LV can be estimated by the following equation [FFA1991]

$$Volume = \left(\frac{7.0}{2.4 + D} \right) D^3 \tag{3.6}$$

where D is the average endocardial diameter from the SA view. [SET1998] measured LV volume changes and LVEF which is used for reporting on the LV health.

LV mass or the LV muscle is based on subtraction of the LV cavity volume from the volume within LV epicardium, as seen in Fig. 3.3 [LANG2005]. This depends on the myocardial area (A_m) which is given by

$$A_m = A_1 - A_2 \tag{3.7}$$

where A_1 is the area within the epicardium and A_2 is the area within the endocardium, which is measured by $A = \pi r^2$.

[SING2002] presented an approach using Echos before and after stress. This approach exploits the fact that the change in LV wall dimensions from rest to stress is uniform if normal. Echo image pre-processing was performed by morphological operators, followed by boundary detection based on active contours and subsequently analysing segments of LV wall. A measure called the Abnormality of Motion (*AoM*) is used by the authors to make a decision on the pathology of a segment n. *AoM* is computed by

$$AoM_n = \frac{VC_n - AV}{AV} \tag{3.8}$$

where VC_n is the variation in contractility given by, $VC_n = |C_{bs} - C_{as}|$, C_{bs} and C_{as} is the contractility before and after stress. AV is the average variation given by,

$$AV = \frac{\sum_n VC_n}{n} \tag{3.9}$$

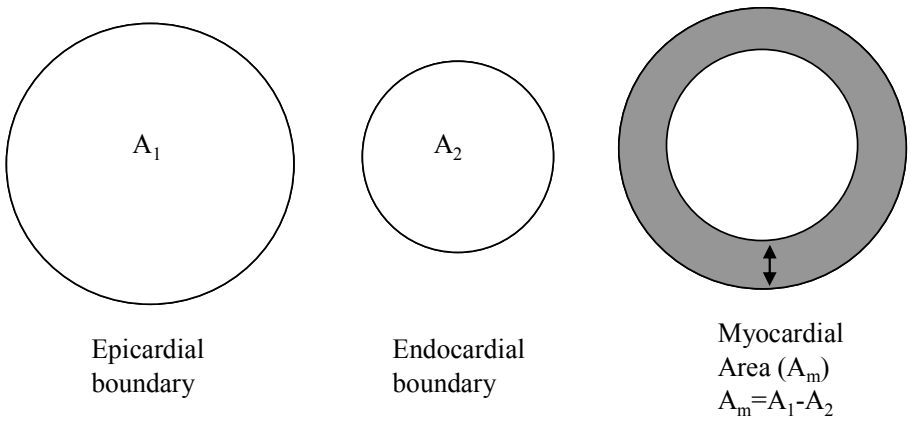

Fig 3.3 Computing myocardial area by calculatingtaking the difference between the area enclosed by the epicardial boundary and the area enclosed by the endocardial boundary

The myocardial area between the epicardial boundary and endocardial boundary in the end-systole image, A_{esn}, and myocardial area between the epicardial boundary and endocardial boundary in the end-diastole image, A_{edn}, is used to compute the contractility of a segment, $C = |A_{esn} - A_{edn}|$.

[QAZI2005] used an automated technique to identify abnormality in hearts. Automatically detected endocardium and epicardium of the LV is used to extract global and local features. A Sparse Linear Fisher Discriminant algorithm with feature selection is used for classification. The local features used for classification were features based on motion, ejection fraction, and area of the heart cavity. In [QAZI2007], a Bayesian network was used to classify the heart based on the local and global features. In [MANS2009], a cardiac motion evaluation using ICA basis neural network is proposed for disease diagnosis. The cardiac motion is estimated by active contours, followed by feature extraction from motion patterns. The features extracted include the energy, standard deviation, mean, zero crossing etc. A neural network was used to classify normal and abnormal myocardial function.

Publication	Enhancement method	Edge detection method	Cardiac parameters extracted	Feature selection techniques and classification
Heart function analysis				
Traditional [LANG2005]	None	Manual edges	LVEF, LV mass	Manual measurements (‘‘eye-ball’’ method)
[CHIA2008]	None	Level sets	LVEF	Manual
Wall motion analysis				
[QAZI2005]	None	Shape Subspace model based approach	LVEF, wall motion , cavity area	Sparse Linear Fisher discriminants
[QAZI2007]	None	Shape Subspace model based approach	Volume, velocity and strain feature	Bayesian networks
[MANS2009]	None	Snakes	Statistical parameters from the motion patterns such as mean, energy, standard deviation etc	Independent Component Analysis with neural networks
[SING2002]	Morphological opening and closing	Snakes	Variance in contractility before and after stress	None

Table 3.1 Overview of automated / semi-automated analysis of Echocardiography for heart function and wall motion abnormality

Publication	**Enhancement method**	**Edge detection method**	**Cardiac parameters extracted**	**Feature selection techniques and classification**
Segmental wall analysis				
Traditional [LANG2005]	None	Manual edges	Systolic wall thickening and wall motion	Manual measurements (‘‘eye-ball’’ method)
[KACH2006]	None	None	parametric analysis of time signal-intensity curves associated to each pixel	None
[NAGY2000]	Morphological opening and closing	Snakes	Contractility measure	Manual
[NOBLE2002]	None	Shape-Space model based approach	Endocardial wall excursion and fractional wall thickening	Logical classification
[OGA2006]	None	Manual contours with image template matching	wall thickness and percent systolic wall thickening	Logical / linear classification
[NOBLE2008]	None	phase-based semi-auto boundary detection	Segmental cavity area	Hidden Markov Model

Table 3.2 Overview of automated / semi-automated analysis of Echocardiography for segmental wall motion abnormality

[KACH2006] proposed an automatic regional wall motion scoring method based on parametric analysis of main motion (which is applied on time signal-intensity curves associated to each pixel [DOMIN2003], and computes wall motion amplitude and transition times index between the high and the low grey scale levels) with new constraints based on time of the mitral valve opening. [NAGY1999] performed pre-processing by morphological operators such as opening and closing, followed by contour detection using active contours and compute a contractility measure by combining the differences between the maximum and minimum amplitudes, the average and the dispersion [NAGY2000]. In [NOBLE2002], a dynamic snakes approach is used for tracking the endocardium and used an assimilated wavelet – based feature (AWF) detection for the endocardium. AWF performs a wavelet decomposition of the intensity profiles; an entropy approximation is used as a cost function to each basis within the decomposition and is reconstructed. For each of the wall segments, endocardial wall excursion and regional wall thickening is computed. Endocardial wall excursion is given by

$$\text{Endocardial Wall excursion} = \frac{(\text{Max Endocardial excursion - Min Endocardial excursion})}{\text{largest excursion of all six segments}} \tag{3.10}$$

The Myocardial wall thickening is defined by fractional thickening, Th%,

$$Th\% = \frac{Th_{ES} - Th_{ED}}{Th_{ED}} \times 100 \tag{3.11}$$

where Th_{ES} is the wall thickness at end systole and Th_{ED} is the wall thickness at end diastole. *Th%* is positive for normal myocardium [NOBLE2002].

In [OGA2006], the endocardial and epicardial boundaries are extracted semi-automatically and few tracking points are selected to be tracked by applying template matching to consecutive frames. The authors used ventricular wall thickness and percent systolic wall thickening as the features for determining the health of the wall segment. The percentage systolic wall thickening is calculated by the previous equation.

In [NOBLE2008], the LV cavity area within the endocardial boundary for each segment was considered for classifying the heart as normal or abnormal. The cavity area (CA) is normalized

$$CA(i) = \frac{CA_{ED} - CA(i)}{CA_{ED}} \tag{3.12}$$

where CA_{ED} = Cavity Area at End of Diastolic.

The parameters extracted from the echocardiography can be used for identifying the abnormality of the heart. These parameters can be classified along with feature selection techniques.

3.7 Feature Extraction Techniques

The features extracted are normalised as the classifiers perform better when the features lie in a relatively small range. The dimensionality is reduced to identify few features that are characteristic and informative for the classification process. The complexity, time and memory to run the classification algorithm are also reduced. The review of the two feature extraction techniques used in this research, Principal Component Analysis (PCA) and Independent component analysis are discussed in this section.

3.7.1 Principal component Analysis (PCA)

Principal Component Analysis (PCA) is a statistical technique that is widely used for pattern identification in datasets with its applications in fields such as face recognition (Eigen faces) [TP11991, TP21991] and image compression [SMITH2002]. Recently, the PCA techniques have been used widely in Electrocardiogram (ECG) analysis [ZHANS2005] and phonocardiogram [GUPTA2005] to extract the principal characteristics of the signal. It is used in ASM [COOT1994,COOT1998], AAMM [BOSCH2006] or in a combination of ACM and ASM [HAMA2000] to detect the contours of the structures in medical images, to learn the heart motion dynamics [MALA1999], and for lungs outline reconstruction [SIEP2003].

PCA identifies patterns in data and express the data in such a way as to highlight the similarities and differences in the data. PCA has an advantage of reducing the dimension of data with insignificant loss of information.

3.7.2 Independent Component Analysis (ICA)

Independent component analysis (ICA), an extension of PCA statistical technique, was originally developed for separating mixed signals in cocktail party problems or blind source separation [HO2000]. It has been used for feature extraction in face recognition [BART2002] and image analysis. In ICA, the observed data is expressed as a linear combination of components that are statistically mutually independent. Recently, ICA has been applied to the processing of different biomedical signals, such as ECG signals [CHOU2008], Electroencephalography (EEG) and Magnetoencephalography (MEG) recordings analysis [POTTER2001]. ICA is used for image segmentation [KL2004], statistical shape analysis [LOT2004], extraction of local myocardial contraction patterns from multislice short-axis MRI [SUIN2009] and echocardiography [MANS2009].

Some of the common ICA algorithms used to estimate the independent source signals are Fast ICA method [HKO2001] (by maximizing non-Gaussianity), the infomax principle [BS1995] (maximizing entropy) and JADE algorithm [CARD1999] (by using fourth-order cumulant matrix).

3.8 Delaunay triangulation

Delaunay triangulation technique is used in this research to select triangular regions for region based enhancement. Delaunay triangulation, introduced by Boris Delaunay in 1934, is a triangular meshing technique which is used to divide the region of interest into smaller regions using the edges obtained in the previous step. This triangulation technique divides a surface into regions with common characteristics that are particularly well-suited for image processing applications [9]. Delaunay has been used to represent shapes in images [TG1999], for image segmentation [LS2006], and used to form a high resolution image from low resolution frames [LB2002]. [LS2006] proposed a segmentation method where the image is divided

into triangular regions called trixels. Neighbouring trixels are fused together (based on simple heuristic criteria) to form polygons that segment the image.

Delaunay triangulation was used in document image processing for text region extraction [XY2003] and location of the title and author regions [XY2004]. This was performed by locating the connected components in a document image with their centroids, followed by performing Delaunay triangulation. The triangles are then classified based on connectivity, side size and the orientation. Rules are given to identify the text, tile or author regions based on the distinguishing triangular features. The handwritten character recognition by extracting the Delaunay triangle descriptor features was proposed by [ZHENG2006].

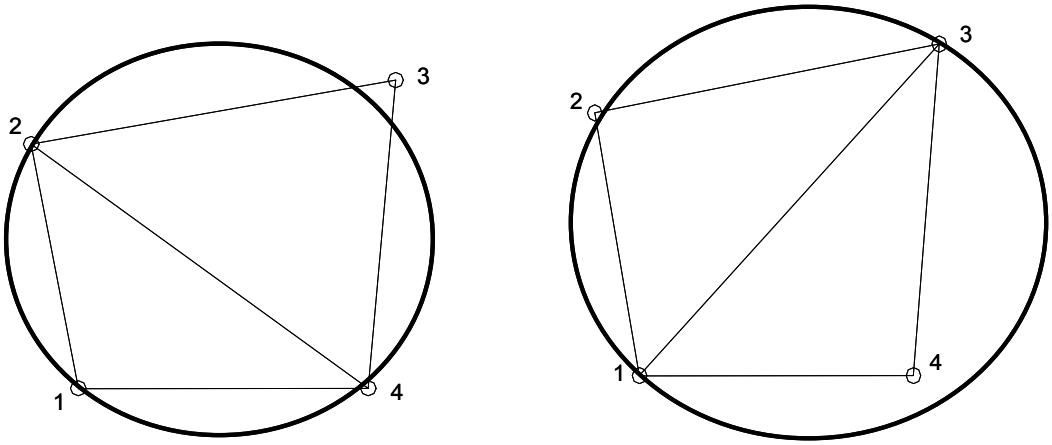

(a) Delaunay triangle (b) Not Delaunay triangle

Fig. 3.4 Shows triangulation of the 4 points satisfying Delaunayin (a) and a triangulation which does not satisfy the Delaunay condition in (b)

In Medical image processing, Delaunay triangulation is used by [SK2006] to develop a vector-based segmentation algorithm. The image is divided into non-overlapping regions with similar characteristics. The improvement in the segmentation is obtained by adapting the triangulation to the image structure by performing edge splitting, triangles splitting and edge suppression. Later, they proposed a 3D Delaunay triangulation based vector segmentation [SK2007]. DT is also used for 3D surface reconstruction of thrombosis using the 2D segmented contours [DHUB2005], generating a volumetric mesh to reconstruct tubular anatomical structures [NAZA1994], left ventricle [ZHUANG2005] and different parts of the body for

finite element analysis [LIAO2005]. A DT based image compression technique for Mammographic images was proposed by [SIL2005].

For a set of V vertices (or points or edges) in a 2 D plane, a triangulation of these vertices produce a set of T triangles , whose interiors do not intersect each other, and whose union is the convex hull of V, if every triangle intersects only at the triangle's vertices [SHEW1999]. Delaunay triangulation is performed in such a way that there is no point in the circumcircle of the triangles (that is, no point is within the circle passing through three vertices of triangle) in the network (as shown in the Fig. 3.4 (a)). Delaunay triangulation is advantageous over other meshing based techniques as it maximizes the minimum vertex angles of the triangles in the network, so that the triangles formed tend towards equiangular triangles, avoiding sharp and stretched triangles.

3.9 Conclusion

This chapter discussed the various image processing techniques used in the field of echocardiography to solve this problem of image enhancement, segmentation and to developing a semi or fully automatic algorithm for wall motion abnormality identification.

When considering the Echo image enhancement, both speckle noise reduction and blood tissue contrast enhancement are essential in processing the echocardiography images. Hence, this research proposes a region based algorithm for blood-tissue contrast enhancement algorithm which incorporates speckle noise reduction and contrast enhancement.

The review of the existing segmentation technique showed that the radial search based approach has advantages such as reducing the boundary detection problem from 2 dimensions to 1 dimension, reducing the computation complexity and processing time. Among the radial search based approaches, Fuzzy logic based multi resolution edge detection technique FMED is chosen and modified to be used in this research.

As the LV wall motion provides significant information on the heart function, the identification of the heart abnormality based on motion information is considered in this project. The global cardiac parameters such as LVEF, cavity area are also used in the decision making of the heart function. A segmental wall analysis is also performed to identify the abnormal segments based on their parameters such as maximum wall excursion, cavity area and fractional myocardial wall thickening.

CHAPTER 4

ECHOCARDIOGRAPHY IMAGE ENHANCEMENT TECHNIQUES

4.1 Introduction

One of the objectives of the research is to improve the contrast between the LV wall region and the blood cavity region in the echo images. Echo in general produces images with low quality. The quality of the echo images is both patient dependent (obesity and presence of air between heart and chest wall produces low quality images) and operator dependent (narrow rib spaces resulting in small acoustic windows affects the ability to obtain good quality images). Despite developments in the ultrasonic imaging techniques, the captured images may still contain various imaging artefacts, such as, large amount of noise, missing structures (those parallel to the ultrasound beam), false echoes, shadowing, and restricted echo windows [KAD2001].

Also, in the process of ultrasound imaging, a random granular pattern is formed due to the constructive and destructive interference of backscattering. This speckle noise is a characteristic of coherent images such as ultrasound images, and depends on the frequency and geometry of the ultrasound transducer [ZYKK2007] used in data acquisition. However, the manual interpretation of the ultrasound image by an expert becomes difficult and time consuming due to the presence of image artefacts including the presence of speckle noise as it reduces the image contrast and blurs the image details. As the segmentation of the heart wall in the echo image is strongly

influenced by the quality of the image and the presence of speckle noise, there is significant inter-observer and intra-observer variability in the diagnosis of heart conditions. This results in the need for research in the field of echocardiography image enhancement techniques.

This chapter presents a novel image enhancement algorithm to reduce the noise and enhance the contrast between the tissue and the blood region in the SA view echo images. An overview of the image enhancement approach is presented in the section 4.2. The overall block diagram of the algorithm is also provided here. Section 4.3 discusses the speckle noise reduction technique used as a pre-processing stage and its benefits. Section 4.4 describes the two stages involved in the edge detection technique to identify the heart wall boundary. It also introduces the local information on the features of the centre point in the left ventricle based on the gray levels and position. The presence of small features that are crucial to locate the wall edges are also mentioned in this section. It tries to imitate the human expert ability to locate the centre point and the heart wall boundary. The local and global knowledge on the tissue and blood regions in the echo images is introduced in the section 4.5. The region based processing for the tissue and the blood region for contrast enhancement is explained in this section. Finally, the results obtained by applying this technique to both synthetic and real echo images of average quality that were obtained from a local hospital is presented in the section 4.6. The performance of the image enhancement approach is also analysed in this section.

4.2 Echo Enhancement Algorithm

A high level overview of the proposed enhancement algorithm is presented in Fig. 4.1. The main steps include wavelet based speckle noise reduction, edge detection, followed by a regional enhancement process that employs Delaunay triangulation based thresholding. From an engineering point of view, speckle is regarded as a main source of noise in ultrasonic images. In this application of finding the inner and outer wall boundaries of the heart in the echocardiography ultrasound images, the speckle noise prevents favourable results from being obtained. The speckle noise reduction acts as a pre-processing stage to get a cleaner ultrasound image, which is

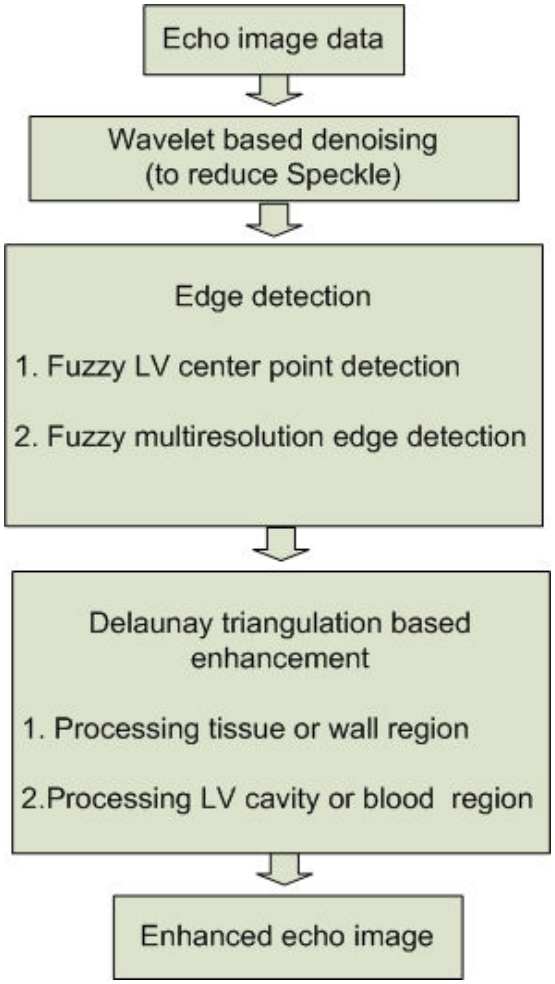

Fig. 4.1 Enhancement Algorithm Overview

more suitable for heart wall boundary detection. Undecimated wavelets based approach is used here to reduce speckle noise in the ultrasound images.

In this work, prior knowledge of the images is taken into account for enhancing the echo images. In case of the SA view echo images, the left ventricle cavity or the blood region is surrounded by the heart wall or the tissue region. The wall region is a bright region with higher pixel values and the blood region is a dark region with lower pixel values. To distinguish the tissue region from the blood region in the echo image, the wall boundaries have to be detected. The automated LV boundary extraction is the next stage, which is performed in two stages the LV centre point

detection to locate the centre in the cavity area, followed by a radial search based LV boundary detection to identify the inner and outer wall of the LV.

After detecting the endocardial and epicardial edges, a triangular meshing technique called Delaunay triangulation [SHEW1999] is used to divide the tissue region and blood region into smaller regions using these edges. This triangulation technique divides a surface into regions with common characteristics that are particularly well-suited for image processing applications. The tissue region and the blood region are processed separately to obtain the enhancement result. The basics of the Delaunay triangulation is given in the section 4.5 along with the thresholding applied for the enhancement of the contrast between the tissue and the blood regions.

4.3 Speckle noise reduction

Speckle noise caused by backscattering, is a random, interference pattern present in coherent images such as the ultrasound images. As the observed speckle pattern affects the edge detection in the radial search, reducing the speckle noise would act as a preprocessing stage. Undecimated wavelets are known to smooth signal independent noise [GS2005, AT2003]. Undecimated wavelets based approach is applied in Synthetic Aperture Radar (SAR) images to reduce speckle noise by preserving edges and textural information [GS2005]. Consequently, this approach could be applied to reduce speckle noise present in echo images. The flow diagram for speckle noise reduction is given in Fig. 4.2. In this algorithm, undecimated wavelet decomposition of the image into approximation and details is performed. The low pass filtering in the horizontal direction and the vertical direction results in the approximation (also known as the coarse sub-band as it is comparable (most like) to the original image). The vertical, horizontal and diagonal details of the image are obtained for each level of decomposition. The low pass filtering of the image in the vertical direction and high pass filtering of the same in the horizontal direction results in vertical details. The horizontal details are obtained as a result of low pass filtering in the horizontal direction and high pass filtering in the vertical direction.

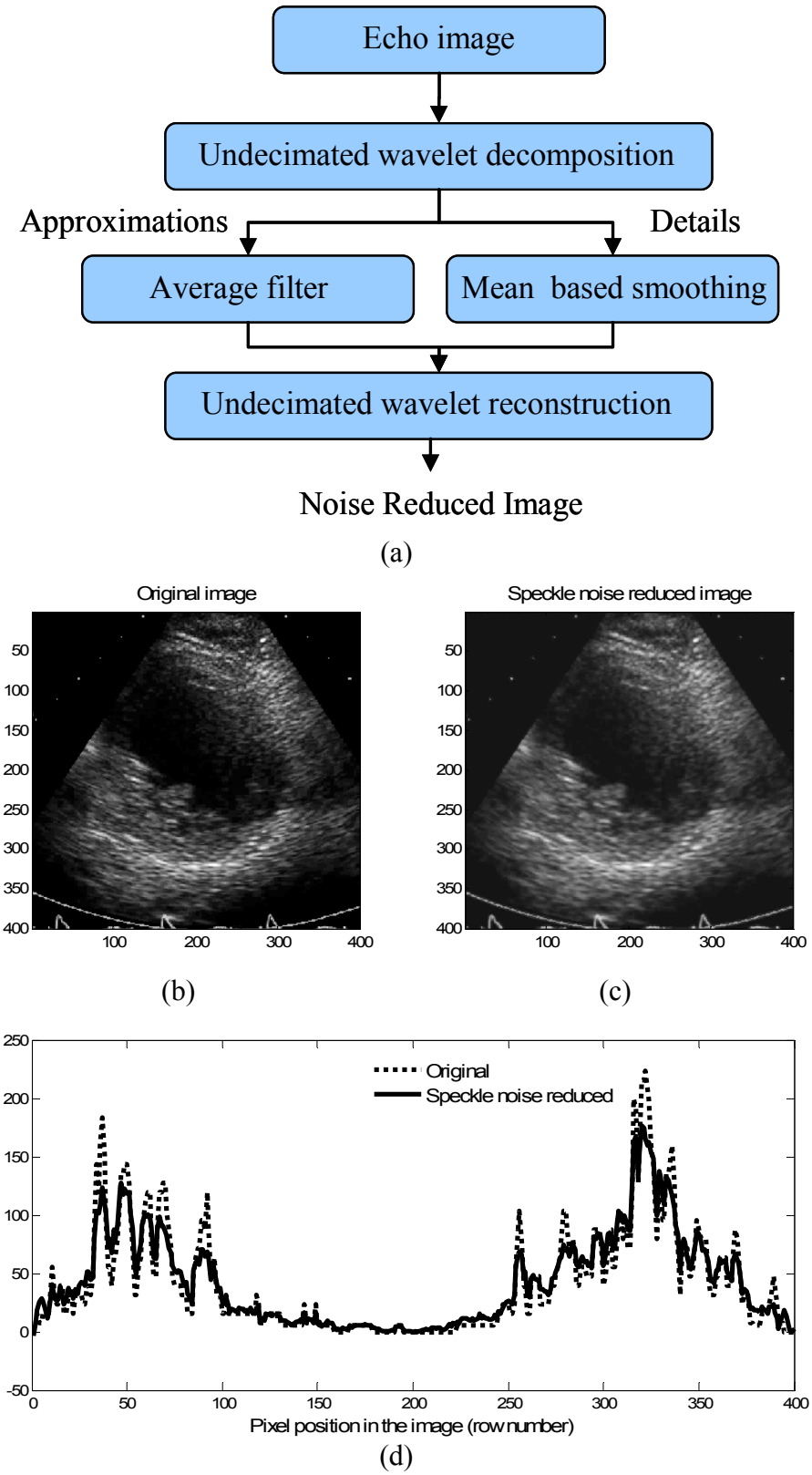

Fig. 4.2 (a) Flow diagram for speckle noise reduction, (b) sample Echo image and (c) speckle noise reduced image and (d) vertical line profile (column 200) before and after speckle noise reduction

The high pass filtering in the horizontal and vertical direction results in the diagonal details. The approximation sub-band is used to obtain the next level of decomposition, resulting in approximations and details. Here, the image is decomposed up to 4 levels. An average filter of size [3X3], is applied to the approximation and a mean based smoothing is applied to all the details, which is defined mathematically for an image I(x, y) as

$$I(x,y) = \begin{cases} I(x,y) & if\ |I(x,y)| \le N \\ N & if\ |I(x,y)| > N \end{cases} \tag{4.1}$$

where N is the trimmed mean value of row of the pixel $I(x, y)$ and x, y are the pixel coordinates. Trimmed mean is used as it is a robust estimate of the center of the body of the data than the mean, if there are outliers in the data. In MATLAB, the trimmed mean of a data X with n values, is the mean calculated by excluding the highest and lowest k data values, where k=n*(p/100)/2 and where p is the percentage to be trimmed. Here 25 % of the outliers are trimmed from the data. However, if the data is all from the same probability distribution, then the trimmed mean is less efficient than the sample mean as an estimator of the location of the data.

The above representation can be explained as follows. Firstly the trimmed mean value (N) of each row is computed. If the absolute value of a coefficient in the row exceeds the trimmed mean value, then it is replaced by the trimmed mean. This operation is used to smooth the sudden changes of coefficient values. The same operation is applied to all rows of the detail sub-bands. Then the image is reconstructed using all the modified sub bands to get the noise reduced image. Fig. 4.2(b) shows the original echo image and Fig. 4.2(c) shows the processed image after speckle noise reduction. The intensity profile of a vertical line (column 200) in the image before and after speckle noise reduction is shown in Fig. 4.2(d). It can be noted that the line profile after processing preserves the peak positions and the overall structure, but smoothes out small noisy structures. The speckle noise reduction stage is advantageous to identify the heart wall edge detection.

4.4 Edge detection

The edge detection performed to identify the heart wall edges in an Echo image is a centre-based approach, where the edges are searched along the radial lines starting from the LV centre. The inner (endocardial) and outer (epicardial) boundary detection is carried out by a fuzzy logic based multi-scale algorithm. This fuzzy multiscale edge detection technique comprises of two main stages, the automatic LV centre point detection for all the echo frames and LV boundary detection on radial lines. The details of the existing algorithm and the modifications performed are described in the following subsections.

4.4.1 Left Ventricle Centre Point (LVCP) detection

The automatic LVCP detection is an essential step as the centre point is critical in all radial search based approaches to detect heart wall boundary. This section describes the existing fuzzy LVCP developed by [SS1998]. LVCP detection is performed by using the prior knowledge of the SA view echo images to set fuzzy rules. They are represented by fuzzy membership functions, which are combined by using fuzzy logic operators to identify candidate LVCP pixels. In other words, fuzzy membership functions are used to represent the structural, intensity and spatial information as discussed below.

4.4.1.1 Structural information

In an SA view echo image, two significantly bright regions representing the myocardium – pericardium interface in the posterior wall region and the epicardial boundary in the anterior wall are present. The vertical centre line (close to the LVCP) is recognized by the lowest point in the posterior wall. The posterior wall step edge is obtained along the vertical columns of the image using the fuzzy multiscale edge detection, and a fuzzy subset for the *Fuzzy Vertical Line (FVL)* is formed with 7 pixels width for a decimated image of (25 x 25). The membership functions for FVL is given by [SET1998]

$$FVL = \{(i,j), \mu_{VL}(i,j)\} \quad i,j = 1 \ldots 25$$

where,

$$\mu_{VL}(i,j) = f_{VL}(i) = \begin{cases} 1 - \dfrac{|i - x_c|}{4} & , \quad |i - x_c| \le 3 \\ 0 & , \quad 3 < |i - x_c| \end{cases} \tag{4.2}$$

$$j = 1 \ldots 25$$

The highest membership value of unity is given to the vertical centre point, progressively decreasing the membership values as distance increases from the centre. The lowest membership value of 0 is given to the pixels other than the 7 pixel width for the FVL.

The high contrast region in the anterior wall is very close to the vertical centre line. So, an average of its neighbouring columns (3 columns on either side) in the reduced resolution image of (50 x 50) is performed and the fuzzy multiscale edge detection technique is used to identify the anterior wall edge. The horizontal centre line along y_c is determined by taking the mid way between the anterior wall edge y_1 and the posterior wall edge y_2 along the vertical centre line $y_c=(y_1+y_2)/2$ as seen in Fig. 4.3. Then, a fuzzy subset for the *Fuzzy Horizontal Line (FHL)* is formed with 9 pixels width for a decimated image of (25 x 25). The membership functions for FHL is given by [SET1998]

$$FHL = \{(i,j), \mu_{HL}(i,j)\} \quad i,j = 1 \ldots 25$$

where,

$$\mu_{HL}(i,j) = f_{HL}(j) = \begin{cases} 1 & , \quad |j - y_c| \le 1 \\ 1.25 - \dfrac{|j - y_c|}{4} & , \quad 1 < |j - y_c| \le 4 \\ 0 & , \quad 4 \le |j - y_c| \end{cases} \tag{4.3}$$

$$i = 1 \ldots 25$$

The highest membership value of unity is given to the horizontal centre point and its immediate neighbours, progressively decreasing the membership values (for the 9 pixel width) on either side as distance increases from the centre. The membership value of 0 is given to the other pixel locations. To reduce the computation time significantly and obtain a satisfactory result, the posterior and anterior wall in the

image to estimate the horizontal and the vertical centre line in the image reduced to a resolution of (50 x 50).

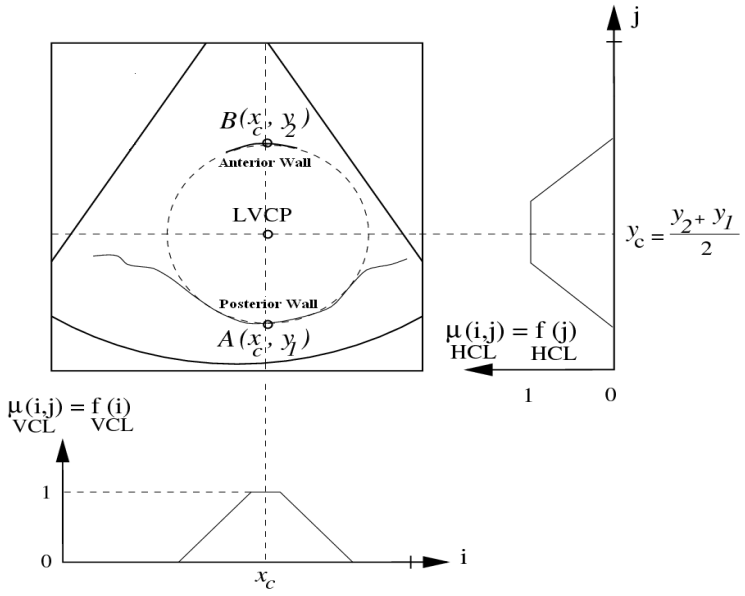

Fig. 4.3 Schematic diagram of a SA view showing the LVCP position and its relation to the VCL and HCL (indirectly to posterior wall and anterior wall)

4.4.1.2 Intensity information

LVCP is a dark pixel in the LV cavity or the blood region. The scale of darkness of the image pixels are represented by a fuzzy subset *Fuzzy Darkness (FD)*. The membership functions for FD is given by

$$FD = \{(i,j), \mu_D(i,j)\}, \quad i,j = 1 \ldots 25$$

where, (4.4)

$$\mu_D(i,j) = f_D(I_{ij}) = \begin{cases} 1 & , \quad I_{ij} \le 10 \\ 1 - \dfrac{I_{ij} - 10}{20} & , \quad 10 < I_{ij} \le 30 \\ 0 & , \quad I_{ij} \ge 30 \end{cases}$$

A statistical study on good echo images stated that the pixels in the LV cavity is below 30 (on a scale of 0 to127) [SS1997].

4.4.1.3 Spatial information

LVCP is located in the centre part of the image plane. In the reduced resolution image of size (25x25), the potential region for LVCP is defined by a circular region (radius = 11) in the image plane. The scale of closeness of the image pixels to the centre of the image place is represented by a fuzzy subset *Fuzzy Centre Proximity (FCP).*

$$FCP = \{(i, j), \mu_{CP}(i, j)\}, \quad i, j = 1 \ldots 25 \tag{4.5}$$

Highest membership value of unity is given to a circular region (radius = 5) covering the potential region with the origin (xc= 13; yc= 13). Progressively decreasing membership values are used as the pixel distance increases from the centre. Fig. 4.7(b) shows the fuzzy membership function for centre part of the image (FCP). The original image size of (400 x 400) is reduced to (25 x 25) for determining the fuzzy dark image pixel and fuzzy centre proximity.

4.4.1.4 Candidate Centre point selection

The pixel that has higher membership value in all fuzzy subsets will have the properties defined for the LVCP. The intersection of the four input membership functions is performed by the fuzzy *min* operator, to select the minimum of the membership values for each element. It is given by

$$FI = FVL \cap FHL \cap FD \cap FCP$$
$$\mu_{FI}(i, j) = \min\left(\mu_{FVL}(i, j), \mu_{FHL}(i, j), \mu_{FD}(i, j), \mu_{FCP}(i, j)\right), \quad i, j = 1 \ldots 25 \tag{4.6}$$

Possible candidates for LVCP can be obtained by performing fuzzy α -cut operator, which is a soft – thresholding method to choose the elements with values greater than the threshold 'α' (approximately). To preserve the relative importance of the pixels, the pixels corresponding to LVCP have membership values between 50% and 90% of the maximum value. The old membership values are translated into new membership values by using a continuous non-decreasing mapping function fα. The membership values of the fuzzy α -cut of the fuzzy set FI is given by

$$\mu_{FI\,\alpha} = f_{\alpha}(\mu_{FI}(i,j)), \quad i,j = 1\ldots 25 \tag{4.7}$$

where FI_{α} is the "soft thresholded" fuzzy set.

4.4.1.5 Template matching

After obtaining the most probable candidates for the LVCP, a template matching is performed for these candidate pixels to obtain the most likely LVCP. A template is an ideal representation of the pattern to be identified within an image [SHB1993]. Template matching is used here to search for specific patterns (circular dark neighbourhood pattern) within the LV cavity. This is performed by moving the template over every position of the candidate pixel in the image and calculating the degree of similarity. A generalised convolution of the image and the template is computed by [WGL1992]

$$I \otimes T_{(i,j)} = < I.T_{(i,j)} >; for\ all\ (i,j) \in R_T \tag{4.8}$$

where A is the input echo image; $T_{(i,j)}$ is the template with its centre positioned at pixel (i,j); R_T is the region of the template and < . > represents the inner product. Then, the mean of the pixels within the template region, is obtained for all candidate pixels to obtain a fuzzy subset F_T. The small mean values correspond to LVCP pixels, which are then combined with FI_{α} to obtain the LVCP.

$$F_{LVCP} = FI_{\alpha} \cap F_T \tag{4.9}$$

4.4.2 Improved fuzzy LVCP detection:

The anterior wall extraction criteria, fuzzy rule for intensity information and the selected template were modified in the fuzzy LVCP detection algorithm, in order to obtain better results. The specific details of the modification together with simulation results are discussed below.

4.4.2.1 Anterior wall extraction criteria

To determine the fuzzy subset for the Fuzzy Horizontal Line (FHL), the anterior wall

and the posterior wall edges is required. The high contrast region in the anterior wall is very close to the vertical centre line. So, an average of its neighbouring columns (3 columns on either side) in the reduced resolution image of (50 x 50) is performed and the fuzzy multiscale edge detection technique is used to identify the anterior wall edge. In some cases, there is a high contrast region above the anterior wall which has a greater value than the anterior wall region as seen in Fig. 4.4 (a). This causes incorrect detection of anterior wall location. If there is a single peak in the top half of the line, it is chosen to be the anterior wall point. In case of two peaks identified in the top half of the line greater than a peak threshold, then the second peak is chosen as the anterior wall. Once the anterior wall is extracted, the horizontal centre line along y_c is determined and a fuzzy subset for the Fuzzy Horizontal Line (FHL) is formed using the equation 4.3. Fig. 4.4 (a) shows the extracted anterior epicardial boundary and the lowest point of the posterior epicardial boundary in a reduced resolution image. Fig. 4.4(b) and Fig. 4.4(c) represent the fuzzy vertical and horizontal membership functions.

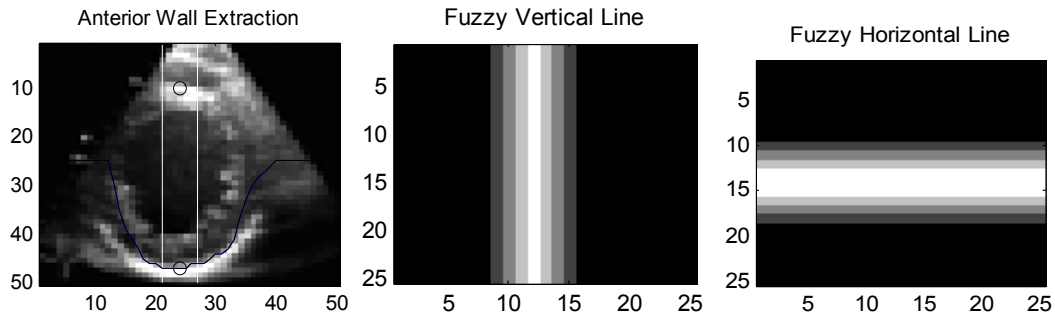

Fig. 4.4 (a) extracted anterior and posterior epicardial boundary and the corresponding fuzzy vertical and horizontal membership functions are shown in (b) and (c).

4.4.2.2 Intensity information

LVCP is a dark pixel in the LV cavity or the blood region. The scale of darkness of the image pixels are represented by a fuzzy subset Fuzzy Darkness (FD). The membership functions for FD is given by

$$FD = \{(i,j), \mu_D(i,j)\}, \quad i,j = 1 \ldots 25$$

where,

$$\mu_D(i,j) = f_D(I_{ij}) = \begin{cases} 1 & , \quad I_{ij} \le a \\ 1 - \dfrac{I_{ij} - a}{b - a} & , \quad a < I_{ij} \le b \\ 0 & , \quad I_{ij} \ge b \end{cases} \tag{4.10}$$

where, $a = mean(I); \quad b = mean(I) + std(I)$

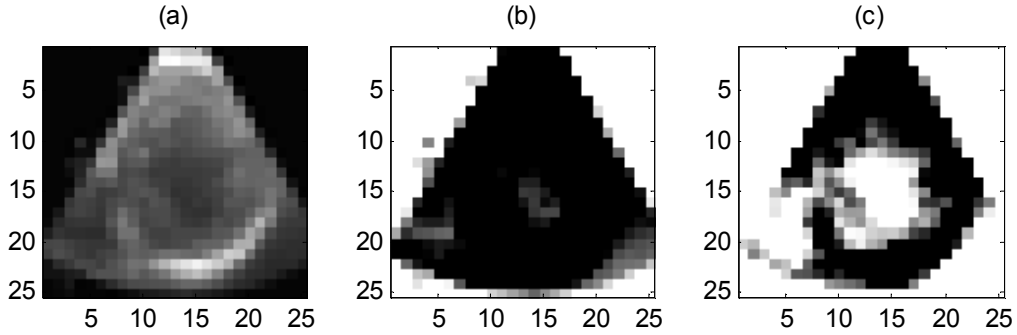

(a) Original low contrast image, (b) FDARK membership function obtained by setting the standard values of a=10 and b=30, (c) FDARK membership function obtained by determining the automatically (a=32; b=45).

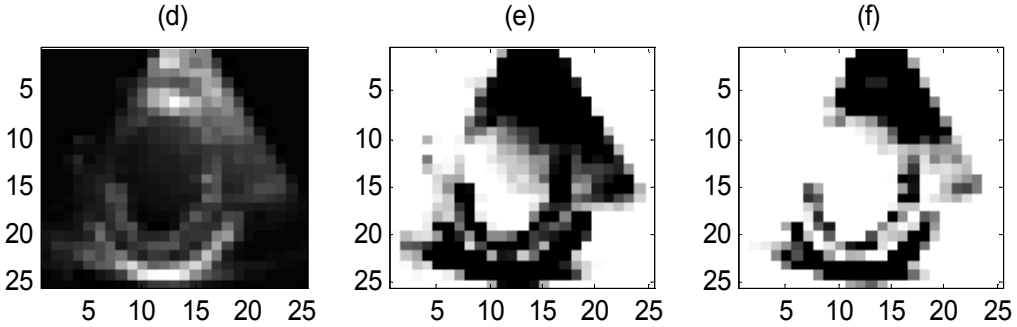

Fig. 4.5 (d) Original good quality image, (e) FDARK membership function obtained by setting the standard values of a=10 and b=30 , (f) FDARK membership function obtained by determining the automatically(a=21; b=43).

In [SS1997, SS1998], the values of a=10 and b=30 was chosen. In case of average quality and poor quality echo images with very low contrast between the LV cavity and the tissue, this scaling resulted in fuzzy subset with membership values, which did not well represent the LV cavity region. This fuzzy set formation was then automated by selecting the threshold value based on the statistics of the image such

as mean and standard deviation as shown in equation 4.4. Fig. 4.5 shows the good quality and poor quality images and the fuzzy membership function for dark pixels of the image by using the fixed thresholds and automatically determined thresholds. It can be seen in Fig. 4.5(b) that entire LV cavity is not represented in the FDARK membership function, when the fixed thresholds are used. When the automatically determined thresholds are used as shown in Fig. 4.5(c), the LV cavity is represented well in the fuzzy subset. The automatic thresholds work well for good quality images as shown in Fig. 4.5(d) to obtain fuzzy subset with well represented LV cavity as shown in Fig. 4.5(f).

4.4.2.3 Template selection

Template matching is performed to search for specific patterns (dark neighbourhood pattern) within the LV cavity. The data driven template shown in Fig. 4.6(c) is chosen for SA views, both in mid cavity level with papillary muscles as seen in Fig. 4.6(a) and basal level as seen in Fig. 4.6(b). The template matching is performed as explained in subsection 4.4.1.5.

The various stages involved in the fuzzy logic based LVCP detection algorithm is shown in the Fig. 4.7. The input image is shown in Fig. 4.7(a). Fig. 4.7(b) shows the fuzzy membership function for centre part of the image (FCP). The fuzzy subset for the intensity information determined by the equation 4.10 is shown in Fig. 4.7(c).

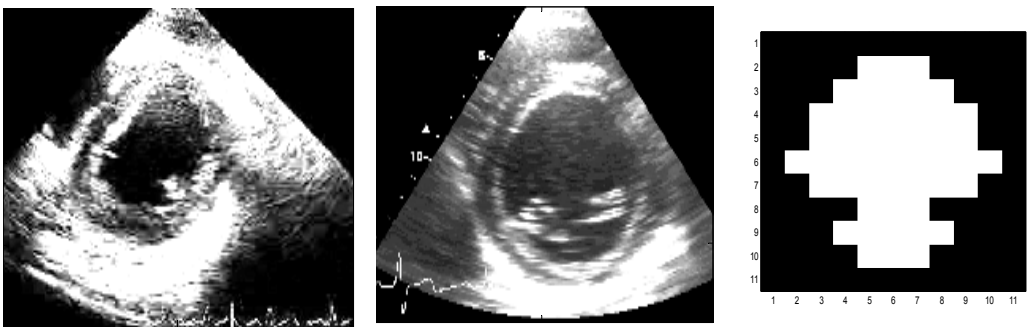

(a) (b) (c)

Fig. 4.6 (a) SA mid cavity level with papillary muscles in the LV cavity area, (b) SA basal level with mitral valve in the LV cavity area, (c) Data driven template to describe the LV cavity area

the extracted anterior and posterior wall are shown in Fig. 4.7(d). Fig. 4.7(e) and Fig. 4.7(f) represent the fuzzy vertical and horizontal membership functions, respectively. Fig. 4.7(g) shows the candidate LVCP pixels obtained by the fuzzy α-cut of the intersection of the four fuzzy subsets. The extracted centre point and an estimated epicardial boundary in the original image are shown in Fig. 4.7(i). Once the centre point is detected, the boundary detection is performed as explained in the following sections.

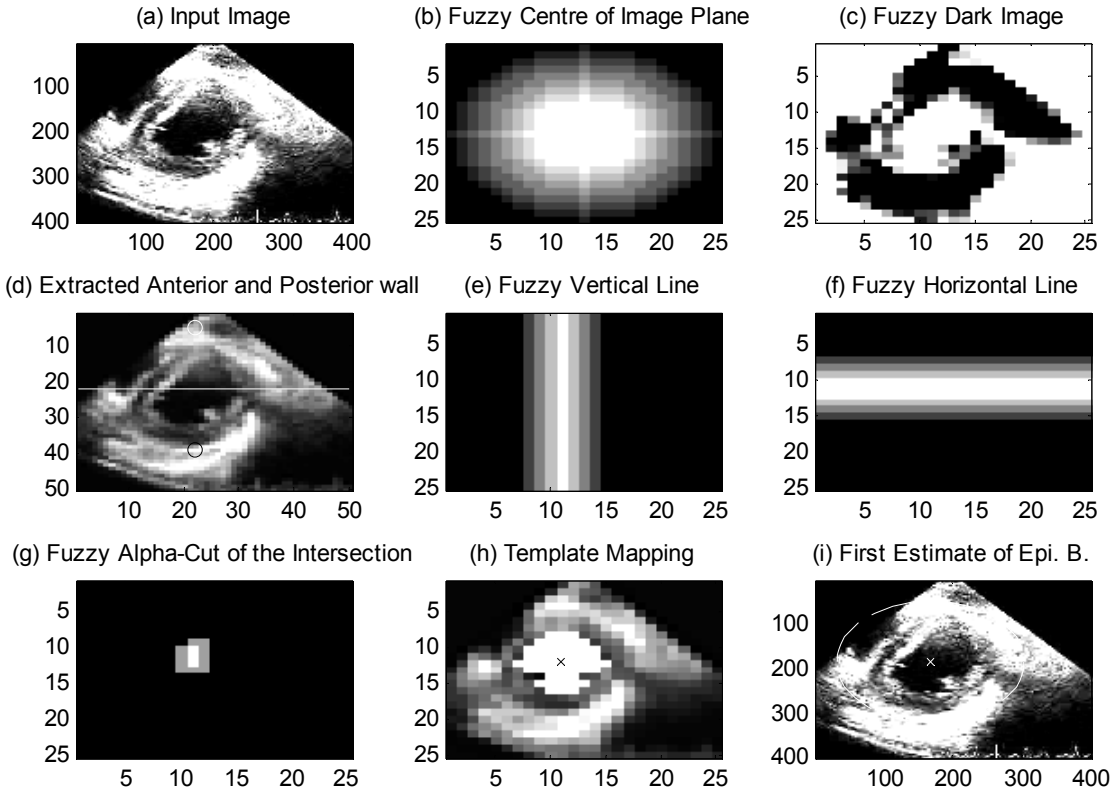

Fig. 4.7 Stages in the left ventricle centre point detection

4.4.3 Left ventricle boundary detection

This section describes the existing fuzzy multiscale edge detection (FMED) algorithm developed by [SS1998] to search the LV boundary edges along the radial lines starting from the LVCP. The radial search based approach is used here as the LV wall has a radial oriented motion in the echo movie. In an Echo frame, 60 radial lines are processed for the extracting the endocardium and epicardium edges. In any frame j, the radial lines through the anterior wall are combined to determine the epicardial, endocardial edges and their difference to get the LV wall thickness, T_j, which is used for defining the region of interest (ROI) in the radial lines for edge detection. The advantage of applying the ROI is to reduce the number of expected step edges and for computational efficiency. The ROI for the epicardial boundary is defined as a circular model using a radius, $\mathbf{R_j^{ep}}$ (estimated rough epicardial edge for the frame j). The ROI includes a region on either side of the estimated edge by scaling it with lower and higher scaling factors S_L and S_H. The upper limit ($\mathbf{R_j^{epH}}$) and lower limits ($\mathbf{R_j^{epL}}$) for the region is defined by the circular regions of radii

$$R_j^{epH} = R_j^{ep} \times S_H \; ; R_j^{epL} = \max\{(R_j^{ep} \times S_L), (R_j^{ep} - T_j)\} \qquad (4.11)$$

The wavelet transform is performed on the 1D signal along the radial line. The signal is decomposed upto 6 levels into approximations and details. The details are used for extracting the step edges which correspond to the endocardium wall edge. The details in the different scales $S_j(n)$, are normalised. In the each scale of the wavelet transform, the local maximum represents the positive transition in the signal. This edge information at different scales is combined to get a robust edge result by defining fuzzy sets. Fuzzy membership functions are used to represent the scales, by assigning a membership value of unity to all the local maximum points. The multiscale edge fuzzy subset is defined by $\mathrm{A_j}$.

$$A_j = \left\{\left(n, \mu_{A_j}(n)\right), n = 1,2,\dots,N\right\}, \; j = 1,2,\dots,J \qquad (4.12)$$

where $$\mu_{A_j}(n) = \begin{cases} 1 & if\ S_j(n)\ is\ a\ local\ maximum \\ |S_j(n)| & else \end{cases}$$

The different scales fuzzy subsets are combined by applying the fuzzy operator for intersection to extract the edge. The coarse scale is excluded for better localization. This edge property is referred as the edge fuzzy set A_E given by

$$A_E = A_1 \cap A_2 \cap \ldots A_{J-1} \tag{4.13}$$

The maximum in the edge fuzzy set corresponds to the actual endocardium edge in the echo image.

The median filtering of filter size [5x1] is performed on the extracted endocardial edges to reduce the effect of the papillary muscle which is a protruding tissue in the wall which connects to the heart valves to keep it in place. The extracted boundaries are refined by applying cubic B-spline approximation to get continuous and smooth boundary for epicardium and endocardium. In Echo movies, the quality of the frames is not necessarily consistent. Some frames have the shadowing effect resulting in missing structures or low contrast regions, while the others do not have that effect. In manual interpretation, the experts consider the temporal information (information on the adjacent frames) for analysing the heart wall motion. While processing of the edges in a frame, the edge information of the previous and the next frame is also considered. The processing is performed by combining the previous and the next frame with less weight compared to the present frame. The statistical information of the radial line is used choose the level of importance given to adjacent frames. This would help in edge detection in the radial lines which intersect with the regions of missing information.

4.4.4 Improved LV boundary detection:

The region of interest in the radial line to search the boundary edge and the criteria for selecting the edge point in the edge fuzzy subset were modified in the FMED algorithm, in order to obtain better results. The specific details of the modification together with simulation results are discussed below.

4.4.4.1 Region of interest (ROI) in the radial line

The advantage of applying the ROI is to reduce the number of expected step edges in the radial line. The FMED algorithm works well, if the LVCP estimation process has a maximum of 10% error. The problem arises when the separation between the calculated and actual LVCP is greater than 10% error (that is, 10% of the LV diameter). Here, the algorithm is modified in such a way that, for the first radial line, using the estimated epicardial edge, a ROI (including either side of the estimated edge) is defined for epicardial boundary. For the radial lines other than the first one, the algorithm is modified to consider the average of the estimated edge R_j^{ep} and the detected edge of the previous radial line, $ED_{i-1,j}^{epi}$ to describe the upper and lower limit for the ROI as given below.

$$R_{i,j}^{epH} = \frac{(R_j^{ep} + ED_{i-1,j}^{epi})}{2} \times S_H$$

$$R_{i,j}^{epL} = \max\left\{\left(\frac{(R_j^{ep}+ED_{i-1,j}^{epi})}{2} \times S_L\right), \left(\frac{(R_j^{ep}+ED_{i-1,j}^{epi})}{2} - T_j\right)\right\} \qquad (4.14)$$

The lower and higher scaling factors are $S_L = 0.7$ and $S_H = 1.3$, so that it includes a region on either side of the estimated edge. This includes approximately 15 pixels on either side of the edge. Similar ROI is modelled for the endocardial edges. For the radial lines other than the first one, the upper ($R_{i,j}^{enH}$) and lower limit ($R_{i,j}^{enL}$) for the endocardial boundary is defined as follows

$$R_{i,j}^{enH} = \min\left\{\left(\frac{ED_{i-1,j}^{endo} + (ED_{i,j}^{epi} - T_j)}{2} \times S_H\right), \left(ED_{i,j}^{epi}\right)\right\}$$

$$R_{i,j}^{enL} = \left(\frac{ED_{i-1,j}^{endo}+(ED_{i,j}^{epi}-T_j)}{2} \times S_L\right) \qquad (4.15)$$

where, $ED_{i,j}^{epi}$ is the calculated epicardial edge for i^{th} radial line.

$ED_{i-1,j}^{endo}$ is the calculated endocardial edge for the previous $(i-1)^{th}$ radial line

Fig. 4.8(a) shows the image to be processed. Fig. 4.8(b) shows the extracted centre point and the estimated epicardial boundary**,** using the centre and the extracted anterior wall point as explained in section 4.4.2.1. Fig. 4.8(c) shows the 60 radial lines which are processed for the extracting the endocardium and epicardium edges. Fig. 4.8(d) shows the ROI modelled for the epicardium (outer wall of the heart) and Fig.4.8(e) shows the extracted epicardium using FMED. Fig. 4.8(f) shows the estimated wall thickness, T_j. Fig. 4.8(g) show the ROI modelled for the endocarium (inner wall of the heart). Fig. 4.8(h) shows the endocardial edge obtained using the edge selection criteria described in the next subsection.

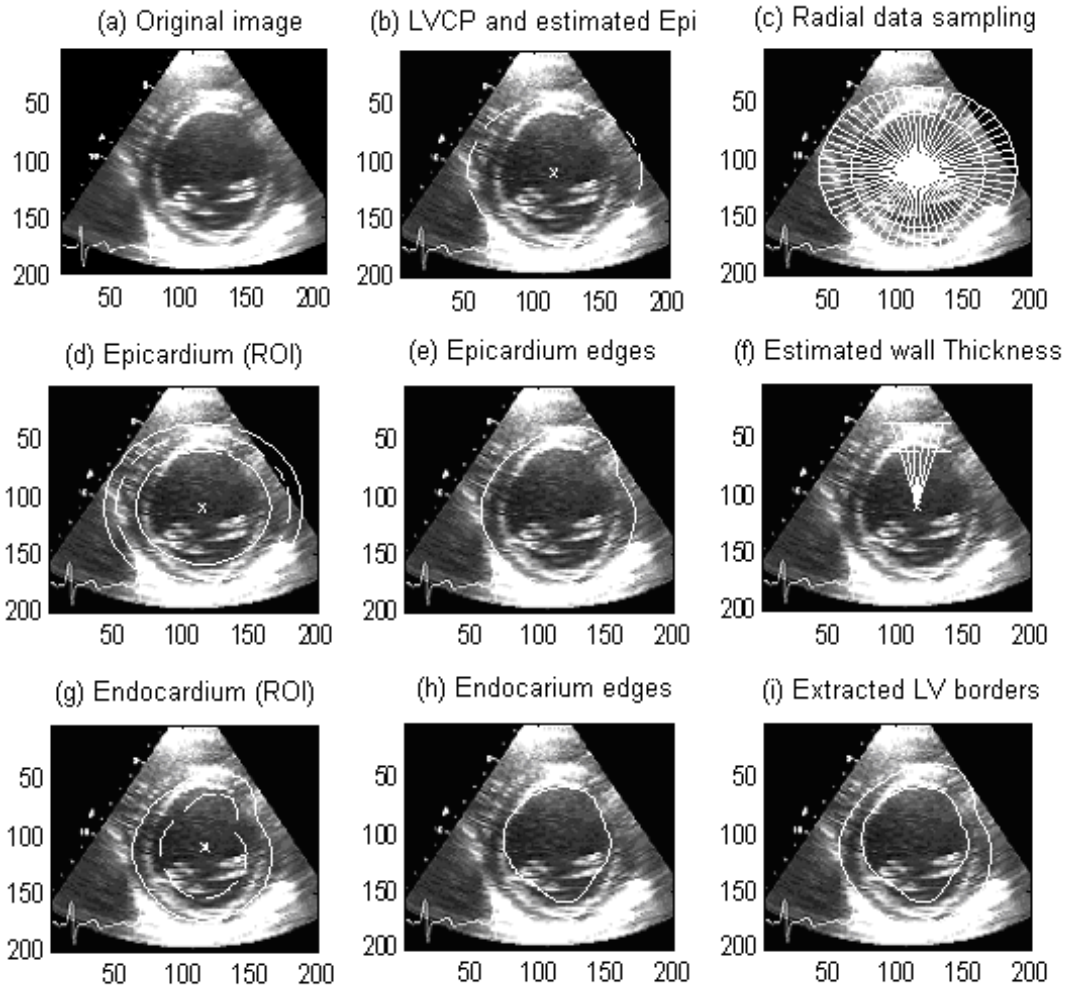

Fig.4.8 Stages in the left ventricle inner and outer wall boundary detection

4.4.4.2 Edge selection criteria

In some cases, due to the presence of papillary muscles or mitral valve in the LV cavity region, more than one strong edge is present in the region of interest. In this case, the clean maximum in the edge fuzzy set does not necessarily extract the actual edge. Fig. 4.9 shows the endocardium edge detection process along the radial line in Fig. 4.9(a). The wavelet transform is performed on the 1D signal along the radial line shown in Fig. 4.9(b). The signal is decomposed upto 6 levels and the details in the 6 different scales $S_j(n)$, are normalised and shown in Fig. 4.9(c-h). In the image shown in Fig. 4.9(a), the mitral valve has a stronger edge that the actual endocardial edge. The clean maximum in the edge fuzzy set as shown in Fig. 4.9(i) detects the valve denoted by a '■' marker in Fig. 4.9 (a). So the extraction of the edge from the edge fuzzy set is performed differently when there is more than one peak in the region of interest. The number of peaks with values greater than the 75% of the maximum in the edge fuzzy set and the peaks are separated with a minimum distance, w=10, are extracted. Then, the second peak is selected as the endocardial edge. Fig. 4.9 (j) shows the extracted endocardial edge in the fuzzy edge subset, which is denoted by a '●' marker in the Fig. 4.9 (a).

The edge detection results for echo image in SA mid cavity view (Fig. 4.10(a)) and SA basal view (Fig. 4.10(e)) is shown here. 4.10(b) shows that the level sets with active contours [LI2005] produces correct edges in the region of good quality and produces incorrect edges in regions of poor quality. It can be seen in Fig. 4.10(c) and (d), that the edges obtained by FMED and modified FMED for SA mid cavity view before further spatial/ temporal processing have no significant difference. The presence of the mitral valve in the LV cavity area affects the edges obtained by the by level sets with active contours as seen in Fig. 4.10(f) and FMED as seen in Fig. 4.10(g). The modified FMED edges are shown in Fig. 4.10(h). On average, the processing time for level sets to detect edges in one frame in MATLAB is 29.11 seconds, while the processing time for modified FMED to detect edges is 1.07 seconds. Modified FMED reduces the edge detection problem from 2 dimensions to 1 dimension, thus reducing the processing time. The edge information obtained is used in the enhancement stage to determine the blood and tissue region in the image.

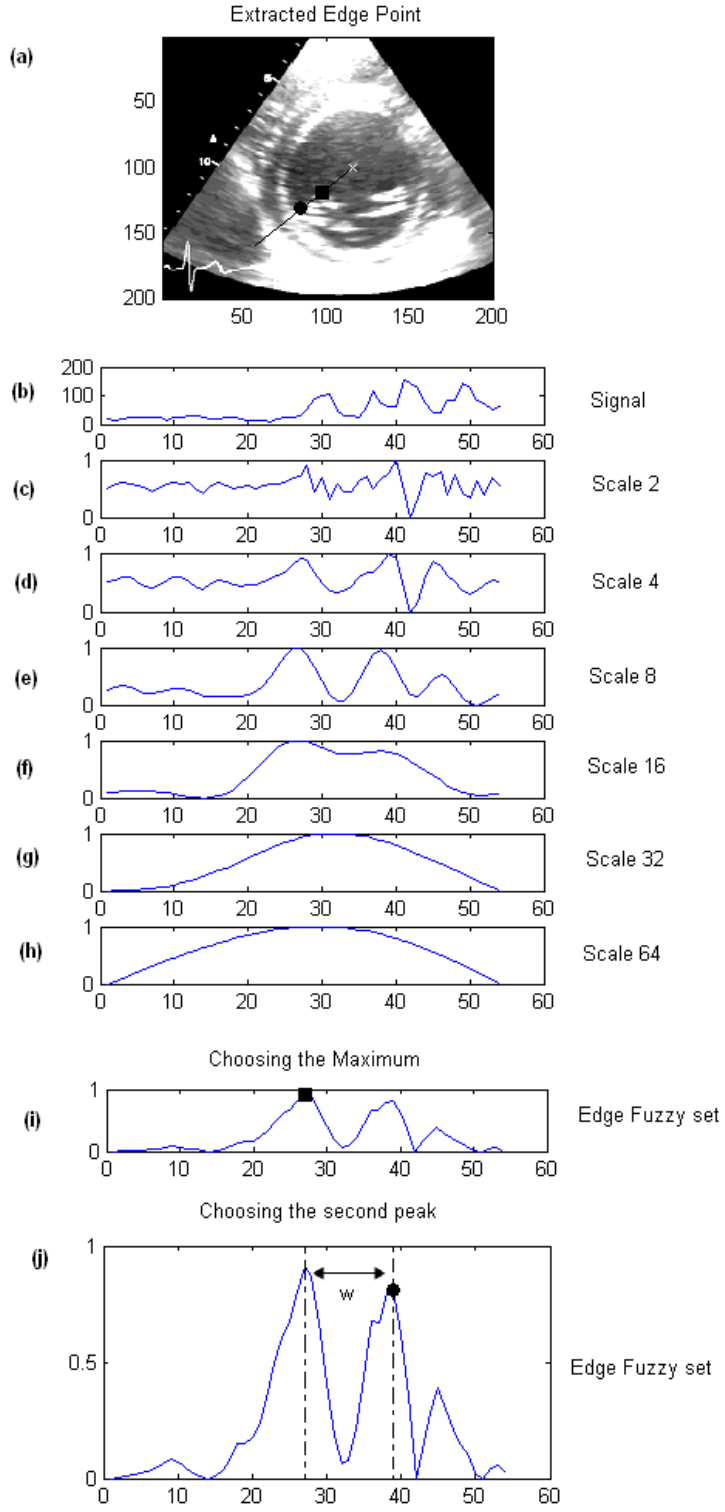

Fig.4.9 (a) Detection of the Endocardium (inner wall) along the radial line, (b) the signal along the radial line, the wavelet details at different scales are shown from (c) to (h). (i) the edge obtained by choosing the maximum of the edge fuzzy subset, and (j) the edge obtained by choosing the second highest peak when the edge fuzzy subset has more than one peak.

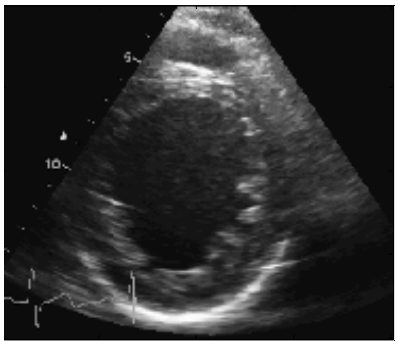

(a) Original image

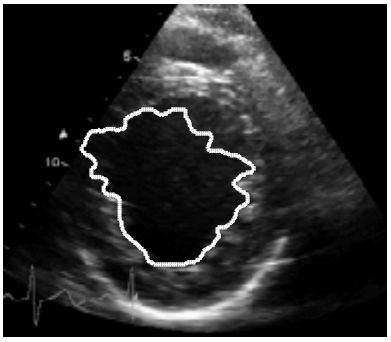

(b) Level sets with Active contours

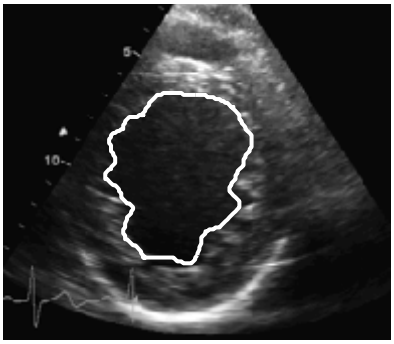

(c) FMED edge

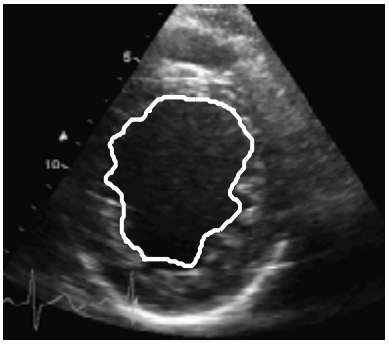

(d) modified FMED edge

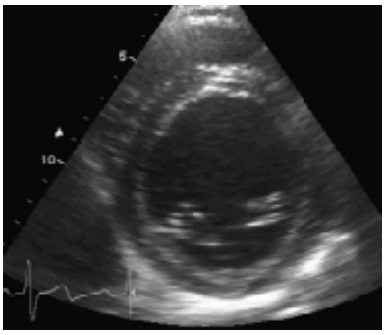

(e) Original image

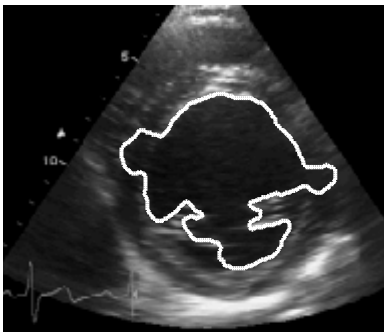

(f) Level sets with Active contours

(g) FMED edge

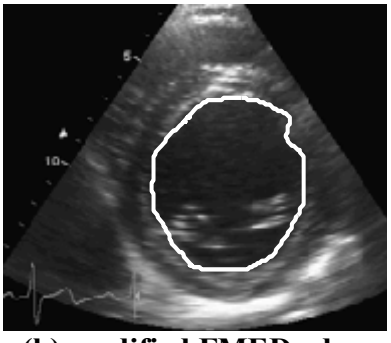

(h) modified FMED edge

Fig.4.10 Edge detection results for echo image in SA mid cavity view (a) and SA basal view (e) using level sets with active contours, FMED and modified FMED

4.5 Delaunay triangulation based enhancement

The tissue or wall region in the echo images is represented as bright regions due to strong reflection, while the left ventricle cavity or the blood region is a dark region. Contrast enhancement is achieved by brightening the wall region and darkening the blood region, by dividing the echo image into smaller regions and performing non-linear processing in those regions. Dividing the entire image into uniform regions does not work as different regions have to be processed differently. It is also computationally expensive and unnecessary. The basics of Delaunay triangulation is explained in the section 4.5.1. The processing of the wall region and processing of the tissue region in detailed in section 4.5.2 and section 4.5.3 respectively.

4.5.1 Delaunay triangulation

Delaunay triangulation, introduced by Boris Delaunay in 1934 is used in this work to divide a surface into triangular regions with common characteristics that are particularly well-suited for image processing applications. This triangulation is performed by using the points or edges obtained from the image. For a set of V vertices (or points or edges) in a 2 D plane, a triangulation of these vertices produce a set of T triangles , whose interiors do not intersect each other, and whose union is the convex hull of V, if every triangle intersects only at the triangle's vertices [SHEW1999]. Delaunay triangulation is performed in such a way that there is no point in the circumcircle of the triangles (that is, no point is within the circle passing through three vertices of triangle) in the network (as shown in the Fig.4. 11(f)). Also

Delaunay triangulation is advantageous over other meshing based techniques as it maximizes the minimum vertex angles of the triangles in the network, so that the triangles formed tend towards equiangular triangles, avoiding sharp and stretched triangles. This triangulation is suitable for interpolation as the pixel values within the region in the final image is directly related to the triangle region in the network. Delaunay triangulation is performed in the heart wall region between the endocardium and the epicardium to divide it into triangular regions and these regions are processed by applying a thresholding technique. This is followed by processing the blood region in a similar fashion.

4.5.2 Processing tissue or wall region

To select the wall region for processing, the endocardial and epicardial boundary edges along with two other set of points formed, 3 pixels and 6 pixels away from both the edges are considered as vertices for triangulation. The wall region closer to the edges is divided into smaller regions by forming two bands with 3 pixels width from the inner and outer wall and the region in-between them is divided into a comparatively larger triangles. The triangulation performed in the wall region can be seen in Fig. 4.11(c). The triangles formed in the blood region are not considered for processing in this stage. The triangles within the blood region are either larger or thin and long when compared to the tissue region triangles. The area of the triangle and the length of the sides of the triangle are used to eliminate the triangles in the blood region, that is, triangles with area greater than 100 (arbitrary unit) and the triangles with one of the side length greater than (1.5 x wall thickness T_j) are omitted. By using this elimination criteria, minimum of 95% of the blood region triangles are eliminated leaving a maximum of 5% of the small triangles close to the edges. These triangles are also processed as the tissue region.

After performing the triangulation, a thresholding is applied within the shortlisted triangular regions within the wall region. In the tissue region, a mean based thresholding is applied, which is defined mathematically for a triangular region $I_i(x,y)$ as

$$I_i(x,y) = \begin{cases} I_i(x,y) + \dfrac{M'}{5} & if\ I_i(x,y) \le M_i \\ I_i(x,y) & if\ I_i(x,y) > M_i \end{cases} \qquad (4.16)$$

where $I_i(x,y)$ is the pixel value and M_i is the mean of the pixels within the triangular tissue region, *M'* is the mean of the pixels in the wall region, x and y are the pixel coordinates. The above representation can be explained as follows. Each pixel within the triangular region is compared with mean of the pixels within the region. If the actual pixel value is less than or equal to the mean, then the pixel value is incremented by 1/5th of the mean, otherwise the pixel is retained. The tissue region is brightened only in the required areas in the image while the high contrast

regions are unaffected. This prevents over enhancing the high contrast sections in the tissue region.

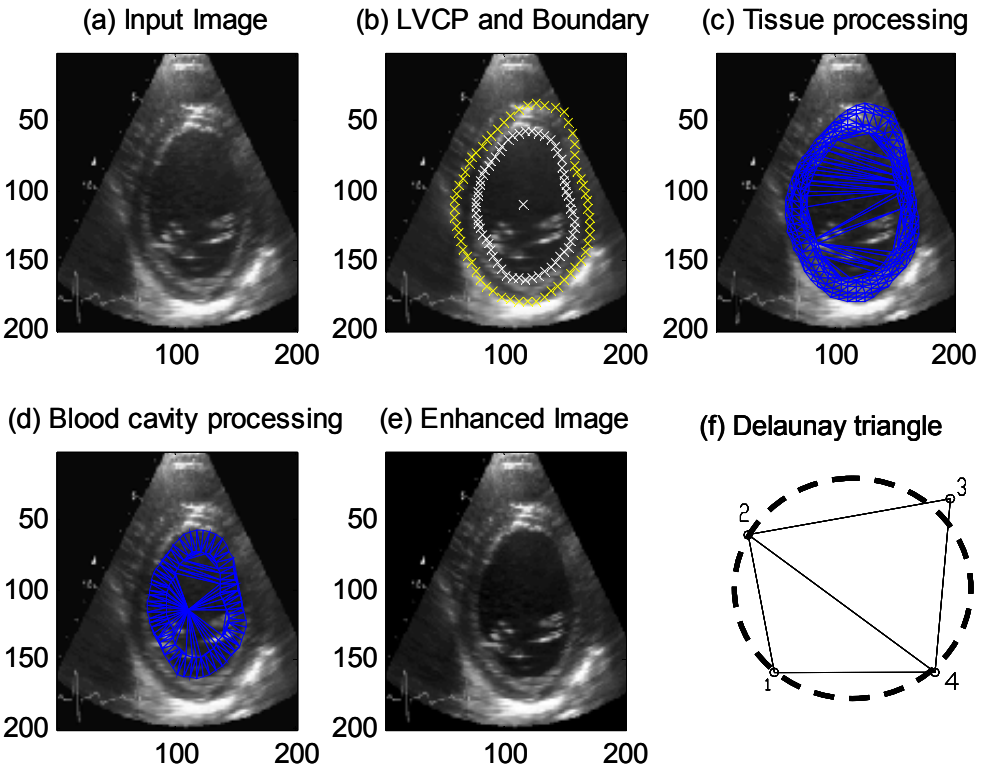

Fig. 4. 11 Shows the different stages in enhancement step for the synthetic Short Axis heart image. (a) Original image (b) image with extracted LVCP and wall boundary (c) Delaunay triangulation for the blood region (using the extracted inner wall and centre), (d) Delaunay triangulation for only the wall region (using the extracted wall boundaries) and (e) Processed image for contrast enhancement. A Delaunay triangle is showed in (f)

4.5.3 Processing LV cavity or blood region

The blood region is selected and divided into triangular regions by considering the centre of the LV cavity and the endocardial boundary edges along with a set of points formed towards the centre (with a distance of 5 pixels from the endocardial boundary edge) as vertices for triangulation (see Fig.4. 11(d), followed by thresholding which is defined mathematically for a triangular region $I_i(x,y)$ as

$$I_i(x,y) = \begin{cases} I_i(x,y) - b & \text{if } I_i(x,y) \le M_i \\ I_i(x,y) - \dfrac{M'}{2} & \text{if } M_i \le I_i(x,y) \le M_i + 20 \\ I_i(x,y) & \text{if } I_i(x,y) > M_i + 20 \end{cases} \tag{4.17}$$

where $I_i(x,y)$ and M_i are the pixel value and the mean of the pixels within the triangular blood region, *M'* is the mean of the pixels in the blood region, x and y are the pixel coordinates. In other words, if the actual pixel value is less than or equal to the mean, then the pixel value is decremented by *b*. If the pixel lies between the mean M_i and $M_i + 20$, then the pixel value is decremented by half of the mean. If the pixel is greater than $M_i + 20$, the pixel is retained so that the heart wall tissue structure if encountered while processing the blood region, will not be affected. The contrast improvement is performed based on the local information, so that the weak regions (lateral wall region) of the image are enhanced more than the strong regions (top and bottom wall region). The new modified image is reconstructed as follows:

$$I_{\text{mod}\,ified}(x,y) = (P_1(x,y) + P_2(x,y))/2 \tag{4.18}$$

where $P_1(x,y)$ is the image after processing the wall region and $P_2(x,y)$ is the image after processing the blood region in the original image. Averaging the processed images is performed to reduce the effect of incorrect modifications to the anatomical structures. For example, if any of the small blood region triangles close to the wall are not eliminated while processing the tissue region, then the effect of incorrect processing in those regions is reduced by averaging the two processed blood regions.

4.6 Experimental Results

This section presents experimental results of the system for echo image contrast enhancement. Echo images can be recorded in different views, each of which is important to identify critical parameters to evaluate different heart conditions. Here, short axis (SA) views are considered. The echo movies are captured over a time period; to cover a complete cardiac cycle consisting of an average of 25 frames. The number of the radial lines used for edge detection in one frame is empirically selected

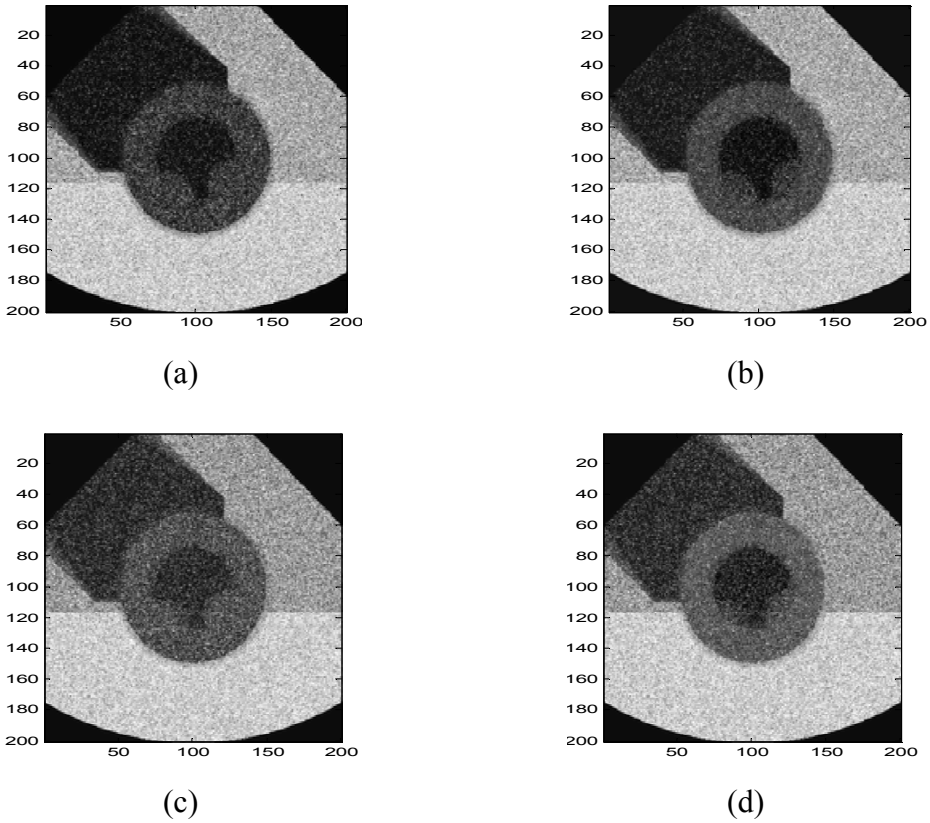

Fig. 4.12 Enhancement result for synthetic Short Axis images, (a) Synthetic image 1(CR =0.5147), (b) Enhanced image 1 (CR=0.5732), (c) Synthetic image 2(CR == 0.4166) and (d) Enhanced image 2 (CR=0.4433)

as 60. Synthetic images models and real image data are used for the experiment. Synthetic images are generated using the method used in [DIAS1996] and consists of 25 frames of 400 x 400 images. The pixel value in the image varies from 0 and 128 which is defined using Rayleigh distribution with different reflectivity factor for the reflected ultrasound signal due to blood, heart wall and tissue other than heart. A Rayleigh distribution with reflectivity factor σ is given as

$$R(n) = \left(\frac{n}{\sigma^2}\right)\exp\left[-\frac{1}{2}\left(\frac{n}{\sigma}\right)^2\right] \tag{4.19}$$

In the first synthetic image shown in Fig.4. 12(a), reflectivity factors defined in the left and right ventricular regions representing blood with σ_1= 20, heart wall region with σ_2= 40, tissue outside the heart in the two lateral regions with σ_3= 80 and the lung tissue outside the posterior wall region with σ_4= 120. The relative contrast

between the regions is $\sigma_1/\ \sigma_2 = \sigma_2/\ \sigma_3 = 0.5$ and $\sigma_2/\ \sigma_4 = 0.33$. For the second synthetic image shown in Fig. 4.12 (c), the relative contrast between the regions is $\sigma_1/\ \sigma_2 = \sigma_2/\ \sigma_3 = 0.33$ and $\sigma_2/\ \sigma_4 = 0.25$. The resultant enhanced images for the two synthetic images Fig.4. 12 (a & c) are shown in Fig.4. 12 (b & d), respectively. The contrast enhancement can be noted visually and an objective measure is given by contrast resolution.

In [GORD1984], the local contrast between a pixel, p, and average of its eight neighbours, a, is given by

$$C = \frac{|p-a|}{(p+a)} \tag{4.20}$$

Here, the contrast resolution (CR) between the tissue region, S_T and the blood region, S_B is measure by

$$CR = \frac{|S_T - S_B|}{(S_T + S_B)} \tag{4.21}$$

where S_T is the pixel average in a small section of tissue region and S_B is the pixel average in a small section of the blood region. The CR in a section of the image is measured to give a quantitative measure of the image enhancement, as well as the subjective measure. Table. 4.1 shows the contrast resolution for sample original images, after applying Average filter, Median filter and Weiner filter in MATLAB, Frost filter [RAJ2006] and the proposed Delaunay triangulation based Enhancement algorithm. The contrast resolution in the wall segment with contrast improvement is provided in the table. From the table, it can be seen that the contrast resolution is improved for the proposed method when compared to the original image, Average, Median, Weiner and Frost filter.

Image	Original	Average	Median	Weiner	Frost	Proposed
1	0.6375	0.6371	0.6531	0.6375	0.6371	**0.7406**
2	0.2451	0.2475	0.2493	0.2486	0.2472	**0.4378**
3	0.4661	0.4818	0.4946	0.4817	0.4780	**0.6382**
4	0.5022	0.5126	0.5266	0.5127	0.5102	**0.7567**
5	0.3320	0.3256	0.3928	0.3251	0.3270	**0.4193**
6	0.4166	0.4169	0.4135	0.4175	0.4179	**0.4433**
7	0.4490	0.4438	0.4399	0.4451	0.4451	**0.5651**
8	0.2925	0.3036	0.3265	0.3037	0.3010	**0.5866**
9	0.7211	0.7220	0.7075	0.7220	0.7218	**0.9424**
10	0.9634	0.9640	0.9704	0.9638	0.9639	**0.9720**

Table 4.1: Comparison of Contrast Resolution measures

The results for the real SA view images are shown in Fig. 4.13. It can be seen that the contrast between the tissue and the blood region is improved and the wall region is well defined in the enhanced images. Fig. 4.13(a) shows a good quality SA basal view showing the mitral valve in the LV cavity area (from a Philips machine) and Fig. 4.13(b) shows the enhanced image. In the enhanced image, it can be seen that the contrast is improved, preserving the structures of diagnostic importance such as the heart wall edges and the mitral valves within the blood region. The arrow markers shows the valve region in the cavity, which is not affected. Also, it can be noted that the enhancement of the wall region is not overdone. Table 4.2 shows the contrast resolution measure before and after enhancement, obtained for the 6 segments in the echo image shown in Fig. 4.13.

Fig. 4.14(a) shows a poor quality SA mid cavity view showing the papillary muscle in the LV cavity area (from a Siemens machine). The shadowing effect that causes poor contrast in certain regions can be seen in the image. Fig. 4.14(b) shows the enhanced image which shows the contrast enhancement in the certain regions shown by arrow markers while regions with good contrast are not affected. Table 4.3 shows the contrast resolution measure before and after enhancement, obtained for the 6 segments in the echo image shown in Fig. 4.14. It can be seen that the contrast is enhanced only in the required region (in the segments 7, 8, 11 and 12), while there is very less contrast improvement in the segments 9 and 10.

Fig. 4.15(a) shows a poor quality SA mid cavity view without papillary muscle in the

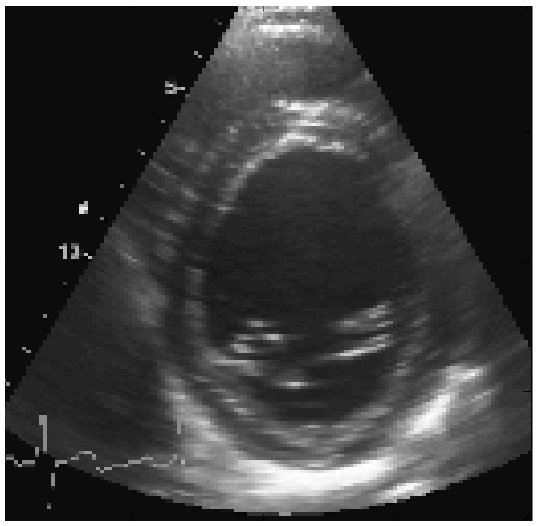

(a)

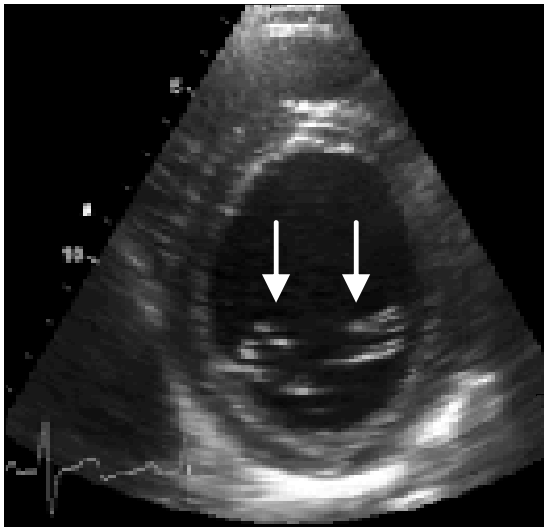

(b)

Fig. 4.13. (a) Good quality SA basal view showing the mitral valve in the LV cavity area obtained from a Phillips machine, (b) enhanced image

Contrast Resolution	Seg 1	Seg 2	Seg 3	Seg 4	Seg 5	Seg 6
Before enhancement	0.5553	0.2296	0.2802	0.5299	0.3108	0.3238
After enhancement	0.5818	0.3060	0.3053	0.5638	0.3399	0.3898

Table 4.2 Contrast Resolution measure in 6 regions for image in Fig 4.13

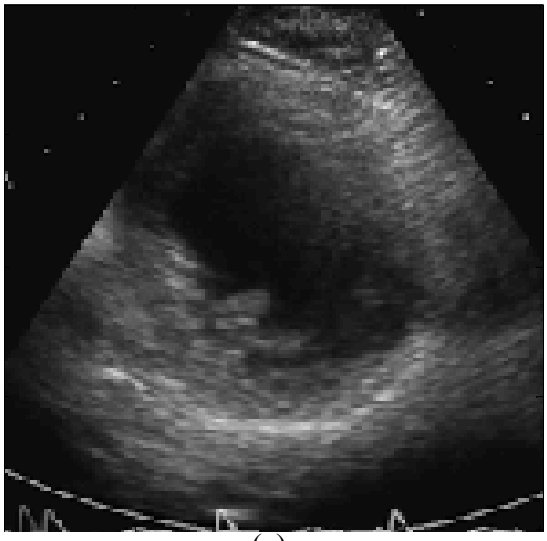

(a)

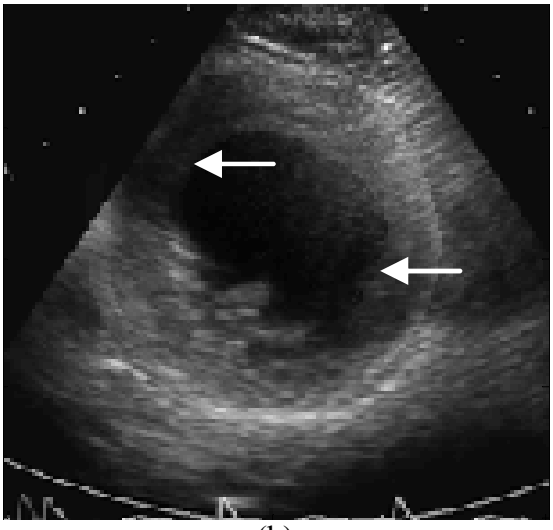

(b)

Fig. 4.14. (a) Poor quality SA mid cavity view showing the papillary muscle in the LV cavity area from a Siemens machine, (b) enhanced image

Contrast Resolution	Seg 7	Seg 8	Seg 9	Seg 10	Seg 11	Seg 12
Before enhancement	0.5038	0.7325	0.9628	0.9070	0.4999	0.4535
After enhancement	0.6631	0.8347	0.9868	0.9290	0.6985	0.5396

Table 4.3 Contrast Resolution measure in 6 regions for image in Fig 4.14

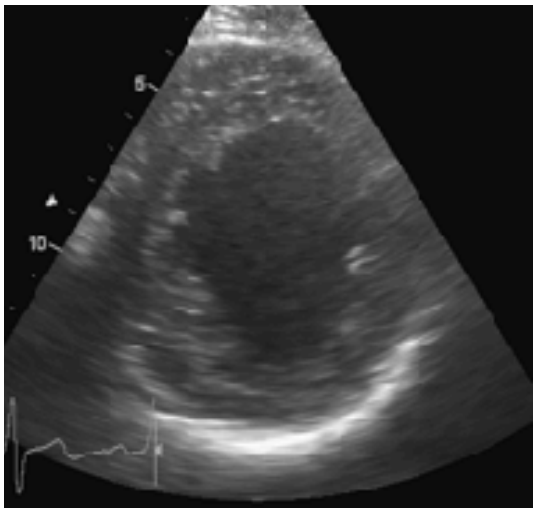

(a)

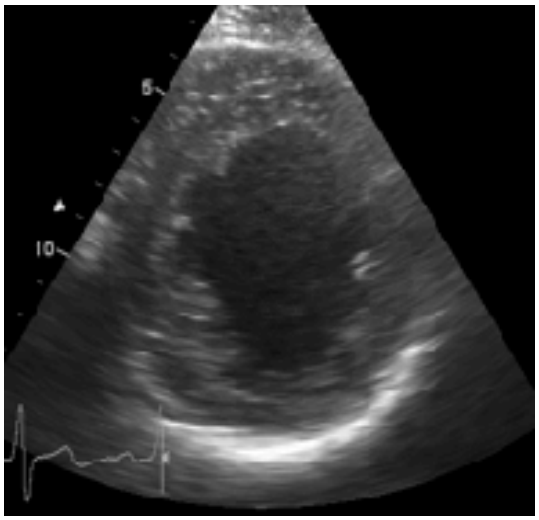

(b)

Fig. 4.15. (a) Poor quality SA mid cavity view without papillary muscle in the LV cavity area from a Phillips machine, (b) enhanced image

Contrast Resolution	Seg 7	Seg 8	Seg 9	Seg 10	Seg 11	Seg 12
Before enhancement	0.2017	0.1244	0.3829	0.3769	0.2685	0.1692
After enhancement	0.2232	0.2082	0.4249	0.4051	0.3179	0.2020

Table 4.4 Contrast Resolution measure in 6 regions for image in Fig 4.15

LV cavity area (from a Philips machine). The poor quality of the image was due to the inappropriate setting in the machine which was used to acquire the image. Fig. 4.15(b) shows the enhanced image, showing enhancement in contrast between the blood and the wall region. Table 4.4 shows the contrast resolution measure before and after enhancement, obtained for 6 segments in the echo image shown in Fig. 4.15. This enhancement will also help manual interpretation, for placing markers on the heart wall to analyse wall motion using the commercially available software which comes with the Echocardiography recording systems. This algorithm is tested on the images obtained from both Siemens and Philips echo machines.

As this image enhancement algorithm is automatic, poor enhancement results were studied in certain cases. The incorrect boundary detection is mainly due to incorrect LVCP detection caused by the incorrect automatic identification of the posterior wall for fuzzy vertical rule. In some cases, incorrect boundaries were due to missing LV wall sections greater than 10% of total LV wall (which is an equivalent to 6 consecutive radial lines used in the LV boundary detection process) in more than 3 consecutive frames or LV wall falling outside the imaging plane as seen in Fig.5.11. Incorrect boundary detection causes poor segmentation of wall region and blood region, resulting in erroneous enhancement of regions.

4.7 Conclusion

In this chapter, a novel echocardiography image enhancement algorithm which combines undecimated wavelet based speckle noise reduction, edge detection, followed by a regional enhancement process that employs Delaunay triangulation based thresholding is presented. The algorithm is applied to both synthetic and real image data sets of short axis view echocardiography sequence. The results are encouraging and suggest that this region based enhancement improves contrast by preserving the edges and the anatomical structures, which are of diagnostic importance. The contrast improvement is performed based on local information so that weak regions of the image are enhanced more than strong regions. This could be beneficial to experts when manually defining the edges for diagnosing purposes and also as a pre-processing stage for the automated analysis of heart function.

CHAPTER 5

AUTOMATED DIAGNOSIS SYSTEM TO DETECT ABNORMAL WALL MOTION

5.1 Introduction

The objective of this research is to develop an automatic diagnosis algorithm to identify myocardial ischemia or heart wall damage, as it is one of the leading cardiac related causes of death worldwide. The damaged heart muscle does not contract as much as the healthy heart muscle, leading to abnormal contractions in the heart wall. In this chapter, Eigenhearts, a novel Principal Component Analysis (PCA) technique based system is proposed to automatically diagnose this abnormality in the contraction of heart wall. Also, the Radon transform is applied in a novel way to extract features from the heart wall motion, which is subsequently used to identify wall motion abnormality.

Studying LV wall motion abnormality in an ischemic heart [KACH2006] using Echo analysis suffers from significant inter and intra observer variability. The proposed automated diagnosis algorithm intends to reduce such variability, to improve accuracy and increase reproducibility of Echo sequence interpretation over visual interpretation. Also, the automated diagnosis tool aims to help in efficient use of the medical expert's time by identifying the abnormality so that they can look into it in detail.

The remainder of this chapter is organized as follows. An overview of the proposed algorithm for abnormal heart wall motion detection along with its block diagram is

presented in the section 5.2. Section 5.3 describes the process of creating the composite motion image by detecting the heart wall boundaries in all the frames of the echo movie. Section 5.4 explains the dimensionality reduction stage of the algorithm, followed by the extraction of feature, called Eigenhearts, in the section 5.5. The classifier used to recognise and classify the extracted features in order to identify the abnormality in the heart is explained in the section 5.6. The different distance metrics used is also described in this section. The results obtained for both synthetic and real echo image database are presented in the section 5.7. Finally, Section 5.8 presents the concluding remarks.

5.2 Overview of Automated Abnormal Wall Motion Diagnosis Algorithm

A high level overview of the automated diagnosis algorithm to detect abnormal heart wall motion is shown in Fig. 5.1. When a patient Echo data is obtained, the image preprocessing is performed and the LV boundary edges are obtained. These boundary edges obtained for the entire echo image are used to create a composite motion image. The automated diagnosis can then be performed. Three different approaches are considered in the following.

In the first approach, Principal Component Analysis (PCA) is applied to the composite motion (CM) image to reduce the dataset and extract the features which are processed by a classifier to identify the abnormality. In the second approach, PCA is applied to the CM image to reduce the dimension of the dataset, followed by feature extraction using Independent Component Analysis (ICA). These features are subsequently used to classify the heart wall abnormality. In the third approach, the Radon transform is applied to the CM image to extract the symmetry features, which are used to classify the abnormality. Once the contraction abnormality is detected, a possible presence of heart wall damage is detected and the risk of heart failure in the future can be diagnosed. These stages in the algorithm are discussed in detail in the following sections.

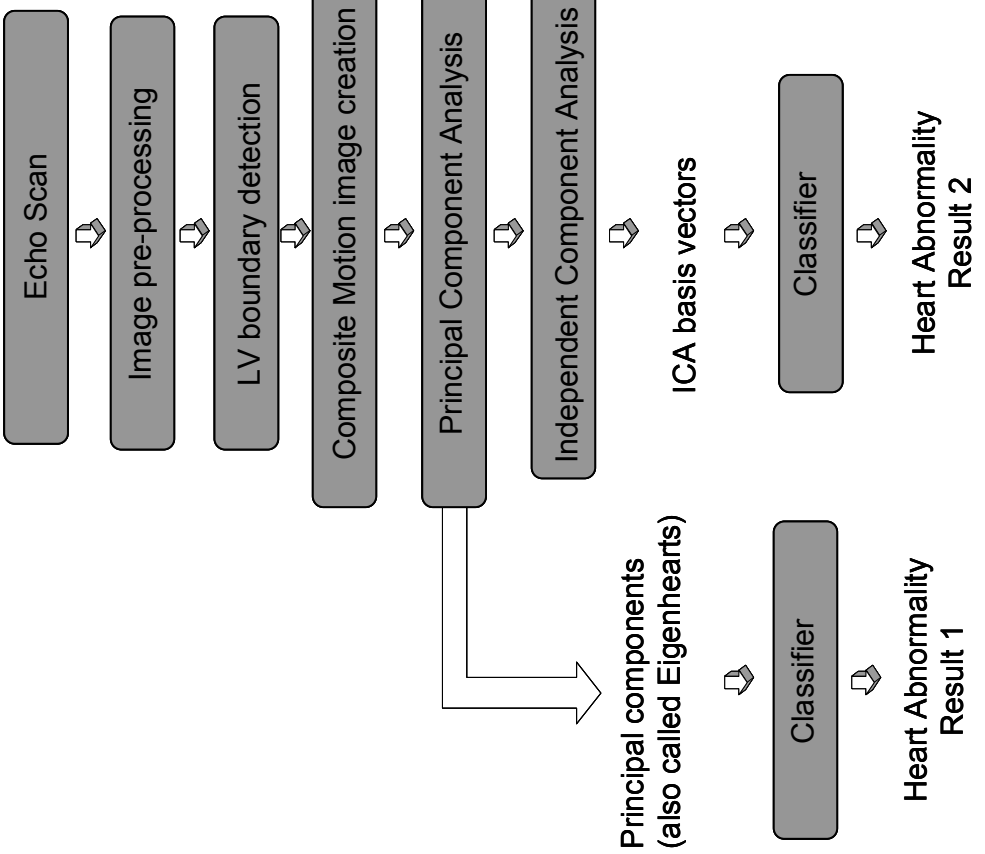

Fig 5.1 Automated Diagnosis for Abnormal Wall Motion

5.3 Composite motion (CM) image creation

An Echo scan is a movie captured over a time period, to cover a complete cardiac cycle. The systole of the left ventricle refers the contracted phase of the chamber, while the diastole refers to the relaxed phase of the chamber. The chamber position at systolic phase and the diastolic phase is significant in order to obtain information on the contractility of the heart wall. An echo movie consists of complete cycle including end-systole to the end-diastole of the LV. The movement of the inner layer of the heart wall (endocardium) and the outer layer of the heart wall (epicardium) are used by experts to identify the wall motion abnormality. Hence, the LV wall boundaries are detected for each frame and the edges obtained for all the frames between the end-systole and the end diastole are used to create a composite motion image. Consequently, a set of composite motion images are obtained from different patients with varied heart wall segment abnormalities, by capturing the end-systole and the end-diastole frame from ultrasound scan movie, are stored in a database.

The basic block diagram for creating a composite motion image is shown in the Fig. 5.2. Once an echo scan movie is obtained, all the frames are extracted from the movie. The LV boundary detection, as described in section 4.4, is performed on individual frames to extract the endocardial (or inner wall) and epicardial (or outer wall) boundaries. Similarly, all the frames including the last frame are processed. The extracted endocardial or inner wall and epicardial or outer wall boundaries for all the frames are put into a composite image to show the movement of the heart wall from the contracted phase to the relaxed phase. This image is referred as the composite motion image. An example of a CM is shown in Fig 5.3 (e). The difference image shows two clear white bands where the inner white band represents the endocardial movement and the outer white band represents the epicardial movement. The LV boundary detection described in the section 5.3.1 and the process of the CM image creation using these edges is described in the section 5.3.2.

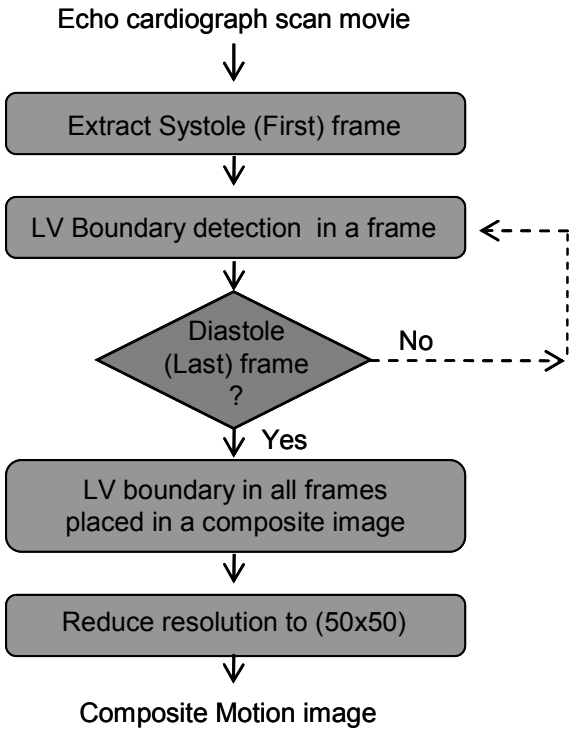

Fig. 5.2 Block diagram to show the stages in creating composite motion image

5.3.1 LV boundary detection

The left ventricular epicardial and endocardial boundary is detected by the Fuzzy multiscale approach as explained in Chapter 4. It is a center-based approach, where the edges are searched along the radial lines starting from the LV center. This Fuzzy multiscale edge detection technique comprises of

- Automatic LV center point detection (as described in section 4.4.1)
- The endocardial and epicardial edge points are extracted along the radial lines (originating from the LV center) using Fuzzy Multiscale Edge Detection (FMED) as described in section 4.4.2.
- Spatial/temporal processing of the extracted boundaries

Once the LV boundaries are extracted for all the frames in the echo movie, the CM image is formed as explained in the next section.

5.3.2 Composite motion image using LV boundaries

A composite image is created by combining the edges obtained for all the frames. The base image used is a black image of the size 200 x 200 with all zeros. The endocardial and epicardial contours obtained for all the frames in the echo movie are plotted in this image with the pixel value 255 (which corresponds to white). This composite image allows visualising the LV wall motion in different directions. The wall motion information in this image is of diagnostic importance, as the movement of the heart wall in a region relates to the health of that region. The composite image formed in some cases might have few outliers due to incorrectly detected edges in few frames of an echo movie, due to missing data in that frame (as shown in Fig. 5.3(a)). As the proposed algorithm involves recognition of patterns in the composite images, the presence of such outliers causes errors. To reduce these errors, the image is resized to 50x50 to produce an image as shown in Fig. 5.3(b) and its thresholded form as in Fig 5.3(c). The location of the LV is different in different echo movies. To eliminate the errors caused by this, the thresholded image is suitably cropped with 2 pixels on either side of the edge information as seen in Fig. 5.3(d). Then the image is resized to 50x50 for consistency through the image database. Fig. 5.3(e) shows clear bands in a composite motion image from a patient where the inner white band represents the endocardial movement and the outer white band represents the epicardial movement.

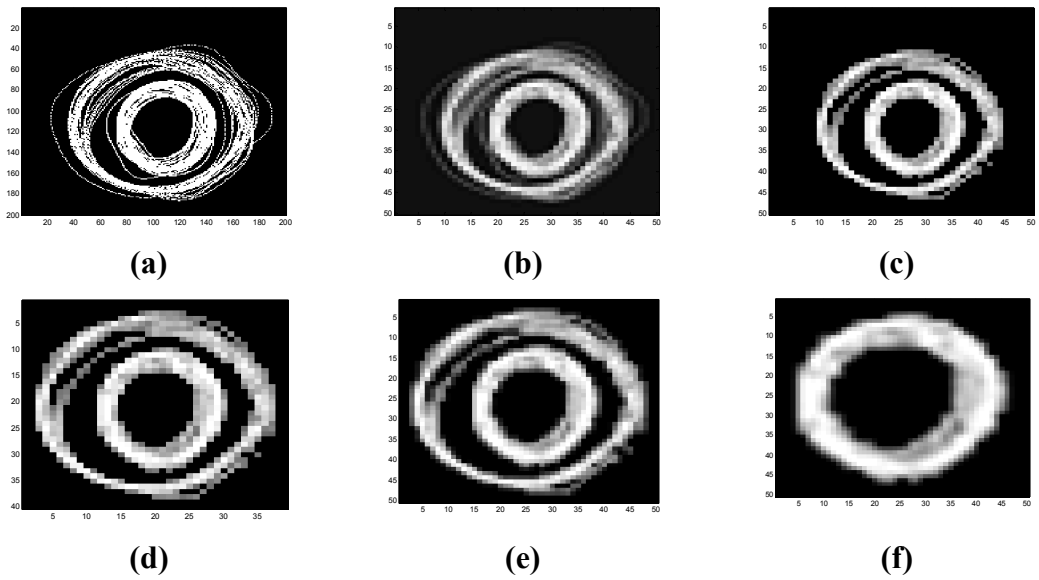

Fig. 5.3 Process of creating the difference image

Considering only the inner wall (endocardial) movement, the composite motion image is obtained as shown in Fig. 5.3(f).

5.4 Principal component analysis (PCA) approach

Principal component analysis (PCA) is a statistical technique that is widely used for pattern identification in large datasets with its applications in fields such as face recognition (eigenfaces) [TP11991, TP21991]. In this approach, PCA is applied to reduce the dimensionality in large datasets. Consider a database formed with a set of M heart scan images, Γ_1, Γ_2, Γ_3… Γ_M, consisting of both normal and abnormal cardiac movements. The average image of the M scan images is calculated by

$$\Psi = \frac{1}{M}\sum_{n=1}^{M}\Gamma_n \tag{5.1}$$

A difference vector between each heart image and the average image is obtained as shown below as:

$$\Phi_i = \Gamma_i - \Psi \tag{5.2}$$

Where $i=1...M$.

The covariance matrix of the image set, C is calculated by

$$C = \frac{1}{M}\sum_{n=1}^{M}\Phi_n\Phi_n^T = AA^T \tag{5.3}$$

where

$$A = \left[\Phi_1\Phi_2...\Phi_M\right]$$

Eigenvectors (which is a set of M orthonormal vectors, u_k) and their associated eigenvalues, λ_k of the above covariance matrix C are calculated [TP11991]. These vectors are arranged in order of significance, based on their eigenvalues. Any heart image can be described and classified using the top m PCA vectors (more significant), while the less significant ones (which typically represent minor features within the images or noise) can be ignored to reduce computation. The required number of top PCA vectors $(m < M)$ is determined heuristically.

In order to classify a new heart image, Γ, it is first converted into its eigenheart components by [TP11991]

$$\omega_k = u_k^T \left(\Gamma - \Psi\right) \tag{5.4}$$

where $k = 1...m$

Then, the weight vector $\Omega^T = \left[\omega_1, \omega_2 ... \omega_m\right]$ is formed which describes the input of each eigenheart in representing the new heart image. The weight vector of the new image and the images in the database are analysed by a classifier to identify the abnormality.

5.5 Independent Component Analysis (ICA) approach

ICA technique, a generalisation of PCA, was originally developed for separating mixed signals in cocktail party problems. In this approach, PCA is applied to reduce the dimensionality in the datasets, followed by applying ICA to extract the features. Independent component analysis is a method for finding underlying factors or components from multivariate (multidimensional) statistical data [HO2000]. This section describes the ICA implemented for heart image classification using the info-max algorithm [BS1995]. The objective of ICA is to find a set of basis images which are statistically independent. Each of the top 'm' PCAs is arranged in a separate row of a matrix X. The ICA algorithm is applied to this matrix producing 'm' independent components (IC).

Sphering of the matrix X is performed to reduce computational complexity. A sphering matrix W_Z is obtained from the matrix X as follows [BART2002]:

$$W_Z = 2 * (Cov(X))^{-(1/2)} \tag{5.5}$$

This step makes the mean and covariance zero so that the first and second order statistics are removed. The ICA algorithm produces a matrix W_I given by

$$W_I = W W_Z \tag{5.6}$$

where W is the weight matrix learned by ICA, which is updated by the learning rule [BS1997],

$$\Delta W = (I + Y' U^T) W \tag{5.7}$$

where I is the identity matrix, $U = WX$ is the linear combinations of inputs, $Y = f(U)$ and the logistic function used is

$$f(u) = \frac{1}{1+e^{-u}} \tag{5.8}$$

The IC representation of the images based on the m statistically independent basis images, U is given by [BART2002]

$$B = R_m W_I^{-1} \tag{5.9}$$

where R_m is the PC representation of the database based on the top m PC vectors. Likewise, the IC representation of any new image can be obtained by,

$$B_{new} = R_{new} W_I^{-1} \tag{5.10}$$

The classification of a new image into one of the predefined heart classes is based on nearest neighbour classifier [CH1967]. The distance between the new image and each heart class is calculated with a different distance metric such as the Euclidean, City-block and Cosine distance metrics, defined as

$$d^2{}_{Euclidean}(a,b) = \|a-b\|^2 \tag{5.11}$$

$$d_{City-block}(a,b) = |a-b| \tag{5.12}$$

$$d_{Cos}(a,b) = -\frac{a \,.\, b}{\|a\| \,.\, \|b\|} \tag{5.13}$$

where a, b denote the vectors and d is the distance between them.

5.6 Radon transform approach

The Radon transform is an integral transform proposed by J. Radon [RADON1917], which is widely used in computerised tomography (CT) medical imaging. The inverse of the transform is used to reconstruct images from CT scans [WEISSTEIN]. The Radon transform is also used in line and curve detection [PETER 1996] applications within image processing, computer vision as it can be considered as a form of template matching [GINKEL2004]. [ROUL1997] proposed a Radon transform based technique to reconstruct a map of a planet's polar region using a spacecraft in a polar orbit. The Radon transform is defined by

$$R_{p\tau}\{f(x,y)\} = \int_{-\infty}^{\infty} f(x, \tau + px)\, dx \tag{5.14}$$

where f(x, y) is a 2-D function in R^2 domain and y coordinate of f(x, y) occurs on the line $y = \tau + px$ in x-y space [DURRANI1984]. Using the sampling property of the delta function, the equation can be written as

$$R_{p\tau}\{f(x,y)\} = \int_{-\infty}^{\infty}\int_{-\infty}^{\infty} f(x,y)\delta[y - (\tau + px)]dy\, dx \tag{5.15}$$

A symbolic representation of Radon transform is given by

$$R_{p\tau}\{f(x,y)\} \equiv U(p,\tau) \tag{5.16}$$

where p is the slope of a line and τ is its intercept.

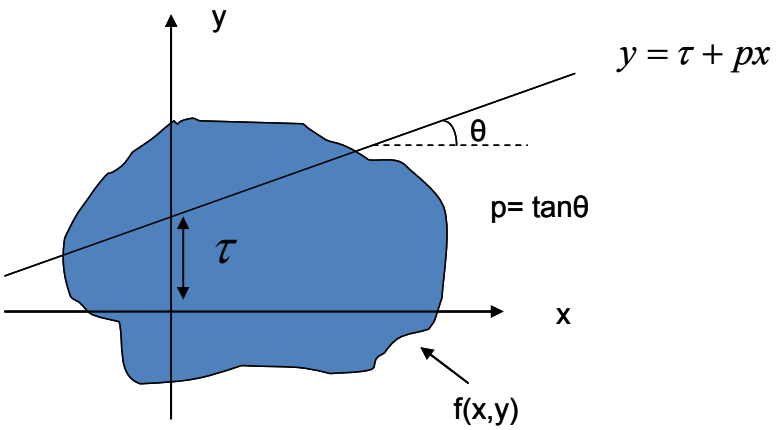

Fig 5.4. Integration of an object along the line $y = \tau + px$

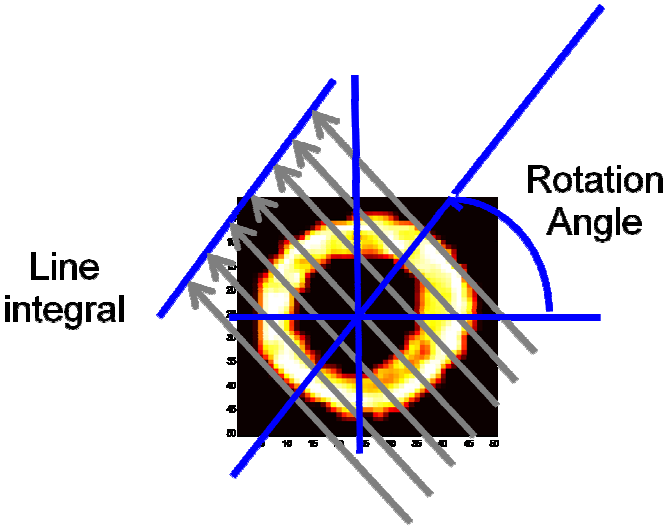

(a)

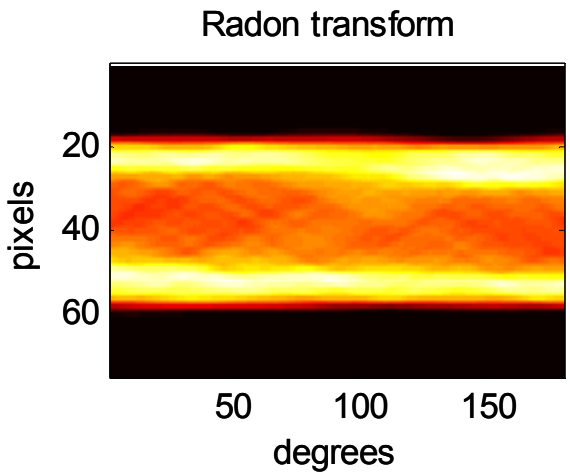

(b)

Fig. 5.5. (a) Concept of line integrals and Radon transform and (b) Radon transform of the Composite Motion (CM) image

In our approach, the Radon transform is applied to identify the symmetry in the composite motion image. The CM image is projected as a set of line integrals. Multiple line integral along parallel paths is obtained. This process is repeated for a different angle from 0 -179 degrees, as the multiple line integral in the angles from 180 -359 degrees is the same as the 0-179degrees. The Radon transform of a CM image with normal wall motion is shown in Fig. 5.5. It can be seen in Fig. 5.5 (b) that the Radon results in two bright bands, which are approximately parallel. Wall motion indicators can be extracted from this to identify abnormal wall motion.

5.7 Results and discussion

Echo images can be recorded in different views, each of which is important to identify critical parameters to evaluate different heart conditions. Here, the short axis mid-cavity view is considered. An average of 25 frames is present in each echo movie. When an Echo scan of a patient is obtained, the composite motion image is obtained and stored in a database. This section describes the experiments that were performed and the results that were obtained. The experiments were carried out with both simulated database and real database. The simulated database was used to prove that the algorithm works for the identification of the abnormality in the heart wall as the real database has limited images with same segment abnormality. The experimental results obtained for classification by performing the PCA approach is discussed in section 5.7.1, the results for the ICA approach is discussed in section 5.7.2 and the Radon transform approach in section 5.7.3.

5.7.1 Heart Abnormality Diagnosis Result 1 - PCA approach

The results obtained by the PCA approach on the simulated and real dataset are discussed in this section.

5.7.1.1 Simulated dataset results

In case of the simulated database, the composite motion (CM) images are stored in a database. The CM images with image resolution of 130 X 123 pixels, is stored in tagged image file format (.tiff file) in a database. The images are gray scale with pixel values ranging from 0 to 255. The database consists of 28 synthesized difference images of short axis mid-cavity echocardiograms representing 4 different classes with 7 images each. Fig 5.6 shows the 28 database images. The images on the first row are normal heart movements, while the rest of the images represent synthesised movement of heart with segment abnormalities.

To locate the contraction failure abnormality, the myocardium and the left ventricular cavity are segmented. The myocardial segments are considered based on the standards [CER2002], which suggest that the left ventricle should be divided into

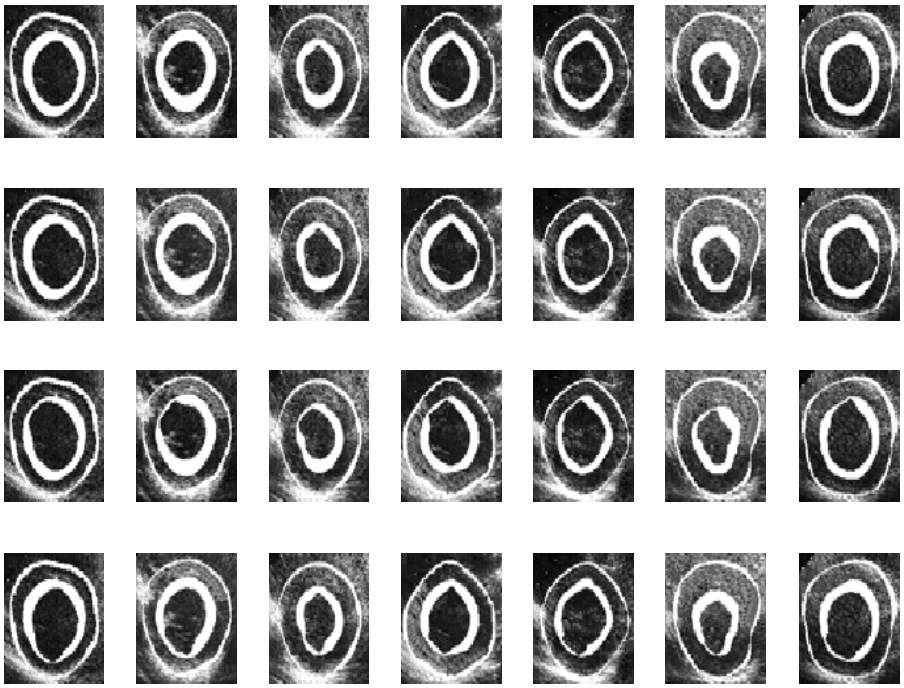

Fig 5.6. Simulated database (28 image)

17 segments. These 17 segments can be assigned to one of the three major coronary arteries, as shown in Fig 2.5. In the short axis view, the mid-cavity slice is divided into 6 segments of 60 degrees each, named mid anterior, mid anterioseptal, mid inferoseptal, mid inferior, mid inferolateral and mid anterolateral. Based on these standards, a database is formed with simulated data. The database consists of normal heart CM images and heart CM images with contraction failure in three different

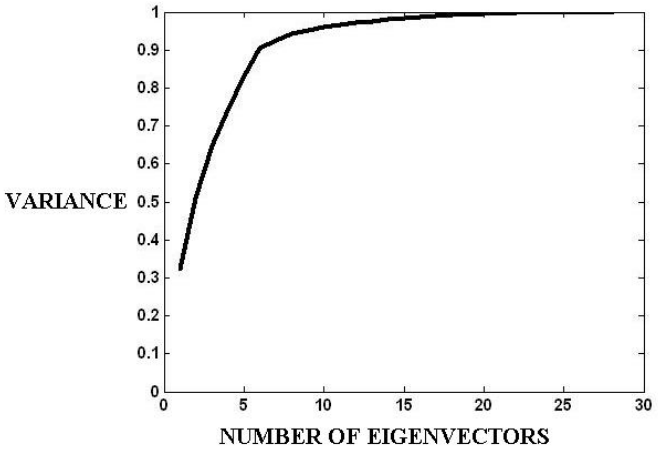

Fig 5.7.Variance plot showing the variance of the images in the simulated dataset (28 image dataset)

regions in the database are grouped into different classes based on the segment abnormality present (same segment failure are grouped into a class). The classes described here are: class 1 - normal; class 2 - 7th and 8th LV segment abnormality; class 3 - 9th and 10th LV segment abnormality; class 4 - 11th and 12th LV segment abnormality. When the new image is classified into one of the classes, 2, 3 or 4, the image is said to have a contraction failure in that particular segments. By locating the segment, the cause for the potential heart failure could be diagnosed. The fault in the corresponding coronary artery that supplies blood can be identified. In this approach, PCA is applied to the composite motion images derived from the heart echo. In this technique, the eigenvalues and eigenvectors of the covariance matrix for the dataset is computed. Any heart CM image could then be represented as a weighted sum of these eigenvectors in a multidimensional heart space. To recognize if a new heart CM image belong to a normal wall motion set or one of the abnormal wall motion set in the database, the image should be within the heart space and should be close to one of the classes in the image data set. The Eigen vectors obtained by performing principal components analysis was used for classification. The first experiment is carried out to investigate the classification of a new image (not in the database) with a segment deformity into the correct class to locate the damaged segment. As the images in the database are limited, when one of the images is considered as a new image, it is removed from the database, also called the 'leave one out method'. The variance between the images in the database is low and hence the number of top eigenvectors used for recognition must be high to give discrimination.

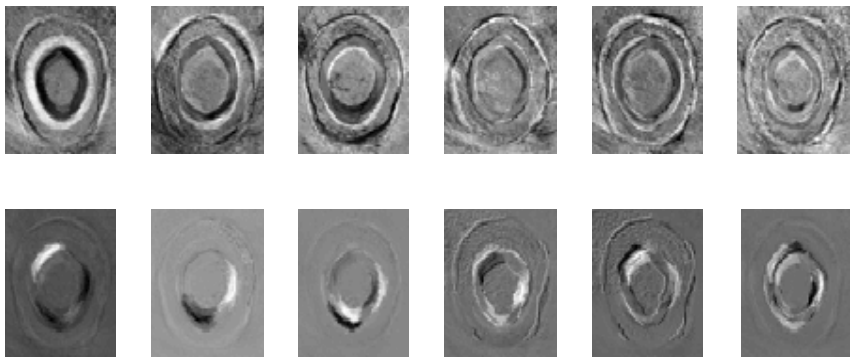

Fig. 5.8. Top 12 eigen vectors used for recognition

Fig 5.7 shows the variance plot for the test performed with 28 images in the database for which 97% variance corresponds to top 12 eigenvectors. The top 12 eigenvectors are presented in the Fig. 5.8. Correct recognition of 69% was obtained when a nearest neighbour classifier was used. In the second experiment, the effects of the severity of the segment contraction abnormality in recognising the segment are investigated. Modifications are made to all images other than the normal images in such a way that the abnormality is reduced representing an earlier stage of the abnormality. An example of the modified segment abnormality is shown in Fig 5.9. The aim of this experiment was to see if the correct segment is identified with the earlier stage deformity. 21 images were used for testing, out of which correct classification was obtained for 14 images.

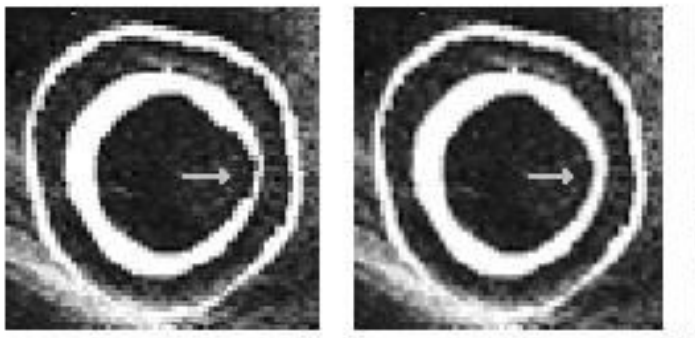

Fig. 5.9 Original image (left), modified image (right). The arrows in the figure show the contraction failure in the segment.

5.7.1.2 Real dataset

The composite motion image obtained from each real echo movie data is stored in a database. The CM images are gray scale with pixel values ranging from 0 to 255 and have image resolution of 50 x 50 pixels. The real database consists of 62 images in total with 27 normal hearts and 35 abnormal hearts, which are annotated by medical experts. The abnormal hearts used in the database had varied levels of wall damage. The scoring of the segments in some cases was 2 (representing hypokinetic segments) and in other it was 3 (representing akinetic segments). In the case of real data, the segmental damage could be present in more than one segment of a heart, that is,

- different wall segments which are supplied with blood by different coronary arteries are damaged
- the segment adjacent to the damaged segment also have wall motion abnormality.

So, the assigning the class for a difference image becomes complicated. For example, an echo movie which has wall motion abnormality in segments 10, 11 and 12 cannot be grouped as Class 3 or Class 4 (as described in the simulated image classification, in Section 5.8.1). In the real data obtained, only 50% of the abnormal heart data had segment abnormality in related segments (wall segments which are supplied by the same coronary artery) such as 7th & 8th segments, 9th & 10th segments, and 11th and 12th segments. The rest had abnormality in segments adjacent to the related segments. There is ambiguity in assigning a class for the heart CM images. Hence, the segmental analysis has to be performed to identify the abnormal segments (which is presented in chapter 6).

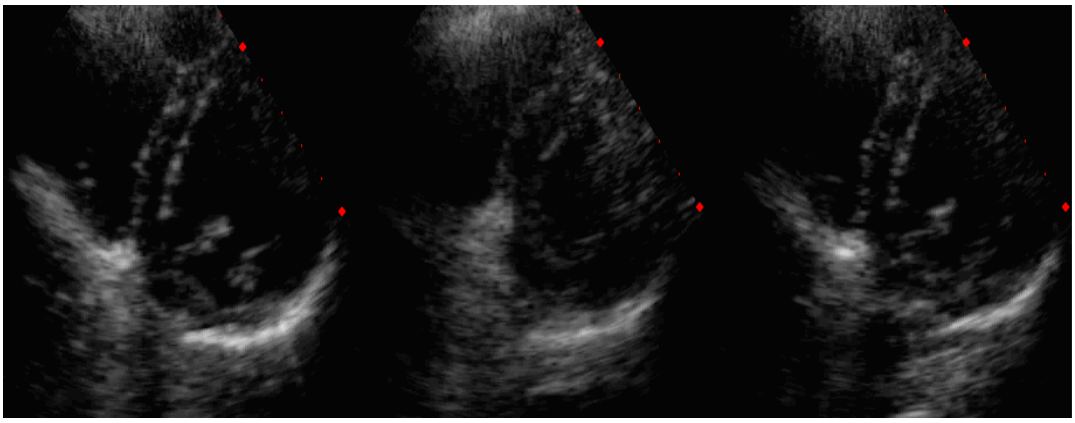

(a) The top right section of the LV epicardium falls outside the image plane

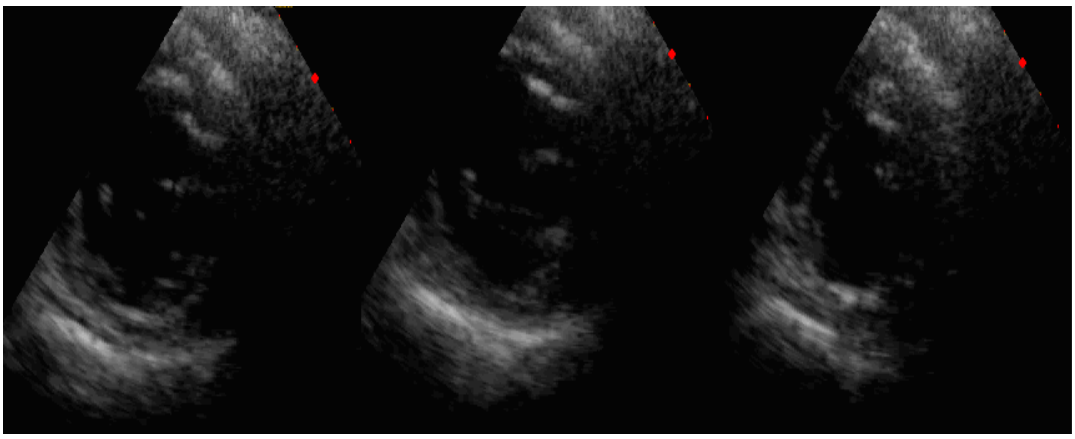

(b) The top left section of the LV falls outside the image plane

Fig. 5.10. Echo frame showing SA echo view where a section of the LV epicardium falls outside the imaging plane

Experiment was performed to analyse the wall motion of the entire LV in order to identify the presence of wall motion abnormality. In the experiment, the CM images used in the database and the new heart CM image considered only the inner wall movement. The outer wall movement is not considered as some of the echo images obtained for analysis had the LV outer wall region outside the imaging plane as seen in the Fig 5.10. Sample CM images in the real dataset which shows normal heart wall motion and abnormal heart wall motion are shown in Fig.5.11.

The PCA based algorithm is used to classify the real heart data using the features extracted from the CM image. The top 18 PC vectors was used out of which top 6 PC vectors are shown in Fig 5.12. The k-Nearest Neighbour classifier was employed with Euclidean distance, City-block distance and Cosine distance metrics. The results obtained are shown in Table 5.1. The Euclidean and the City block distance metric provided a correct classification of 81%, while the Cosine distance metric provided a correct classification of 77%. The correct classification of the negative cases and the positive cases are referred as True negatives (TN) and True positives (TP) respectively. In the case of diagnosis of an abnormality, the experts consider the incorrect recognition as either false positives (FP) or false negatives (FN). A False positive is the term which refers to incorrectly categorizing a heart to be abnormal. A False negative is the term which refers to incorrectly categorizing a heart to be normal. The performance of a classifier can also be measured by sensitivity and specificity.

Sensitivity is a measure of correctly identified actual positives, which is given by

$$Sensitivity = \frac{Number\ of\ True\ Positives}{Number\ of\ True\ Positives + Number\ of\ False\ Negatives} \quad (5.17)$$

Specificity is a measure of correctly identified negatives, which is given by

$$Specificity = \frac{Number\ of\ True\ Negatives}{Number\ of\ True\ Negatives + Number\ of\ False\ Positives} \quad (5.18)$$

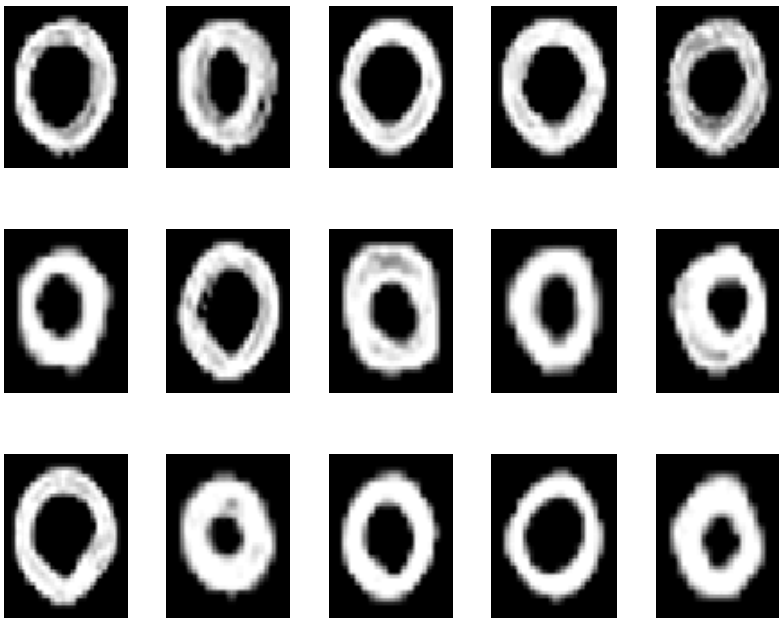

(a) Sample images showing normal heart wall motion

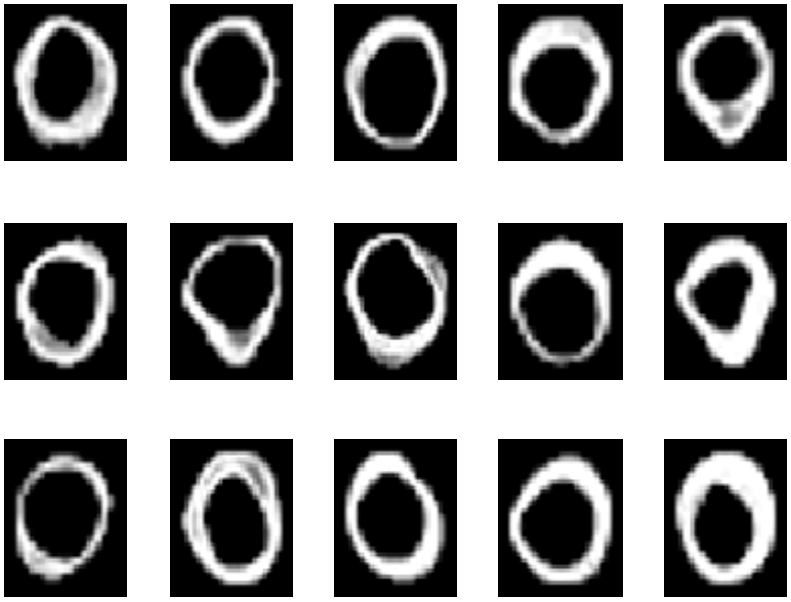

(b) Sample images showing abnormal heart wall motion

Fig. 5.11 Composite motion images (constructed using the inner wall motion) in the real heart image database.

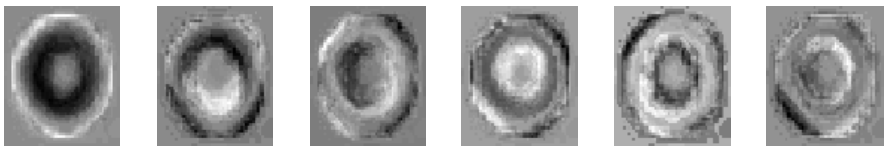

Fig. 5.12 Sample PC vectors obtained from the real dataset (Top 6)

The sensitivity and specificity measures obtained for the classifiers are shown in Table 5.1. The classifier with good sensitivity is required as the abnormal hearts should not be classified as normal hearts. The three k-NN outputs can be combined by various rules such as sum, product rule, max rule, min rule etc[ALEX2001][KIT1998]. In a comparative study between the rules on combining the classifiers, [KIT1998] concluded that sum rule outperformed. For this purpose of identifying the abnormal heart wall motion, the outputs of the classifiers are summed along with conditions as shown in Fig.5.13. The outputs are combined by voting scheme as shown in Fig. 5.13(a) which provided a correct classification of 79%. The outputs are combined as shown in Fig. 5.13(b), in such a way that even if one classifier identifies a heart to be abnormal, it is classified as abnormal. This provides a correct classification of 84% and the highest sensitivity of 83%. In Table 5.2, it can be seen that the combined k-NN has better classification and sensitivity when compared to Bayes classifier, binary SVM and Linear classifiers.

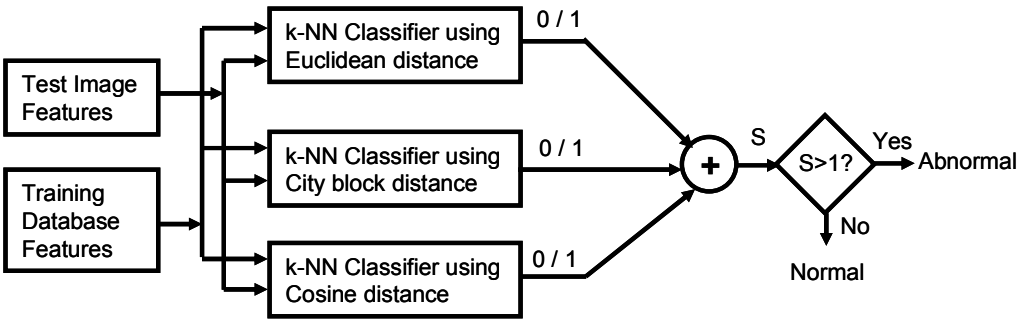

(a) Combining k-NN outputs by voting

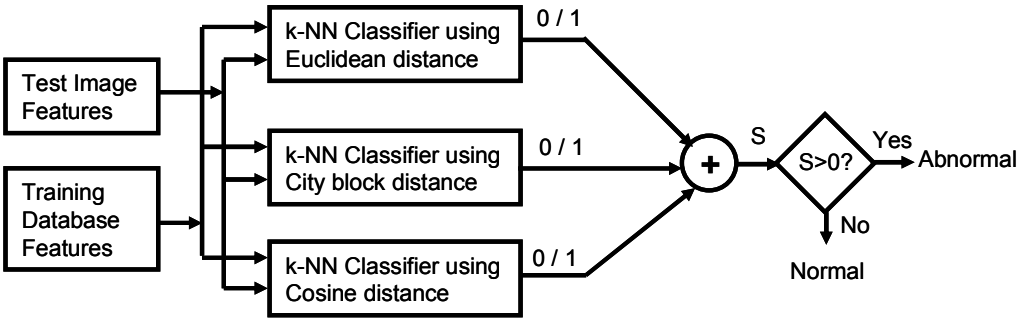

(b) Combined k-NN

Fig. 5.13 Combining the classifier output

Classifier	k-NN using Euclidean distance	k-NN using City block distance	k-NN using Cosine distance	Combining the 3 k-NN outputs by voting	Combined k-NN
% Correct Recognition	81	81	77	79	**84**
Specificity (%)	89	89	96	96	**85**
Sensitivity (%)	74	74	63	66	**83**
True Negatives	24/27	24/27	26/27	26/27	**23/27**
True Positives	26/35	26/35	22/35	23/35	**29/35**
False negatives	9/35	9/35	13/35	12/35	**6/35**
False Positives	3/27	3/27	1/27	1/27	**4/27**
Correct Recognition	50/62	50/62	48/62	49/62	**52/62**

Table 5.1 Performance of PCA approach using k-NN classifiers

Classifier	Combined k-NN	Bayes	SVM	Linear
% Correct Recognition	**84**	76	81	79
Specificity (%)	**85**	81	96	96
Sensitivity (%)	**83**	71	69	66
True Negatives	**23/27**	22/27	26/27	26/27
True Positives	**29/35**	25/35	24/35	23/35
False Negatives	**6/35**	10/35	11/35	12/35
False Positives	**4/27**	5/27	1/27	1/27
Correct Recognition	**52/62**	47/62	50/62	49/62

Table 5.2: Performance of PCA approach using different classifiers

5.7.2 Heart Abnormality Diagnosis Result 2 - ICA approach

The results obtained by ICA approach on the simulated and real dataset are discussed in this section.

5.7.2.1Simulated dataset

The ICA approach is performed on the same dataset with 28 images, as explained in section 5.7.1.1. Experiments are carried out to investigate the classification of a new image (not in the database) with a segment deformity into the correct class to locate the damaged segment. The 'leave one out method' is considered due to the number of images in the dataset. The top 12 eigenvectors obtained from the PCA are used as input to the ICA to extract the 12 ICA basis vectors. The ICA basis vectors obtained are shown in the Fig. 5.14. The recognition performance of the ICA approach for the three cost functions is observed. A correct recognition of 81% is obtained using Euclidean distance metric. The city block and cosine distance metric yield correct recognition of 72% and 75% respectively.

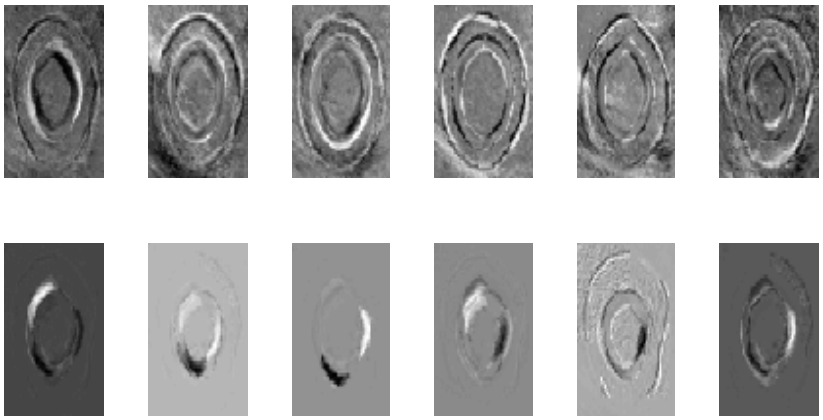

Fig. 5.14. Top 12 ICA basis vectors used for recognition

5.7.2.2 Real dataset

The real dataset which consists of composite motion images as described in section 5.7.1.2. The ICA based algorithm is used to classify the real heart data using the features extracted from the CM images with only the inner wall movement. The total number of data used for testing was 62 out of which 27 hearts had normal wall

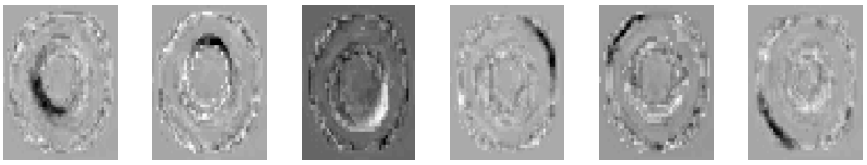

Fig. 5.15. ICA basis vectors obtained from the real dataset (Top 6)

movement and 35 hearts had abnormal wall movement. The top 6 ICA basis vectors out of the 18 vectors used, are shown in Fig. 5.15.

Table 5.3 shows the performance of the ICA approach using the different distance metrics used with the k-NN classifiers. The k-NN classifier using the Cosine distance metric provided the best classification. The combined k-NN classifier also provided the classification result of 84% (with a sensitivity of 74%), same as the cosine metric, while the Euclidean and City block distance metrics provided 74% and 79% respectively.

Classifier	k-NN using Euclidean distance	k-NN using City block distance	k-NN using Cosine distance	Combined k-NN
% Correct Recognition	74%	79%	84%	84%
Specificity	100%	96%	96%	96%
Sensitivity	54%	66%	74%	74%
True Negatives	27/27	26/27	26/27	26/27
True Positives	19/35	23/35	26/35	26/35
False Negatives	16/35	12/35	9/35	9/35
False Positives	0/27	1/27	1/27	1/27
Correct Recognition	46/62	49/62	52/62	52/62

Table 5.3 Performance of ICA approach using k-NN classifiers

5.7.3 Heart Abnormality Diagnosis Result 3 - Radon Transform approach

The Radon transform is applied on the CM images and the abnormal wall motion indicator is extracted. The radon transform of a normal CM images has approximately parallel continuous bright bands. To extract an indicator, sum of the projections is performed. Fig. 5.16 shows sample normal and abnormal heart CM images, its Radon transform and the sum of the projections. It can be seen in row sum of a normal CM image's Radon transform,(as seen in Fig. 5.16 (c)), that the two peaks corresponding to the bright bands are approximately of the equal in value and the area under the two peaks is approximately equal. In the row sum of an abnormal CM image's Radon transform,(as seen in Fig. 5.16 (f and i)), the two peaks corresponding to the bright bands and the area under the two peaks are significantly different. So the ratio of the peak values and the ratio of the area under the two peaks are considered as two measures for classifying the heart as normal or abnormal. By performing multiple experiments, 1:0.85 was set as the ratio of the peak values and 1:0.75 was set as the ratio of the area under the peaks. The classification result obtained was 73%, with a sensitivity of 66% and specificity of 81%.

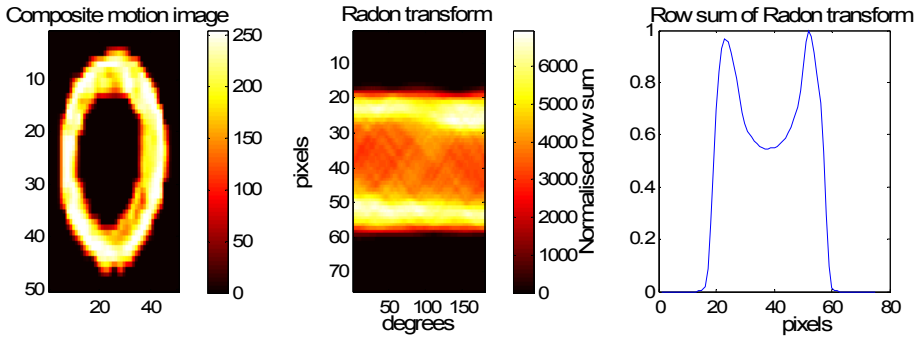

(a) (b) (c)

Normal heart wall motion (sample1)

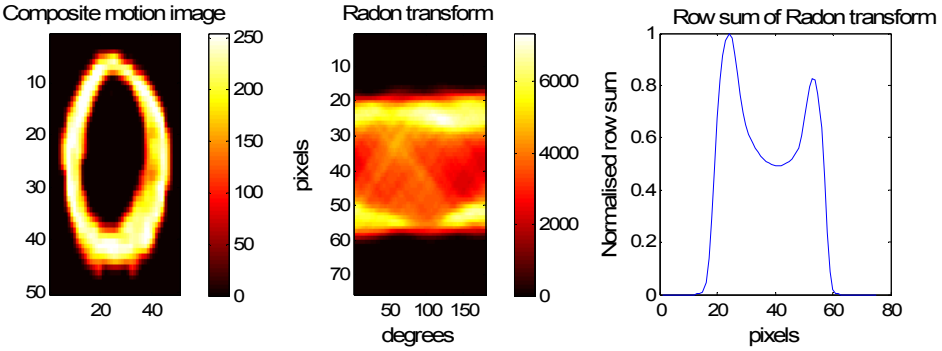

(d) (e) (f)

Abnormal heart wall motion (sample1)

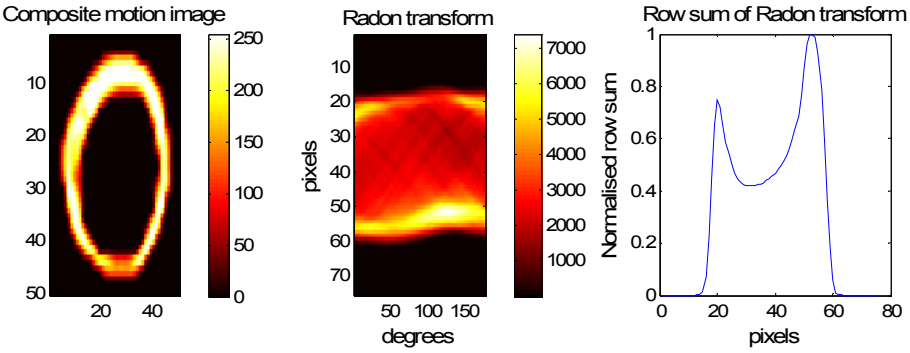

(g) (h) (i)

Abnormal heart wall motion (sample2)

Fig. 5.16 Composite motion images (a, d, g), its corresponding Radon transform in (b, e, f) and the sum of the projections in (c, f, i)

5.7.4 Comparison between PCA, ICA and Radon approach

The confusion matrix of the PCA, ICA approach and Radon approach is shown in Table 5.3 to show the actual classification and predicted classifications performed by the system. Radon transform approach provided a correct classification of 73%, which is notably less than the 84% obtained by the PCA and ICA approaches suggesting that the PCA and ICA features perform better than the Radon transform based features extracted from the row sum of the projections.

In the simulated dataset, the data with the same segment abnormality was put in a class and the correct identification of the class corresponding to the abnormal segment was performed. For the simulated dataset, ICA performed significantly better than PCA to identify the segment abnormality from the composite motion image. As ICA decomposes the CM image into local shape descriptors, it has advantages over PCA for local shape classification.

In the case of the real dataset, the data was grouped into normal and abnormal CM images and a binary classification of the CM image to identify wall motion abnormality was performed. For this dataset, ICA and PCA performed similar, as the presence of abnormality was important, while the position of the abnormality was not important. For this particular dataset, ICA and PCA with combined k-NN classifier perform similar to provide same correct classification, but the sensitivity of the PCA approach is 83%, which is higher than the ICA approach (74%).

As the sensitivity of the approach has to be high to avoid the abnormal hearts to be classified as normal, the PCA approach is more appropriate for the overall Myocardial Ischemia Detection Algorithm, which is discussed in the next chapter.

Correct Classification=52/62 Specificity=85% Sensitivity=83%		Predicted	
		Negative (Normal)	Positive (Abnormal)
Actual	Negative (Normal)	True Negative 23/27	False Positive 4/27
	Positive (Abnormal)	False Negative 6/35	True Positive 29/35

(a) Using the PCA approach

Correct Classification=52/62 Specificity=96% Sensitivity=74%		Predicted	
		Negative (Normal)	Positive (Abnormal)
Actual	Negative (Normal)	True Negative 26/27	False Positive 1/27
	Positive (Abnormal)	False Negative 9/35	True Positive 26/35

(b) Using the ICA approach

Correct Classification=45/62 Specificity=81% Sensitivity=66%		Predicted	
		Negative (Normal)	Positive (Abnormal)
Actual	Negative (Normal)	True Negative 22/27	False Positive 5/27
	Positive (Abnormal)	False Negative 12/35	True Positive 23/35

(c) Using Radon approach

Table 5.4: Confusion matrix for the heart wall motion abnormality classification (Tested images = 62, Normal hearts = 27, Abnormal hearts = 35)

5.8 Conclusion

In this chapter, echocardiography image sequences are processed using a PCA, ICA and Radon transform based system to locate abnormality in heart wall contraction. The results obtained here are the classification results for identifying the wall motion pattern in the composite image. The results to date indicate that the peak ratio and the area under the peak ratio extracted from the Radon transform are not alone sufficient to classify the heart abnormality correctly. The PCA and ICA based features that are extracted from the composite motion images are more suitable for recognising the patterns and the results indicate that it can be effective in identifying the presence of wall motion abnormality. Also, it is anticipated that the percentage of correct recognition of 83 % can be further improved using a larger database and optimising the program for the current dataset.

The wall motion abnormality is a manifestation of the ischemic heart disease or the heart wall damage. Being able to identify the heart wall abnormality with different levels of scoring indicate that the heart wall damage can be identified accurately, at any stage. Once the system automatically diagnoses the wall motion abnormality, the cardiologist can analyse that heart in detail. This could act as a beneficial tool to experts when assessing the health of the heart. The performance of locating a segmental deformity can be improved by considering the movement of individual segments for classification rather than the heart movement as a whole. This automatic detection system is never a replacement for the medical experts, but it is a diagnostic tool to make their life easier.

CHAPTER 6

MYOCARDIAL ISCHEMIA DETECTION ALGORITHM: MIDA

6.1 Introduction

One of the aims of this research is to identify the presence of heart wall damage, when an Echo scan is recorded. Though the echocardiography sequence analysis is performed to assess the overall performance of the left ventricle, segmental analysis is required to identify wall abnormalities within individual segments. An algorithm based on the FMED heart wall boundary detection is developed by incorporating the principal component analysis based approach (described in chapter 5) to identify the presence of heart wall damage and locating the abnormal segment in the short axis view. The Myocardial Ischemia Detection Algorithm (MIDA), heart abnormality diagnosis and a wall segment classification algorithm to identify the abnormal movement and indirectly the wall damage or myocardial ischemia is presented in this chapter. The algorithm uses the wall edges to extract the characteristic features of the wall segments and combine them using a voting scheme to decide on the normality of the heart segment.

This chapter is structured as follows. An overview of the Myocardial Ischemia Detection Algorithm (MIDA) with the overall block diagram is presented in the section 6.2. The section 6.3, presents the details on the extraction of global features (that provide information on the health of the heart) and the local features (that provide information on the health of the heart wall segment) from the LV borders to

describe the health of the heart wall segments. Section 6.4 provides details on the regional wall motion synchrony analysis which is performed by the extracting the displacement of the wall segments in the complete cardiac cycle. Section 6.5 provides the result obtained for the identification of the heart abnormality and the location of the segmental damage. Finally, conclusions are presented in section 6.6.

6.2 Myocardial Ischemia Detection Algorithm (MIDA) overview

This section gives an overview of the Myocardial Ischemia Detection Algorithm, which is proposed to perform heart abnormality analysis and heart wall segmental analysis of the echocardiography to detect the myocardial ischemia in the left ventricle. The different stages involved in this algorithm are discussed here. Fig. 6.1 shows the high level overview of the MIDA algorithm.

1. When a patient Echo scan is obtained, the image pre-processing (noise reduction and Delaunay triangulation based image enhancement) is performed on the echo image as explained in the Chapter 4.

2. The centre point in the LV cavity is identified. Fuzzy membership functions to represent the local and global knowledge, which are then combined by fuzzy logic operators to identify candidate LVCP pixels. A template matching is performed to obtain the most likely LVCP from the candidates.

3. Then, the LV boundary is identified by searching along the radial lines originating at the LVCP, by applying Fuzzy Multi-resolution Edge detection technique as explained in section 4.4. This radial search based approach is particularly suitable as the LV wall motion is oriented in the radial direction.

4. For performing the heart abnormality analysis, the PCA based approach on the Composite Motion image constructed by the LV edges extracted from the Echo images (as discussed in Chapter 5) is applied to extract the feature describing the abnormal wall motion which are then used to classify a heart into normal or abnormal heart.

5. Global features are extracted from the LV boundary edges, which describe the health of the heart. The different features extracted are discussed in detail in section 6.3.1. The global features are also used to decide on the heart abnormality.

6. The segmental features are extracted from the LV boundary edges, which describe the health of the heart segments. The different features extracted are discussed in detail in section 6.3.2

7. The segmental features are used individually to make a decision on the segment abnormality, which consecutively helps identify the myocardial ischemia in the segment.

8. The decision outputs obtained by using all the features are combined to make a final decision on the segment damage or abnormality.

The algorithm also provides graphs which show the variation in the heart feature, which are helpful in visualising the changes in a complete cardiac cycle. The variation in segmental features along the entire cardiac cycle are also visualised to check the relative measures of the six segments in the mid cavity SA view. The algorithm also performs regional wall motion synchrony analysis by the extracting the displacement of the wall segments in the complete cardiac cycle. When there is blockage in the path of the 'Bundle of His' or the conducting cells, the message sent from the from the Sinu Atrial node to the wall muscle to contract is not received on time resulting in irregular or asynchronous contraction or wall movement.

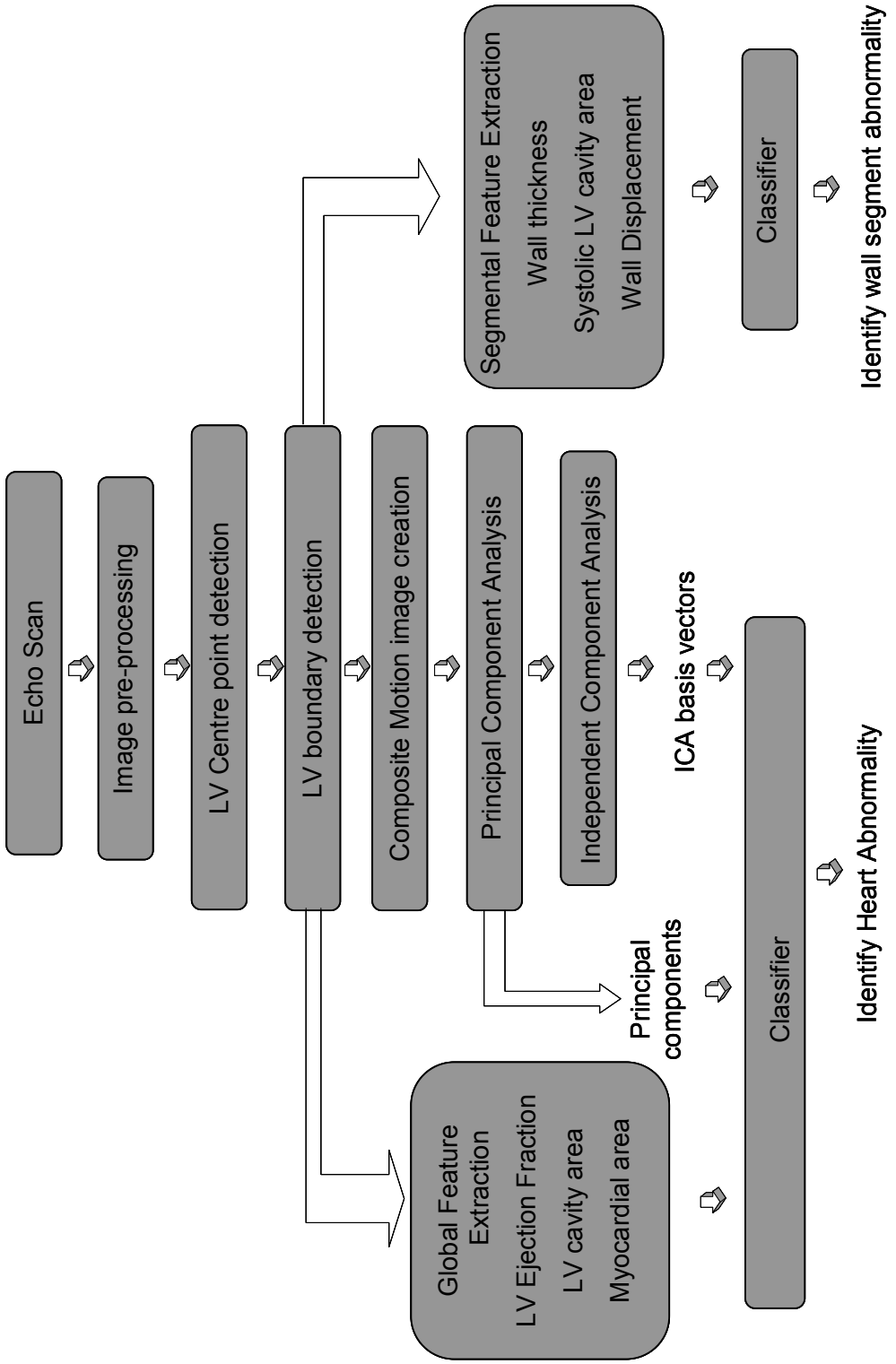

Fig. 6.1 Myocardial Ischemia Detection Algorithm (MIDA) overview

6.3 Features extracted from the LV boundary

The heart wall boundary, both the inner and outer wall contains global and local information about the heart wall which determines the health of the heart. The global features extracted from the heart wall boundaries include ejection fraction, LV cavity area, and myocardial area. The local or segmental features extracted from the boundaries area LV segmental cavity area, average wall thickness in the segment, maximum wall excursion in the segment. The steps involved in extracting the different features are described in this section.

6.3.1 Global features

The global features extracted from the LV are based on the average radius of the endocardial and epicardial LV boundary. The average radius of the LV endocardium is determined from the endocardium to compute average diameter. The average radius of the inner has a maximum value at the end- diastole and has a minimum value at the end systole. Fig. 6.3(a) shows the average radius along the complete cardiac cycle.

6.3.1.1 Ejection fraction

The Volume of the LV is determined by using the equation 3.6 and the ejection fraction is determined by computing the end – diastole volume (which is the largest volume measured in the complete cardiac cycle) and the end-systole volume (which is the smallest volume measured in the complete cardiac cycle). Ejection fraction is obtained for one cycle to determine the volume of blood ejected during that heart beat. The ejection fraction in healthy individuals typically have ejection fractions greater than 0.5 (50%) [VASAN1999]

6.3.1.2 LV cavity area

The LV cavity area along the complete cardiac cycle, determined in the previous step is normalized by dividing it by the end-diastole cavity area. The LV cavity area has a maximum value at the end- diastole and has a minimum value at the end systole. Fig. 6.3(c) shows the LV cavity area over the complete cardiac cycle. It can be seen that the normalized systolic LV cavity area is around 0.3 for a sample healthy heart with

an ejection fraction of 73.26%. The normalized systolic LV cavity area is around 0.6 for the sample heart with abnormality, which has an ejection fraction of 40.7%.

6.3.1.3 Myocardial area

The myocardial area or the tissue area in the LV wall can also be determined as the difference between the total LV area and the LV cavity area, as shown in equation 3.7. The total LV area is determined by using the average radius of the epicardium or the outer wall. The LV cavity area is determined by using the average radius of the endocardium or the inner wall. The variation of the myocardial area in an echo scan is given in Fig. 6.3(b)

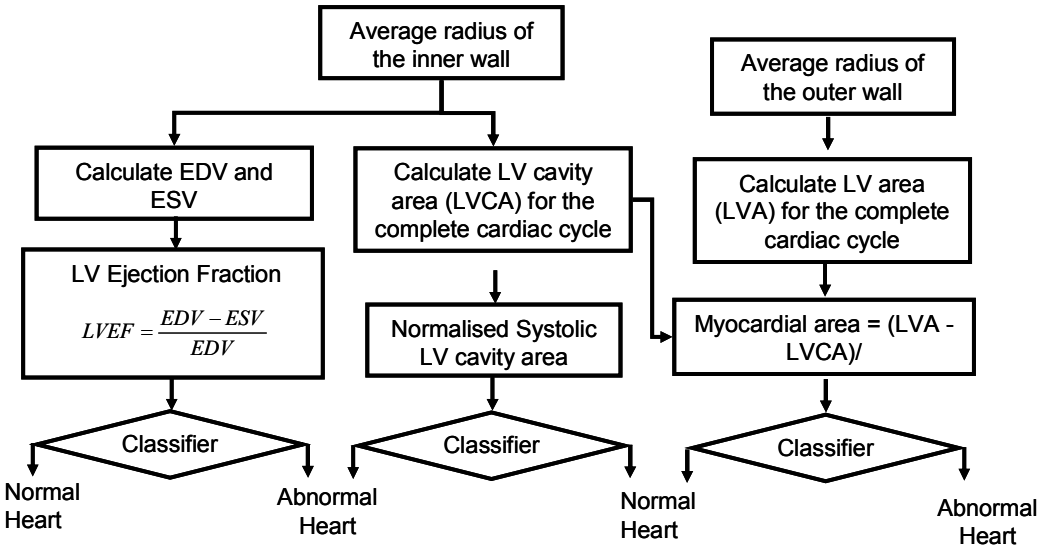

Fig. 6.2 Extraction of global features from the LV inner wall and outer wall edges

These global features give information on the health of the heart and are used for identifying abnormality. To analyze the health of the segmental tissue in the heart wall, local features extracted from the segments is essential, which is discussed in the next sub-section.

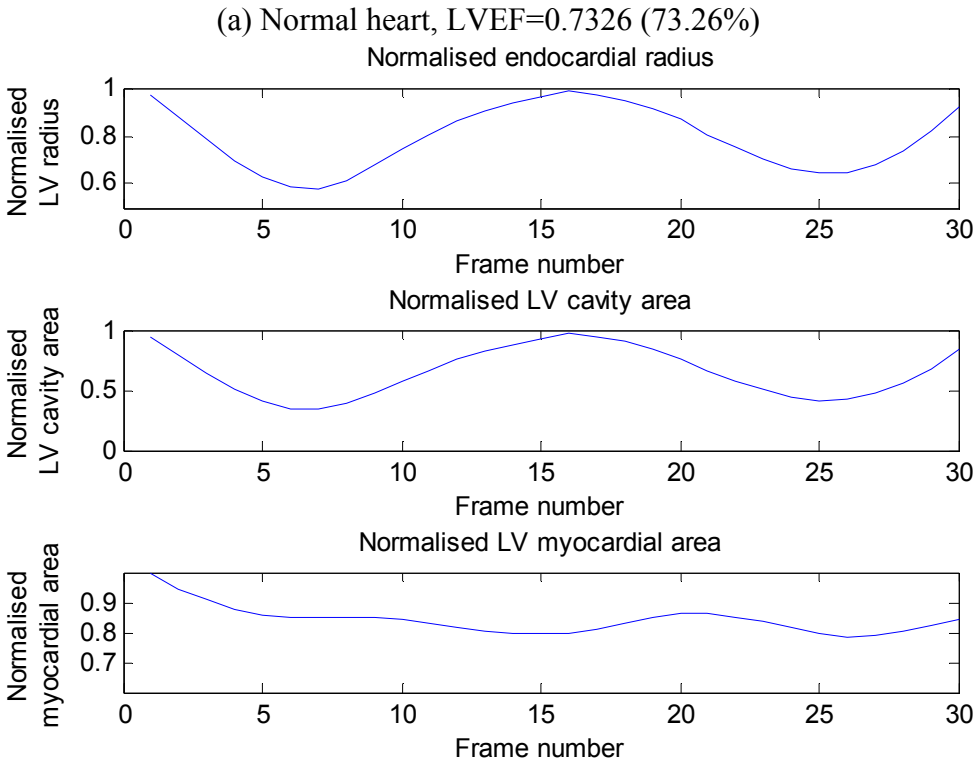

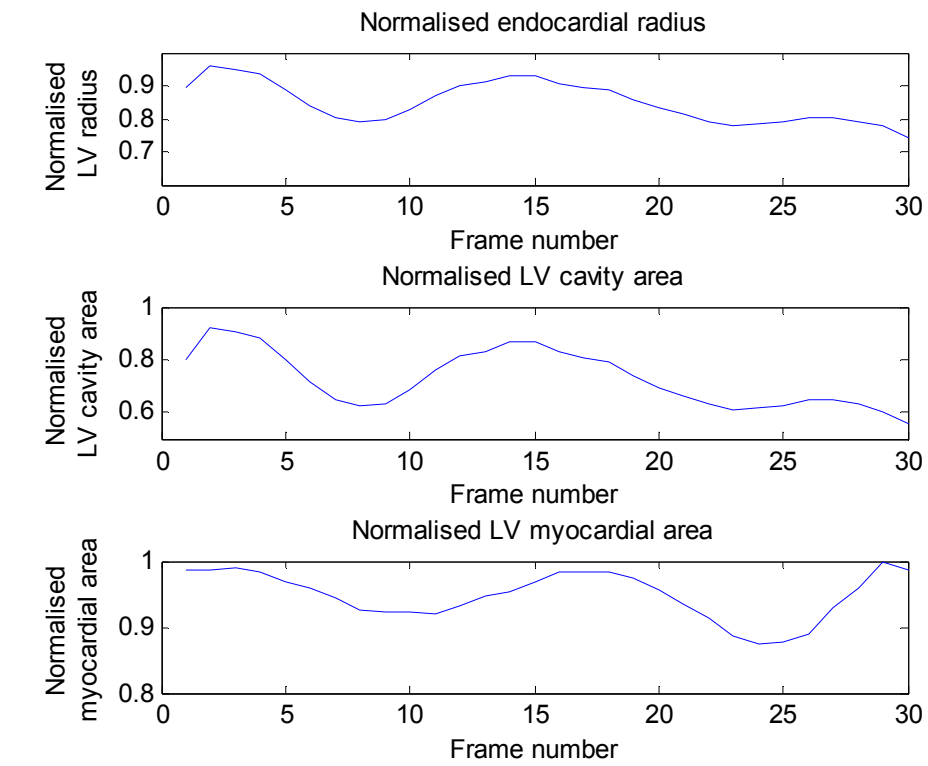

Fig. 6.3 Global features extracted from the LV boundary showing the normalized radius, cavity area and myocardial area for the entire Echo scan

6.3.2 Local or Segmental features

The short axis (SA) view of the heart obtained in the mid-cavity (or papillary muscle) level and basal level is divided into 6 segments based on the segmentation standards [CER2002]. We consider the mid-cavity SA view in this research, which is divided into 6 segments with each segment angle of 60^o, as shown in Fig. 6.4. As the LV wall boundary edge point is extracted along the radial lines in the SA view, the extraction of segmental features is straight forward and is discussed next.

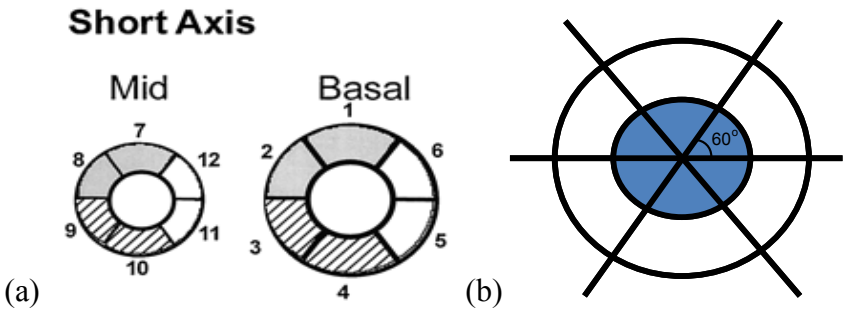

Fig 6.4 (a) Standard segmentation for mid cavity and basal SA view
(b) Dividing the LV into 6 segments with each segment angle of 60^o

6.3.2.1 Local cavity Area

Each segment is considered to be a circular sector with a central angle of 60^o. The local cavity area of the ith segment is determined by the following equation

$$Local\ Cavity\ Area_i = \frac{\theta}{360} \times \pi r_i^2 \tag{6.1}$$

where i =1,2….6,

θ is the central angle and r is the average radius of the LV endocardium for the ith segment . The LV centre point and the endocardial boundary is used for determining the cavity area. Fig. 6.5 shows the segmental LV cavity area variation along the entire Echo scan of a normal heart and an abnormal heart. The local cavity area varies with a minimum value at the end-systole and maximum value at the end-diastole for a normal heart as seen in Fig 6.5(a). The systolic cavity area for all the segments is lower showing that the segments are normal Fig 6.5(b) shows the local

cavity area of an abnormal heart, which has larger systolic cavity area for abnormal segments or probable abnormal segments.

6.3.2.2 Wall thickness measurement

Instantaneous wall thickness is measured as the difference between the radius of the epicardium and the endocardium. The wall thickness within each segment is averaged to get a wall thickness measure for that segment. The myocardial wall thickness variation for the 6 segments is shown in Fig. 6.6. The difference between the wall thickness at ES and ED is normalised by ED wall thickness to obtain the Fractional Myocardial Wall Thickening (FMWT) (by equation 3.11).

For a normal heart, the heart wall has maximum thickness at the systole. Therefore, the positive value for the fractional myocardial wall thickening suggests that the myocardium is normal [NOBLE2002]. Fig. 6.6(a) shows the segmental wall thickness of a healthy heart which has a positive fractional myocardial wall thickening measure for all the segments. Fig. 6.6(b) shows the segmental wall thickness of a unhealthy heart which has a negative fractional myocardial wall thickening measure for the segments 7 and 9, indicating the presence of abnormality. The segmental wall thickness variation is also not in line with the normal variation. The Fractional Myocardial Wall Thickening measure for all the six segments for more images is provided in Appendix A. The graphs showing the change in the global and segmental features along the entire cardiac cycle is also presented in the Appendix B.

(a) Normal heart IS_Img2

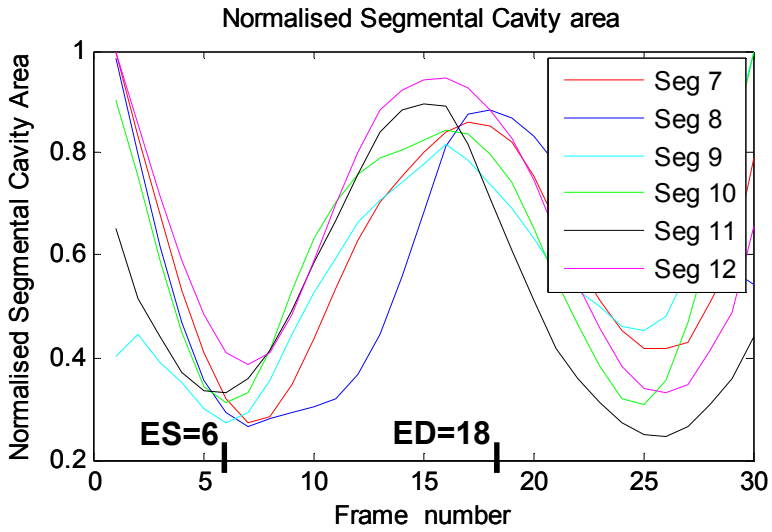

(b) Abnormal heart IS_Img4

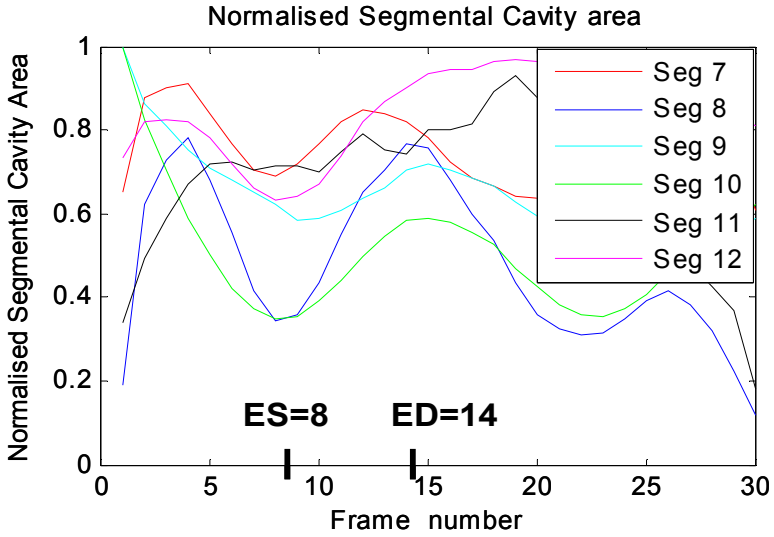

Fig. 6.5 Normalised segmental cavity area for the entire scan

(a)Normal heart IS_Img2

Fractional Myocardial Wall Thickness is positive for all the segments

Seg 7	Seg 8	Seg 9	Seg 10	Seg 11	Seg 12
0.5816	0.1341	0.2271	0.2763	0.0739	0.4029

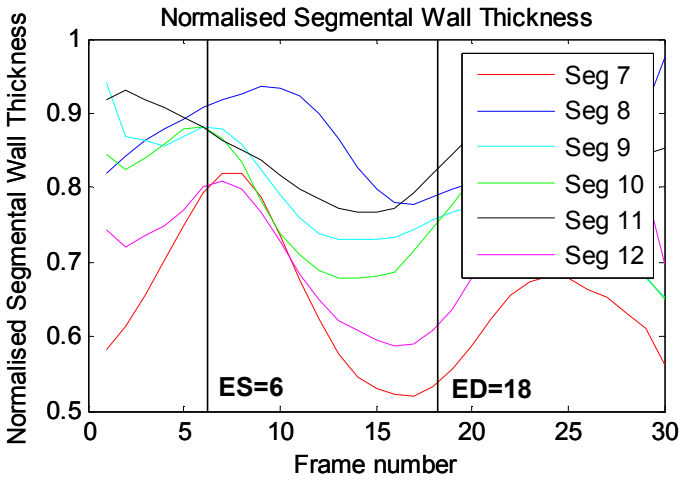

Abnormal heart IS_Img4

Fractional Myocardial Wall Thickness is negative for Segment 7 and 9

Seg 7	Seg 8	Seg 9	Seg 10	Seg 11	Seg 12
-0.1273	0.3780	-0.0573	0.1209	0.0384	0.3920

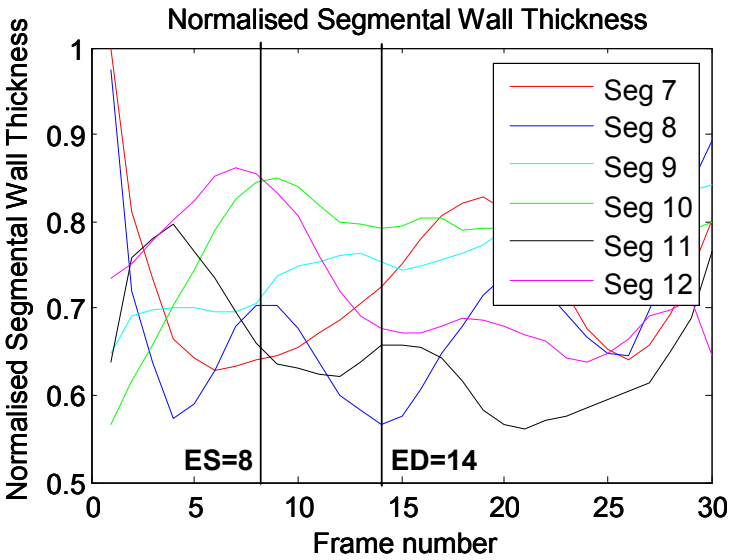

Fig 6.6 Normalised segmental wall thickness for the entire scan

6.3.2.3 Wall Displacement measure

The motion distance between the endocardial wall edges in ES frame and the rest of the frames is determined. The wall displacement within each segment is averaged to get a wall displacement measure for that segment. A wall displacement (WD) or maximal endocardial wall excursion measure is also determined by computing the difference between the maximum wall displacement of the wall edge and the minimum wall displacement of the wall edge, which is then normalised by the largest wall displacement (Equation 3.10). The variation in the wall displacement for the 6 segments of a normal heart is shown in Fig. 6.7. It can be noted that all the segments move synchronously, but the maximum movement differs for different segments. The regions where the right ventricle is attached to the left ventricle, the movement of the left ventricle is slightly restricted. In an abnormal segment, the wall displacement is significantly reduced, as seen in Fig. 6.8(c).

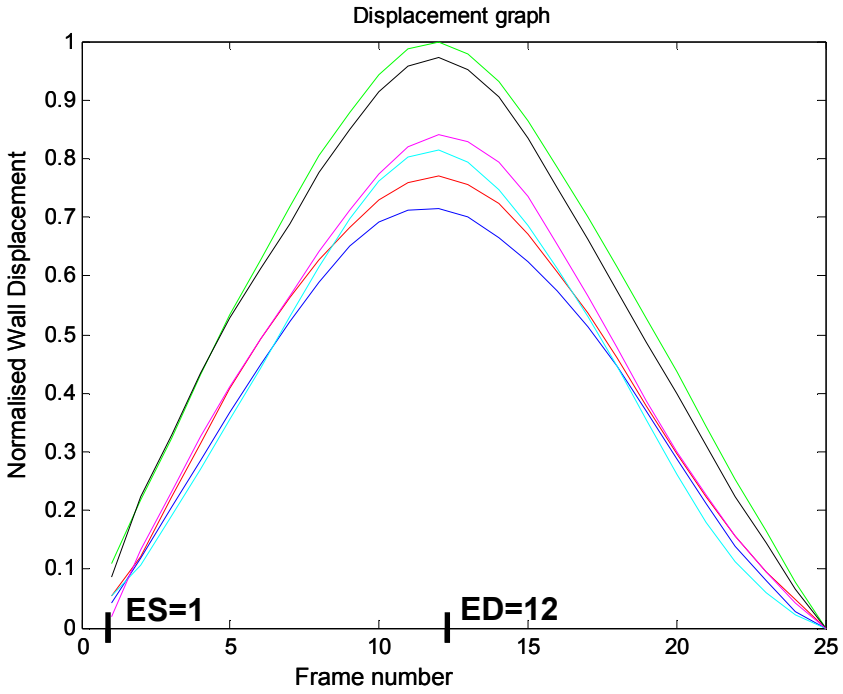

Fig 6.7 Displacement Graph showing the wall displacement from the systole to the end diastole

6.4 Regional wall motion synchrony analysis

The synchrony of the heart muscle contraction is an important factor which determines the overall performance of the heart, as it depends on the amount on the blood pumped. The regional asynchrony is responsible for a global decrease in diastolic filling in patients with myocardial ischemia. Though the increased asynchrony observed in patients with a normal left ventricular function generally has no clinical consequences, in patients with congestive heart failure (CHF), even a small decrease in ejection fraction may affect the diagnosis [EYLL1995]. The regional wall motion synchrony can be seen in the wall displacement graph obtained for a normal healthy heart in Fig.6.7.

The asynchronous movement in the wall segments is caused when different segments contract and relax at different times. To measure the asynchrony in segment motion, the peak position in the wall displacement graphs of all the segments is determined. The frame in which the segment is moving the maximum (that is the relaxed state of that segment) is identified. When all the segments have the maximum movement in the same frame, then they are synchronous. In an asynchronous case, one of the frames, which is close to the ED is considered to be a reference frame and the time difference between the peak positions of all other segments from the reference frame is measured. Regional wall motion asynchrony can be present in both normal and abnormal hearts. Fig.6.8 (a) shows a synchronous movement in normal hearts, (b) shows an asynchronous movement in normal hearts (a delay of 40ms in the relaxation of the segments 9, 11 and 12) and asynchronous movement (a delay of 40ms in the relaxation of the segments 7 and 12, and a delay of 280ms in segment 9) in abnormal hearts can be seen in (c). The displacement graph is a good visual representation of the wall motion asynchrony.

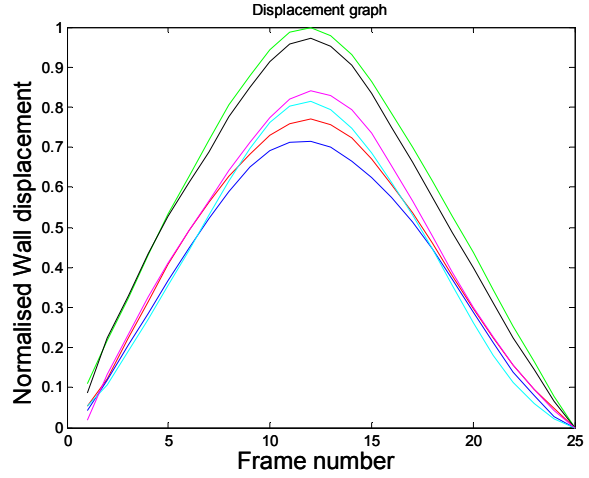

(a)

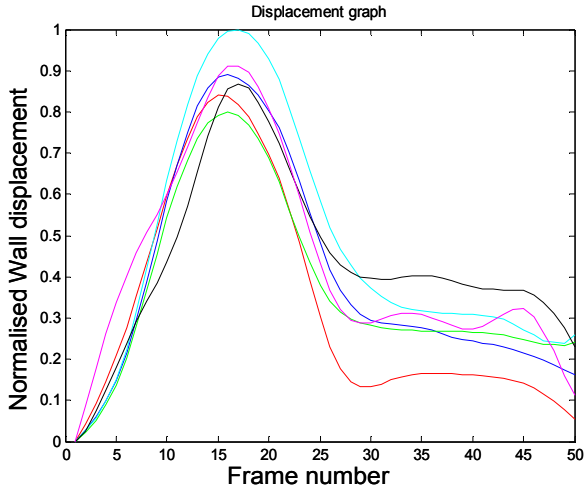

(b)

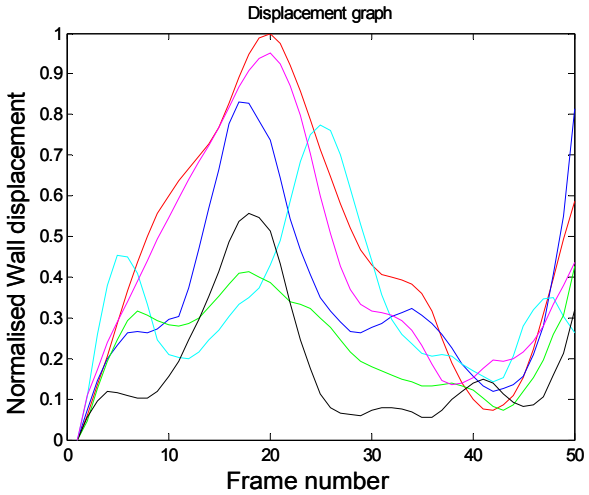

(c)

Fig 6.8 Wall Displacement graphs showing (a) synchrony in normal heart motion (b) asynchrony in normal heart motion, (c) asynchrony in abnormal heart motion

6.5 Results and discussion

As fractional myocardial wall thickness (FMWT) is one of the important measures that describe the health of the segment (or the presence of the myocardial ischemia), both endocardial wall (the inner wall) edges and the epicardial edges are required for the segmental analysis. The short axis mid-cavity Echo view patient data which had complete epicardial wall (outer wall) of the LV within the image plane was chosen for this experiment. The total number of patient data used for this experiment was 37, out of which 22 were normal hearts and 15 were abnormal hearts with abnormality in 31 segments (on an average 5 data had abnormal region in each segment). For example, in the case of identifying the abnormality in the 7th segment, there were 5 abnormal 7th segments and 32 normal 7th segments. For each Echo, both global and segmental features are extracted from the endocardial and epicardial wall boundaries and used for classification. This section discusses the classification results obtained for segmental damage and overall heart abnormality.

6.5.1 Regional features to identify segmental damage

The results obtained for the identification of segmental damage using the regional features such as normalised systolic segmental cavity area (SSCA), fractional myocardial wall thickening (FMWT), wall displacement (WD) measure is given in this section. The segments are analysed separately as the normal feature vary for different regions of the heart wall, for example, some segments have restricted wall motion, etc. The regional features are used individually to make a decision on the segment abnormality, which consecutively helps identify the myocardial ischemia in the segment.

The classification results obtained for the segments using the segmental cavity area, fractional myocardial wall thickening and maximum wall displacement measure can be seen in Table 6.1. It can be seen that the average accuracy for classification based on the normalised systolic segmental cavity area was 77%. The classification results obtained for the segments using the fractional myocardial wall thickening had a higher overall accuracy of 82%. The accuracy for classification of the segments using the wall displacement measure was 78%. It can also be noted that the FMWT

provided a better classification result for segments 7 and 12, WD provided better classification for segments 8 and 9, and, SSCA provided better classification for segments 10 and 11.

Segment	% Correct Classification using Systolic Cavity Area	% Correct Classification using fractional wall thickness	% Correct Classification using segmental wall excursion	% Correct Classification voting of all three features
S7	73	**92**	76	86
S8	76	73	**78**	78
S9	76	84	**95**	86
S10	**86**	84	81	89
S11	**84**	73	70	81
S12	70	**86**	70	86
Mean	**77**	**82**	**78**	**85**

Table 6.1 Classification result using the segmental features

Though the overall classification accuracy was better for the fractional wall thickening measure, none of the three segmental features gave better performance in more than two segments. This could be one of the exceptional cases due to the outliers in the dataset, but the manual interpretation incorporates all these factors in making a decision. The manual interpretation of the Echo data to identify the abnormal segments depends on the how the wall is moving, how far it is moving and how the thickness of the wall varies. Hence, these classification results from the features were combined to get a better classification result. Identifying the segments to be normal or abnormal based on the local cavity area, fractional myocardial wall thickness and maximum wall displacement can be combined in such a way that if any two of the segmental features suggest that the segment is abnormal, it is classified as abnormal segment, or vice versa. This method is called the voting scheme for combining the classifier output (represented in Fig. 6.9) to obtain better classification.

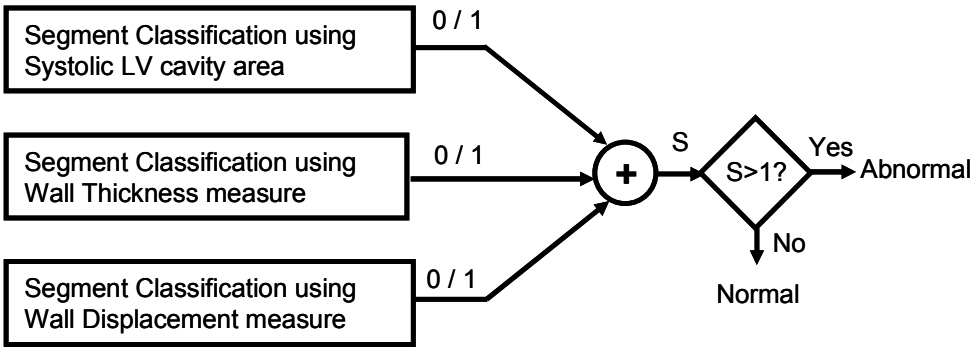

Fig 6.9. Voting scheme combination of classifier output
Normal, if S = 0, 1
Abnormal, if S = 2, 3

A	B	C	S=A+B+C	Normal/Abnormal
0	0	0	0	N
0	0	1	1	N
0	1	0	1	N
0	1	1	2	A
1	0	0	1	N
1	0	1	2	A
1	1	0	2	A
1	1	1	3	A

While combining the classification results, the logical AND operator is used to say that if it satisfies all the three conditions, it is classified as an abnormal segment. The classification result for the different combination of three features (SSCA & FMWT & WD, SSCA & FMWT, SSCA & WD, FMWT & WD and the combination using the voting from all the three features) is given in Table 6.2, showing that highest overall accuracy of 94% was obtained for the AND combination of the three features. Though, the AND combination of all the three features gave the best result among all the combination, to made a decision on the best combination based on the data used, the sensitivity has to be considered as each segment had only about 5 abnormal data. An overall sensitivity was best for the voting scheme which was 80% which was 14% greater that the AND combinations.

Segment	SSCA & FMWT & WD	SSCA & FMWT	SSCA & WD	FMWT & WD	Voting from SSCA & FMWT & WD
S7	93	92	86	92	86
S8	89	81	86	89	78
S9	97	89	95	97	86
S10	95	89	95	95	89
S11	95	89	92	89	81
S12	95	95	86	95	86
Mean	**94**	**89**	**90**	**93**	**85**

Table 6.2 Classification results by combining the segmental features

6.5.2 Heart function classification using global and regional features

The overall heart function classified based on the global features is discussed in this subsection. The global features used in this section for determining the health of the heart are normalised systolic LV cavity area and ejection fraction. As the two measures depend only on the endocardial boundary (the inner wall) edges, the total number of patient data used for this experiment was 62 patient data, which had 27 normal healthy heart data and 35 unhealthy hearts with abnormality. While using the systolic LV cavity area as a feature, a correct classification of 79% with a sensitivity of 89% and specificity of 67% is obtained. When the ejection fraction was used as a feature for classification, a correct classification of 76% with a sensitivity of 86% and specificity of 63% is obtained. The identification of the abnormality based on the PCA and ICA components from the composite motion image as the feature for classification gave an accuracy of 84%.

Feature used for classification	LVEF	Systolic LV cavity area	ICA components from CM image	PCA components from CM image
% Correct Recognition	76	79	84	84
Sensitivity (%)	86	89	96	83
Specificity (%)	63	67	74	85

Table 6.3: Comparison of the features used for classifying the heart abnormality

6.6 Conclusion

This chapter presented a Myocardial Ischemia Detection Algorithm (MIDA) which uses heart wall boundaries obtained using the FMED technique, to analyse the segments in the heart wall to identify the location of the heart wall damage. A good accuracy of 84.69% for identifying abnormality in the segments is obtained for the limited dataset consisting of 37 images. This system combines the three main segmental features to identify the abnormal segment. The results show that for the given data set, the voting scheme provides the good classification results with high sensitivity , when compared with classification using the feature alone and the combination to satisfy all the feature criteria. The present result is encouraging suggesting that using the suitable features and the classifiers can improve the performance of the identification of the abnormal segments.

Further work has to be performed with a larger dataset, which has approximately equal numbers of normal and abnormal segments in the dataset, so that the percentage of correct classification, sensitivity and specificity of the classification can be fairly assessed.

Further work has to be performed with a larger dataset which has a wide variety , that is, different levels of scoring to the segments. Analysis on the normal, hyperkinetic, hypokinetic, akinetic, or dyskinetic segmental feature have to be done so that the segmental features can be used to identify an automatic scoring level for the abnormal segments. For any segment, a percentage confident for different scoring level can be obtained so that it can be used to decide the score, which is most appropriate for that segment.

CHAPTER 7

CONCLUSION AND FURTHER DEVELOPMENTS

7.1 Concluding Remarks

This thesis investigated the various stages involved in the Echocardiography sequence analysis. The main focus of this research was to develop an automated Echo sequence analysis system for detection of heart wall motion and myocardial ischemia. A new integrated approach for myocardial ischemia detection was developed, including the left ventricle boundary detection, feature extraction, heart function parameters calculation and classification has been presented in this thesis.

A novel Delaunay triangular region based echocardiography image enhancement algorithm to improve the contrast between the tissue and the blood region is presented in this thesis. The algorithm integrates undecimated wavelet based speckle noise reduction, edge detection, followed by a regional enhancement process that employs Delaunay triangulation based thresholding. The fuzzy logic based centre detection and fuzzy multi resolution edge detection (FMED) are modified to identify the heart wall boundary. The results to date are encouraging and suggest that this region based enhancement improves contrast by preserving the edges and the anatomical structures, which are of diagnostic importance. The weak regions of the image are enhanced more than the strong regions as the processing is based on the local information. This could be beneficial to experts when manual markers are placed for defining the heart wall edges for diagnosing purposes. This acts as a pre-

processing stage for the automated analysis of Echo images to assess the heart function.

A novel Myocardial Ischemia Detection Algorithm (MIDA) for automated diagnosis of abnormality in the heart wall is developed. The system incorporates image enhancement, heart wall boundary detection, heart classification based on principal component based feature extraction, and segmental wall analysis. The composite motion image which is created using the heart wall boundaries provides information on the heart wall movement in a complete cycle. Principal component analysis, independent component analysis are applied to the composite images to extract heart abnormality detecting features, which is subsequently used to identify abnormal hearts. Radon transform is also applied to the composite images to determine the symmetry of the wall motion, which can be used to identify the abnormality. The segmental wall analysis is performed to identify the location of the heart wall damage. This system combines the three main segmental features such as normalised systolic segmental cavity area, fractional myocardial wall thickening and wall displacement measure to identify the abnormal segment. The results show that for the given data set, the voting scheme provides the good classification results with high sensitivity, when compared with classification using the features individually. The combination to satisfy all the feature criteria provide a very high classification rate, but the sensitivity is lower when compared to the voting scheme. In this study, a binary classification between normal and abnormal motion is proposed. The present result is encouraging suggesting that using the suitable features and the classifiers can improve the performance of the identification of the abnormal segments.

Being able to identify the heart wall abnormality with different levels of scoring indicate that the heart wall damage can be identified accurately, at any stage. Once the system automatically diagnoses the heart segment with wall motion abnormality, it indicates the possible presence of ischemia or wall damage in that segment. The abnormal segment can be related to the coronary artery that supplies blood to that segment based on the segmentation standards, to diagnose the possible cause for the ischemia (possible blockage in that artery) . This could act as a beneficial tool to

cardiology experts when assessing the health of the heart, the automatic identification of heart abnormality can lead to a detailed analysis by the experts.

7.2 Suggestion for Further developments

The remainder of this chapter highlights some of the further work opportunities arising from this work.

7.2.1 Improvements to MIDA algorithm

The results show that for the given data set, the voting scheme provides the good classification results with high sensitivity, when compared with classification using the features individually. The combination to satisfy all the feature criteria provide a very high classification rate, but the sensitivity is lower when compared to the voting scheme. Based on the study on this limited data set, a claim cannot be made on which feature is appropriate to identify the abnormality and the best method to combine the segmental features. In this study, the classifiers used hard decisions (0 or 1) to classify the abnormality based on the features. Using, classifiers which use soft decisions would provide better classification results when combining the classifier output. Also, further work has to be performed with a larger dataset, which has approximately equal number of normal and abnormal segments in the dataset, so that the percentage of correct classification, sensitivity and specificity of the classification can be fairly assessed. The pattern recognition techniques can be applied along with artificial neural networks to improve the classification performance of the system. Multilayer Perceptron (MLP) network and Radial Basis Function (RBF) network are the most popular neural network architectures, out of which RBF has provided better performance than MLP [VENKAT2006].

In the present study, a binary classification to identify normal and abnormal motion is proposed. The scoring of an abnormal motion, i.e., hypokinetic, akinetic, and dyskinetic, is not presented yet. The method is proposed as a computer-aided tool for the clinicians to identify the suspected abnormal motion areas in the myocardium. Further work has to be performed with a larger dataset which has a wide variety, that is, different levels of scoring to the segments. Analysis on the normal, hyperkinetic,

hypokinetic, akinetic, or dyskinetic segmental feature have to be done so that the segmental features can be used to identify an automatic scoring level for the abnormal segments. In this case of identifying different abnormalities, a multiclass classifier could be used to identify the classes with different abnormality. For any segment, a percentage confident for different scoring level can be obtained so that it can be used to decide the most appropriate score for that segment. This can be performed by fuzzy clustering, where each data is assigned with a set of membership levels that specify the level of the association between that data and a particular

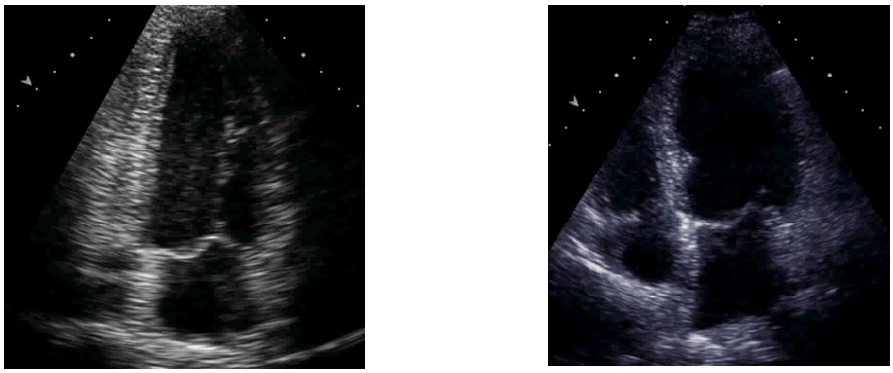

(a) (b)

Fig. 7.1 (a) 2 chamber view and (b) 4-chamber view Echocardiography

class. Fuzzy clustering using these membership levels to classify data to one or more classes [SHAH2000].

7.2.2 Extend to other views of Echocardiography

For illustration purposes, mainly the Short Axis view Echocardiography is considered within the scope of this work. The contrast image enhancement algorithm and Myocardial Ischemia Detection Algorithm (MIDA) can be extended to 2-chamber (2C) and 4-chamber (4C) views of echo scans to identify heart wall abnormality. Fig. 7.1 shows (a) 2 chamber view and (b) 4-chamber view Echocardiography. EVALECHOCARD [FRO2006] is a reference echocardiograph scan image database, which was created with an aim to compare methods dedicated to the estimation of regional wall motion abnormalities [FRO2006]. The database consists of 2-chamber (2C) and 4-chamber (4C) views of echo scans in specific export format or DICOM format. The MIDA algorithm can be extended to 2C and

4C views and then evaluated by applying on the EVALECHOCARD database to compare its performance with other methods.

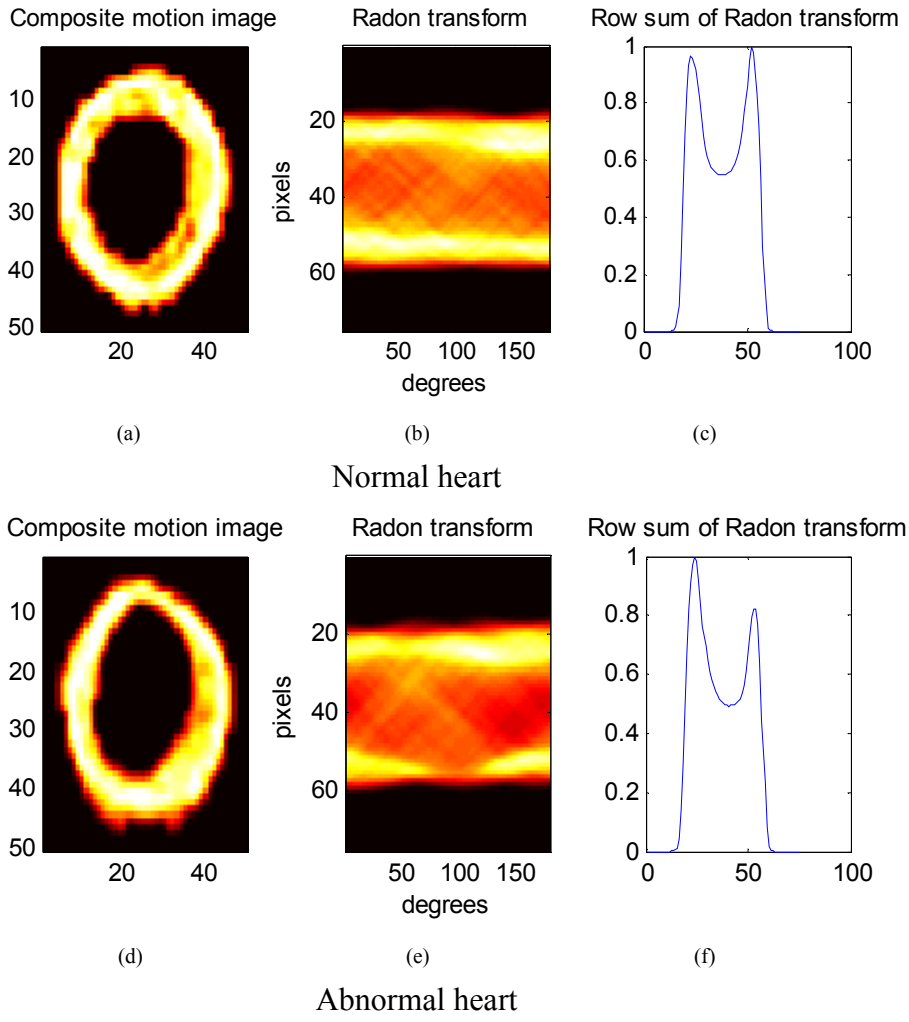

Fig. 7.2 Radon transform of a composite motion image of a normal healthy heart and an abnormal heart with 7th and 8th segment abnormality

7.2.3 Radon Analysis of the composite motion image

The Radon transform was applied to identify the symmetry in wall motion. The results are very encouraging when the area below the sum of the projections and the peak of the projection were used as the parameters for classification. Further study on the radon transform of the composite motion image could help identify other

parameters that could be used for classification. Fig. 7.2 shows (a) the composite motion image of a healthy heart, (b) Radon transform of the composite motion image (a), and (c) row sum of Radon transform, that is, the sum of projections from 0 to 179 degrees, (d) the composite motion image of an abnormal heart with 7th and 8th segment abnormality, (e) Radon transform of the composite motion image (d), and (f) row sum of Radon transform. It can be seen that the two side bands in the radon transform of the normal image is continuous, while one of the two side bands in the radon transform of the abnormal image is discontinuous. The possibility of linking the position of the discontinuity in the side bands to establish the exact location and severity of defect has to be explored.

References:

A

[ADSF2008] H. D. Allen, D. J. Driscoll, R. E. Shaddy, T. F. Feltes, "Moss and Adams' Heart Disease in Infants, Children, and Adolescents: Including the Fetus and Young Adults", 7th Edition, Lippincott Williams & Wilkins (2008).

[AKSEL2006] A. Aksel, A.D. Gilliam, J.A. Hossack, S. T. Acton, "Speckle Reducing Anisotropic Diffusion for Echocardiography", Fortieth Asilomar Conference on Signals, Systems and Computers, pp. 1988 - 1992 (2006).

[ALEX2001] L. A. Alexandre, A. C. Campilho, M. Kamel, " On combining classifiera using sum ans product rules », Pattern Recognition Letters, Vol. 22, pp. 1283-1289 (2001)

[ALLE2008] S. Allender, V. Peto,P. Scarborough, A. Kaur and M Rayner, "Coronary heart disease Statistics 2008 edition", British Heart FoundationStatistics Database, http://www.heartstats.org/ homepage.asp. (2008)

[AMOR2009] J. C. Amorim, M. C. dos Reis, J. L. A. de Carvalho, A. F. da Rocha, and J. F. Camapum, "Improved Segmentation of Echocardiographic Images Using Fusion of Images from Different Cardiac Cycles", International Conference of the IEEE EMBS pp.511-514, (2009)

[AT2003] F. Argenti, G. Torricelli, Speckle Suppression in Ultrasonic Images Based on Undecimated Wavelets, EURASIP Journal on Applied Signal Processing, 5, pp. 470–478 (2003)

B

[BALES1997] A. C. Bales, M. J. Sorrentino. "Causes of congestive heart failure: Prompt diagnosis may affect prognosis", Postgraduate Medicine symposium, 101(1), (1997).

[BAN2007] P. Bansod, U.B. Desai, N. Burkule, "Multi Frame Guided Local Search for Semiautomatic Endocardial Contour Estimation in Echocardiography Sequences" , 6th International Conference on Information, Communications & Signal Processing, (2007)

[BAR1999].M. Baroni, "Contour evaluation of left ventricular wall motion by means of shape-based tracking and symbolic description", Medical Engineering and Physics, Vol 21, pp. 73-85 (1999)

[BART2002] M. S. Bartlett, J.R. Movellan and T. J. Sejnowski, "Face recognition by Independent Component Analysis", IEEE Trans. Neural Networks, 13 (6), pp. 1450-1464, 2002.

[BEY2008] D. Beymer, T. Syeda-Mahmood, F. Wang, "Exploiting Spatio-temporal Information for View Recognition in Cardiac Echo Videos", Computer Vision and Pattern Recognition Workshops, CVPRW '08, pp.1-8, 2008

[BHF2010] "Diastolic heart failure", British Heart Foundation Fact file, http://www.bhf.org.uk/publications/view_publication.aspx?ps=1001232 (2010)

[BOSCH2002] J. G. Bosch, S. C. Mitchell, B. P. F. Lelieveldt, F. Nijland, O. Kamp, M. Sonka, J. H. C. Reiber, "Automatic Segmentation of Echocardiographic Sequences by Active Appearance Motion Models", IEEE Transaction on Medical Imaging, Vol. 21 (11), pp. 1374-1383 (2002)

[BOS2005] J. G. Bosch, F Nijland, S. C. Mitchell, B. P. F. Lelieveldt, O. Kamp, J. H. C. Reiber and M. Sonka. "Computer-aided Diagnosis via model-based shape analysis: Automated classification of wall motion abnormalities in echocardiograms", Academic Radiology, 12 (3), pp. 358-367, (2005)

[BOSCH2006] J. G. Bosch, "Automated contour detection in Echocardiographic images", Thesis 2006

[BS1995] A. J. Bell and T. J. Sejnowski, "An information-maximisation approach to blind separation and blind deconvolution", Neural Computation, 7 (6), pp. 1129-1159, 1995.

[BS1997] A. J. Bell and T. J. Sejnowski, "The independent components of Natural scenes are edge filters", Vision Res., Vol. 37, No. 23, pp. 3327-3338, (1997)

[BURNS2006] H. Burns, "The Chief Medical Officer's Report to Scottish Ministers on the health of the Nation", (2006).

[BUSH1999] S. C. Bushong, "Diagnostic Ultrasound", The McGraw-Hill Companies, Inc.

C

[CARD1999] J.-F. Cardoso, "High-order contrasts for independent component analysis," Neural Computat., vol. 11, pp. 157–192, 1999.

[CER2002] M. D. Cerqueira, N. J. Weissman, V. Dilsizian, A. K. Jacobs, S. Kaul, W. K. Laskey, D. J. Pennell, J. A. Rumberger, T. Ryan., M. S. Verani, 'Standardized myocardial segmentation and nomenclature for tomographic imaging of the heart', Circulation, 105, pp. 539 – 542 (2002)

[CH1967] T.M. Cover and P.E. Hart, "Nearest neighbor pattern classi'cation", IEEE Trans. Information Theory, 13, pp. 21–27, 1967.

[CHEN1997] L. Chen, C. W. Chen, and K. J. Parker, "Adaptive feature enhancement for mammographic images with wavelet multiresolution analysis", Journal of Electronic Imaging, Vol. 6(4), pp. 467–478 (October 1997).

[CHEN2007] G. Chen, X. Liu,; Z. Zhou, "Modified frost speckle filter based on anisotropic diffusion", IET International Conference on Radar Systems, pp. 1 – 4 (2007)

[CHENG2006] J. Cheng, S. W. Foo, and S. M. Krishnan, "Watershed-Presegmented Snake for Boundary Detection and Tracking of Left Ventricle in Echocardiographic Images", IEEE Transactions on Information technology in Biomedicine, Vol. 10 (2), pp.414-416 (2006)

[CHIA2008] F Chiarugi, S Colantonio, D Emmanouilidou, D Moroni, F Perticone, A Sciacqua, O Salvetti, "ECG and Echocardiography Processing for Decision Support in Heart Failure", Computers in Cardiology, Vol. 35, pp. 649−652.(2008)

[CHOU2008] K. Chou and S. Yu, "Categorizing Heartbeats by Independent Component Analysis and Support Vector Machines", International Conference on Intelligent Systems Design and Applications, ISDA '08, Vol. 1, pp. 599 – 602 (2008)

[CHOY1998] M. M. Choy, J. S. Jin, "Extractin Endocardial Echocardiographic Images Borders from Sequential Using Mathematical Morphology ond Temporal lnformation to lmprove Contour Accuracy", IEEE Engineering in Medicine and Biology, pp. 116-121 (1998)

[CHU1988] C. H. Chu. E. J. Delp. and A. J. Buda. "Detecting left ventricular endocardial and epicardial boundaries by digital two-dimensional echocardiography." IEEE Transcations on Medical Imaging, MI-7, no. 2. pp. 81- 90, (1988)

[COL2004] S Colombo, M Martini, L Delfino, M Llambro, M Turie, EG Caiani, "Development of a User-Friendly Database for Combined Assessment of Doppler Coronary Now Reserve and Wall Motion Abnormalities" Computers in Cardiology, Vol. 31. pp. 589-592 (2004)

[COOT1994] AD Parker, A Hill, CJ Taylor, TF Cootes, XY Jin, DG Gibson, "Application of Point Distribution Models to the Automated Analysis of Echocardiograms"

[COOT1994] T. F. Cootes, A.Hill, C. J. Taylor and J. Haslam. "The use of active shape models for locating structures in medical images", Image and Vision Computing, 12 (6), pp. 335-366, 1994.

[COOT1995] T. F. Cootes, C. J. Taylor, D. H. Cooper, and J. Graham., "Active shape models- their training and application", Computer Vision and Image Understanding, Vol. 61(1):38-59, 1995.

[COOT1998] T.F. Cootes, G.J. Edwards, and C.J. Taylor, "Active Appearance Models",H. Burkhardt, B. Neumann (Eds.): Computer Vision ECCV '98,Vol II, LNCS 1407, pp. 484 - 498,1998.

[COOT2006] P.Kittipanya-ngam and T.F.Cootes, "The effect of texture representations on AAM performance", International Conference on Pattern Recognition (ICPR'06) (2006)

[CS2001] C. Chinrungrueng, A. Suvichakorn, "Fast edge-preserving noise reduction for ultrasound images", IEEE Transactions on Nuclear Science, 48, 849–854 (2001).

[CZK2004] D. Comaniciu, X. S. Zhou, and S. Krishnan, "Robust Real-Time Myocardial Border Tracking for Echocardiography: An Information Fusion Approach", IEEE Transactio on Medical Imaging, Vol. 23 (7), pp. 849-860 (2006)

D

[DYDEN2006] I. Dydenko, F. Jamal, O. Bernard, J. Dhooge,.I. E. Magnin, D. Friboulet, "A level set framework with a shape and motion prior for segmentation and region tracking in echocardiography", Medical Image Analysis, Vol. 10, pp. 162–177 (2006)

[DALE1993] R.Dale-jones and T.Tjahjadi, "A study and modification of local histogram equalization algorithm", Pattern Recognition, Vol. 26 (9), pp. 1373-1381 (1993)

[DIAS1996] J. Dias and J.Leitao, "Wall position and thickness estimation from sequences of echocardiographic images" IEEE Transactions on Medical Imaging, Vol. 15 (1), pp. 25-38 (1996)

[DHUB2005] M. Dhubi1, J. Puentes, L. Bressollette, B. Guias, B. Solaiman, "Volume Calculation of Venous Thrombosis Using 2D Ultrasound Images", Proceedings of the IEEE Engineering in Medicine and Biology, pp. 4002-4005, (2005)

[DOMIN2003] C R. Dominguez, F Frouin, O. G´erard, P. Lim, B. Diebold, and A. Herment, "Parametric Analysis of Main Motion to Study the Regional Wall Motion of the Left Ventricle in Echocardiography" Springer-Verlag Berlin Heidelberg, I. Magnin et al. (Eds.): FIMH 2003, LNCS 2674, pp. 173–183, (2003)

[DUN1991] F. Dunn, "Ultrasound", IEEE Transactions on Education, 34(3), pp. 266-268 (1991)

[DURRANI1984] T.S. Durrani and D. Bisset, "The Radon transform and its properties", Geophysics, Vol. 49, pp. 1180-1187 (1984)

E

[EH1954] I. Edler and C.H. Hertz, "Use of ultrasonic reflectoscope for continous recording of movements of heart walls", Kurgl Fysiogr. Sallad i Lund Forhandl, 24(5), 1954

[ESC2007] K. Thygesen, J. S. Alpert and H. D. White, "Universal definition of myocardial infarction", European Heart Journal, Vol. 28, pp. 2525–2538 (2007)

[EYLL1995] C van Eyll, M F Rousseau, J Etienne, L Stoleru, AA Charlier, H Pouleur, "High Performance Regional Wall Synchrony Analysis in Severe Systolic Dysfunction: A New Program Based on Reverse Polish Notation", Computers in Cardiology, pp. 509-512 (1995)

F

[FANG2008] W. Fang, K. L. Chan, S. Fu, S. M. Krishnan, "Incorporating temporal information into active contour method for detecting heart wall boundary from echocardiographic image sequence", Computerized Medical Imaging and Graphics, Vol. 32 590–600 (2008)

[FFA1991] T.L. Force, T.D. Folland, N Aebischer, S. Sharma, A.F. Parisi, "Echocardiographic Assessment of Ventricular function", Cardiac Imaging, pp. 374-401 (1991)

[FIL2004] E.S. Filho, M. Yoshizawa, T. Iwamoto, A. Tanaka, Y. Saijo, "Morphological-fuzzy filter for enhancement of intravascular ultrasound images" SICE 2004 Annual Conference, Vol. 2, pp. 1394 - 1397 (2004)

[FJ1980] A. C. Fleischer, A. E. James, "Introduction to Diagnostic Sonography", John Wiley & sons, Inc (1980)

[FRO1982] V. S. Frost, J. A. Stiles, K. S. Shanmugan, and J.C. Holtzman, "A model for radar images and its applications to adaptive digital filtering for multiplicative noise", IEEE Transaction on Pattern Anal. Machine Intell, 4, pp. 157 – 165. (1982)

[FRO2006] F Frouin, N Kachenoura, A Delouche, P Dumee, T Kalikian, H Guillemet, L Sarry, O Nard, B Diebold, "EVALECHOCARD: A Database in Echocardiography for the Comparison of Methods Dedicated to the Estimation of Regional Wall Motion Abnormalities", Computers in Cardiology, Vol. 33, pp. 517−520 (2006)

[FU2000] J.Fu, Lien H., Wong S., "Wavelet based histogram equalization enhancement of gastric sonogram images", Computerized medical imaging and graphics, Vol.24, pp.59-68, (2000)

[FUNG2005]G. Fung, M. Qazi, S. Krishnan, J. Bi, R. B. Rao, and A. Katz, "Sparse classifiers for Automated Heart Wall Motion Abnormality Detection" (2005)

G

[GA1997] R. G. Grainger and D. Allison, "Grainger & Allison's Diagnositic radiology: A textbook of medical imaging", Third edition, Churchill Livingstone, (1997).

[GAND2006] G. Gandelman, "Heart Failure",

http://www.nlm.nih.gov/medlineplus/ency/article/000158.htm, (2006).

[GIAC1998] A. Giachetti, "On-line analysis of echocardiographic image sequences", Medical Image Analysis, Vol. 2 (3), pp.261-284 (1998)

[GINKEL2004] M. van Ginkel, C.L. Luengo Hendriks and L.J. van Vliet, "A short introduction to the Radon and Hough transforms and how they relate to each other" Number QI-2004-01 in the Quantitative Imaging Group Technical Report Series

[GORD1984] R Gordon, R. Rangayyan, "Feature enhancement of film mammograms using fixed and adaptive neighborhoods", Applied Optics, Vol. 3(4), pp. 560–4 (1984)

[GORD1986] R. Gordon, G. Buelloni, A. P. Dhawan, "Enhancement of mammographic feature by optimal adaptive neighborhood image processing", IEEE Transactions on Medical Image, Vol 5(1), pp.8–15(1986)

[GS2005] D. Gnanadurai, V. Sadasivam, Undecimated wavelet based speckle reduction for SAR images, Pattern Recognition Letters, 26, (2005) 793–800.

[GUPTA2005] C. N. Gupta, R. Palaniappan, S. Rajan, S. Swaminathan, S.M.Krishnan, "Segmentation and Classification of heart sounds", Canadian Conference on Electrical and Computer Engineering, pp. 1674 - 1677 (2005)

[GZ2006] S. Garas, A. M. Zafari, "Myocardial Infarction",

http://www.emedicine.com/med/topic1567.htm, (2006)

H

[HAMA2000] G Hamameh, T Gustavsson, "Combining Snakes and Active Shape Models for Segmenting the Human Left Ventricle in Echocardiographic Images", Computers in Cardiology, Vol. 27, pp.115-118 (2000)

[HE2006] X. He, W. Jia, Q. Wu, T. Hintz, "Description of the cardiac movement using hexagonal image structures, Computerized Medical Imaging and Graphics, Vol. 30, pp. 377–382 (2006)

[HES2004] T. F. Heston, "Myocardial Ischemia - Nuclear Medicine and Risk Stratification", http://www.emedicine.com/med/topic1568.htm , (2004)

[HG1999] X. Hao, S. Gao, A novel multiscale nonlinear thresholding method for ultrasonic speckle suppressing, IEEE Trans. Med. Imag.,Vol. 18 (9), pp. 787–794 (1999)

[HKO2001] A. Hyvärinen, J. Karhunen, and E. Oja, Independent Component Analysis. New York: Wiley (2001)

[HO2000] A. Hyvarinen and E. Oja, "Independent Component Analysis: Algorithms and Applications", Neural Networks, 13 (4-5), pp. 411-430 (2000)

[HOSS2003] F. Xu, Y. Yu, S. T. Acton and J. A. Hossack, "Detection of myocardial boundaries from ultrasound imagery using active contours", IEEE Ultrasonics Symposium, pp. 1537- 1540 (2003)

[HOSS2004] J. E. Pickard, R. L. Janiczek, S. T. Acton, J. Sklenar, J. A. Hossack, S. Kaul, "Segmentation of myocardium from myocardial contrast Echocardiography", ASILOMAR Conference on Signals Systems and Computers, Vol. 2, pp. 1616-1619 (2004)

[HS2007]_"Heart Disease and Stroke Statistics — 2009 Update", American Heart Association (2009)

[HUNT2005] S. A. Hunt et al., "ACC/AHA 2005 Guideline Update for the Diagnosis and Management of Chronic Heart Failure in the Adult", Circulation, Vol. 112, pp. 154-235 (2005)

[HUS1985] Matthew Hussey, "Basic physics and technology of medical diagnostic ultrasound", Macmillan Publishers Ltd (1985)

J

[JAIN1989] A. K. Jain, Fundamentals of Digital Image Processing, Englewood Cliffs, NJ: Prentice-Hall, (1989)

[JESS2009] M. Jessup et al., "Focused Update Incorporated Into the ACC/AHA 2005 Guidelines for the Diagnosis and Management of Heart Failure in Adults", Circulation, Vol. 119, pp. 1977-2016 (2009)

K

[KACH2006] N Kachenoura, A Delouche, C R. Dominguez, S Mule, D Balvay, T Kalikian, A Herment, O Nardi, F Frouin, B Diebold, "Automatic Scoring of Segmental Wall Motion in Echocardiography Using Quantified Parametric Images", Computers in Cardiology, Vol. 33, pp.721−724 (2006)

[KAD2001] S. Kaddoura, "Echo Made Easy", Churchill Livingstone, (2001).

[KANG2005] S. Kang, "Heart Attack",

http://www.nlm.nih.gov/medlineplus/ency/article/000195.htm, (2005)

[KANG2006] S. Kang, "Coronary heart disease", http://www.nlm.nih.gov/medlineplus/ency/article/007115.htm , (2006)

[KASS1988] M. Kass, A. Witkin, and D. Terzopoulos, "Snakes: Active Contour Models", International Journal of Computer Vision, pp. 321-331 (1988)

[KAUN1987] D.T. Kaun, A. A. Sawchuk, T. C. Strand, and P. Chavel, Adaptive restoration of images with speckle, IEEE Transaction on Acoustic Speech Signal Processing 35, (1987) 373 – 383.

[KIM1997] J. K. Kim, J. M. Park, K. S. Song, and H. W. Park, "Adaptive Mammographic Image Enhancement using First Derivative and Local Statistics" IEEE Transactions on Medical Imaging, Vol. 16, NO. 5, pp. 495-502(1997)

[KIT1998] J. Kittler, M. Hatef, R. P. W. Duin and J. Matas, „ On combining Classifiers", IEEE Transcations on Pattern analysis and machine intelligence, Vol. 20(3), pp. 226 -239 (1998)

[KL2004] J. Koikkalainen and J. Lotjonen, "Image segmentation with the combination of the PCA- and ICA-based modes of shape variation," in IEEE International SymposiumBiomed. Imag.: Nano Macro, 2004, vol. 1, pp. 149–152.

[KOVESI2003] P. Kovesi, "Phase Congruency Detects Corners and Edges" , Proc. VIIth Digital Image Computing: Techniques and Applications, DICTA2003, pp. 309-318, (2003) http://www.csse.uwa.edu.au/~pk/Research/MatlabFns/

[KRE2006] F.W. Kremkau, "Diagnostic ultrasound : principles and instruments", (2006)

L

[LAC2008] S. G. Lacerda, A. F. da Rocha, D. F. Vasconcelos, J. L. de Carvalho, L. A .Joao, I. G. Sene, F. J. Camapum, "Left ventricle segmentation in echocardiography using a radial-search-based image processing algorithm", International Conference of the IEEE Engineering in Medicine and Biology Society, EMBS 2008, pp. 222 – 225 (2008)

[LAINE1995] A. F. Laine, J. Fan, W. Yang, "Wavelets for contrast enhancement of digital mammography", IEEE Engineering in Medicine and Biology Magazine, Vol. 14, pp. 536-550 (1995)

[LAINE1996]X. Zong, A. F. Laine, E. A. Geiser, and David C. Wilson, "De-Noising and contrast enhancement via wavelet shrinkage and nonlinear adaptive gain", Wavelet Applications III, Proceedings of SPIE, vol. 2762, pp. 566-574 (1996)

[LAINE1998] X. Zong, A. F. Laine, and E. A. Geiser, "Speckle Reduction and Contrast Enhancement of Echocardiograms via Multiscale Nonlinear Processing", IEEE Transactions on Medical Imaging, Vol. 17 (4), pp. 532 - 540(1998)

[LAMB1990] C. Lamberti, F. Sgallari, "A Workstation-Based System for 2-D Echocardiography Visualization and Image Processing", IEEE Transactions on Biomedical Engineering, Vol. 37 (8), pp. 796-802 (1990)

[LANG2005] R. M. Lang, M. Bierig, R. B. Devereux, F. A. Flachskampf, E. Foster, P.A. Pellikka, M. H. Picard, M. J. Roman, J. Seward, J. S. Shanewise, S. D. Solomon, K.T. Spencer, M. J, Sutton, W.J. Stewart, "Recommendations for Chamber Quantification: A report from the American society of echocardiography's guidelines and standards committee and the chamber quantification writing group, developed in conjunction with the European Association of echocardiography, a

branch of the European society of Cardiology", Journal of the American Society of Echocardiography, 18 (12), pp. 1440-1463 (2005)

[LB2002] S. Lertrattanapanich, N. K. Bose, High resolution image formation from low resolution frames using Delaunay Triangulation, IEEE Transaction on Image processing, 11(12), (2002) 1427-1441.

[LC2002] P.-C. Li and M.-J. Chen, Strain compounding: A new approach for speckle reduction, IEEE Trans. Ultrason. Ferroelect. Freq. Contr., 49 (1), (2002) 39–46.

[LEE1986] J. S. Lee, Speckle suppression and analysis for synthetic aperture radar, Opt.Eng. 25 (5), pp. 636-643 (1986)

[LF2000] F.L. Lizzi, E. J. Feleppa, "Image processing and pre-processing for medical ultrasound", 29th Applied Imagery Pattern Recognition Workshop 2000, Proceedings. , pp. 187 – 192 (2000)

[LI2000] P. Li and M. Chen, "A New Compounding Approach for Speckle Reduction", IEEE Ultrasonics Symposium, pp. 1699 – 1702 (2000)

[LI2002] P.-C. Li and M.-J. Chen, "Strain compounding: A new approach for speckle reduction," IEEE Trans. Ultrason. Ferroelect. Freq. Contr., vol. 49, no. 1, pp. 39–46, Jan. (2002)

[LI2005] Formulation. C. Li , C. Xu, C. Gui, M. D. Fox "Level Set Evolution Without Re-initialization: A New Variational Formulation", IEEE Computer Society Conference on Computer Vision and Pattern Recognition,. CVPR 2005.Vol. 1, pp. 430 - 436 (2005)

[LI2007] H. Li; J. Gao, D. C. Liu, "Adaptive Edge Enhancement of the Ultrasound Image", Fourth International Conference on Image and Graphics, ICIG 2007, pp. 86 – 91 (2007)

[LIN2003] N. Lin, W. Yu, and J. S. Duncan, "Combinative Multi-Scale Level Set Framework for Echocardiographic Image Segmentation" , Medical Image Analysis, Vol. 7 (4), pp. 529-537, (2003)

[LIAO2005] S.Liao; R. Tong; M. Wang; J. Dong, "Rapidly Generate Lumbar Spine Volume Mesh", Ninth International Conference on Computer Aided Design and Computer Graphics (CAD/CG 2005)

[LOT2004] J. Lotjonen, S. Kivisto, J. Koikkalainen, D. Smutek, and K. Lauerma, "Statistical shape model of atria, ventricles and epicardium from short- and long-axis MR images," Med. Image Anal., vol. 8, no. 3, pp. 371–386, (2004).

[LOUP1989] T. Loupas, W. N. Mcdicken, and P. L. Allan, "An adaptive weighted median filter for speckle suppression in medical ultrasonic images", IEEE Trans. on Circuits and Systems, Vol. 36, pp.129-135 (1989)

[LS2006] L. Prasad, A. N. Skourkhine, Vectorized image segmentation via trixel agglomeration, Pattern Recognition, 39, pp. 501-514 (2006)

[LYN2006] P. J. Lynch, C. C. Jaffe, Yale University Center for Advanced Instructional Media Medical Illustrations generated for multimedia teaching projects by the Yale University School of Medicine, Center for Advanced Instructional Media, 1987-2000, Creative Commons Attribution 2.5 License 2006

M

[MALA1999] S. Malassiotis and M. G. Strintzis, "Tracking the Left Ventricle in Echocardiographic Images by Learning Heart Dynamics" (1999)

[MAN2005] J. Maniam and S. Narainasamy. "Search of Dynamic Magnetic Resonance images using active shape model", Sunway Academic Journal, 2, pp. 77-83, 2005.

[MANS2009] M. S. Mansoory, M. Ashtiyani, T. N. Hojjat, "Cardiac Motion Evaluation for Disease Diagnosis Using ICA Basis Neural Network", International Association of Computer Science and Information Technology - Spring Conference, IACSITSC '09, pp. 496 – 500 (2009)

[MART2004] F. H. Martini, "Fundamentals of Anatomy and Physiology", Pearson Education Ltd, (2004).

[MCD1981] W. N. McDicken, "Diagnostic ultrasonics- priciples and use of instruments", second edition, John Wiley & sons, Inc (1981)

[MEY2004] R. A. Meyer,"History of Ultrasound in Cardiology", Journal of Ultrasound in Medicine, 23, pp. 1–11 (2004)

[MH2008] S.C. Mukhopadhyay, R.Y.M. Huang, "Sensors - Advancements in Modeling, Design Issues, Fabrication and Practical Applications", Lecture Notes Electrical Engineering, Vol. 21(2008)

[MIK1998] I. Miki´c, S. Krucinski, and J. D. Thomas, "Segmentation and Tracking in Echocardiographic Sequences: Active Contours Guided by Optical Flow Estimates", IEEE Transaction on Medical Imaging, Vol. 17 (2), pp. 274 - 284 (1998)

[MITC2005] R. Mitchell, G. Fowkes, D. Blane and M. Bartley, "High rates of ischaemic heart disease in Scotland are not explained by conventional risk factors", Journal of Epidemiology and Community Health, 59, pp. 565-567, (2005).

[MON1988] Monteiro, A.P.; Marques de Sa, J.P.; Abreu-Lima, C., "Automatic detection of echocardiographic LV-contours-a new image enhancement and sequential tracking method", Computers in Cardiology, pp. 453 – 456 (1988)

[MPT2008] S. J. McPhee, M. A. Papadakis and L. M.Tierney, " Current Medical Diagnosis and treatment 2008", McGraw Hill (2008)

N

[NAG1999] E. Nagel, H. B. Lehmkuhl, W. Bocksch, C. Klein, U. Vogel, E. Frantz, A. Ellmer, S. Dreysse, E. Fleck, "Noninvasive diagnosis of Ischemia-induced Wall Motion Abnormalities with the use of high-dose Dobutamine stress MRI - Comparison with Dobutamine stress echocardiography", Circulation, 99, pp. 763-770 (1999)

[NAGY1999] L. Nagy, "Echocardiography image processing and analysis-Wall motion detection", Proceedings of Conference of Serving Humanity, Advancing Technology, pp. 1044 (1999)

[NAGY2000] L. Nagy, E. Nagy, "Detection of Ischaemic Cardiopathy Analysing 2D-Echograms", Proceedings of the 22"d Annual EMBS International Conference, 2000, pp. 545-547 (2000)

[NAZA1994] B. Nazarian, C. Chedot, J. Sequeira, "Interactivity and Delaunay triangulation for the reconstruction of tubular anatomical structures", IEEE conference on Engineering in Medicine and Biology Society, pp. 706-707 (1994)

[NOBLE2001-1] D. Boukerroui, J. A. Noble, M. Brady, "Feature enhancement in low quality images with application to echocardiography", Lecture Notes In Computer Science; Vol. 2082, Proceedings of the 17th International Conference on Information Processing in Medical Imaging, pp. 453 - 460 (2001)

[NOBLE2001-2] D. Boukerroui, J. A. Noble, M. C. Robini and M. Brady, "Enhancement of contrast regions in suboptimal ultrasound images with application to Echocardiography", Ultrasound in Med. & Biol., Vol. 27 (12), pp. 1583–1594, (2001)

[NOBLE2002] G. Jacob, A. Noble, C. Behrenbruch, A. D. Kelion and A. P. Banning, "A Shape –Space based approach to tracking myocardial borders and quantifying regional left ventriculat function applied in Echocardiography", IEEE Transaction on Medical Imaging, Vol. 21(3), pp. 226- 238 (2002)

[NOBLE1998] M. Mulet-Parada and J. A. Noble, "Intensity-invariant 2D+T Acoustic Boundary Detection", Proceedings of the IEEE Workshop on Biomedical Image Analysis, pp. 133 (1998)

[NOBLE2006] J. A. Noble and D. Boukerroui, "Ultrasound Image Segmentation: A Survey", IEEE Transaction on Medical Imaging, Vol. 25 (8), pp. 987-1010 (2006)

[NOBLE2008] S. Mansor, J. A. Noble, "Local wall motion classification of stress echocardiography using a hidden markov model approach", IEEE International Symposium on Biomedical Imaging ISBI2008, Vol., pp.1295-1298 (2008)

[NOBLE2008-2] K. Rajpoot, J. A. Noble, V. Grau, N. Rajpoot, "Feature Detection from Echocardiography Images Using Local Phase Information", Proceedings of the 12th Annual Conference on Medical Image Understanding and Analysis (2008)

[NOBLE2010] J. A. Noble, "Ultrasound image segmentation and tissue characterization", Journal of Engineering in Medicine, Vol. 224, pp.307-316 (2010)

O

[OGA2006] K. Ogawa, T. Hozumi, K. Sugioka, Y. Matsumura, M. Nishiura, R. Kanda, Y. Abe, Y. Takemoto, M. Yoshiyama, J. Yoshikawa, "Usefulness of automated quantification of regional left ventricular wall motion by a novel method of two-dimensional echocardiographic tracking", The American Journal of Cardiology, Vol. 98 (11), pp. 1531-1537 (2006)

[OS1988] M. O'Donnell and S. D. Silverstein, Optimum displacement for compound image generation in medical ultrasound, IEEE Trans. Ultrason. Ferroelect. Freq. Contr., 35 (4), pp. 470–476, (1988)

[OSHER1988] S. Osher and J. A. Sethian, "Fronts Propagating with Curvature Dependent Speed: Algorithms Based on Hamilton-Jacobi Formulations", Journal of Computational Physics, Vol. 79, pp.12-49, (1988)

[OTEY2006] M. E. Otey, J. Bi, S. Krishnan, B. Rao, J. Stoeckel, A. Katz, J. Han, and S. Parthasarathy, "Automatic View Recognition for Cardiac Ultrasound Images", In MICCAI-CVII, (2006)

P

[PARK2007] J. Park, S. Zhou, C. Simopoulos, J. Otsuki, and D. Comaniciu, "Automatic cardiac view classification of echocardiogram", In International Conference on Computer Vision, pp. 1–8, (2007)

[PER2009] A. Perperidis, D. Cusack, N. McDicken, T. MacGillivray, T. Anderson, "Temporal compounding of cardiac ultrasound data: Improving image quality and clinical measurement repeatability", International Conference of the IEEE Engineering in Medicine and Biology Society, EMBC 2009, pp. 3661 – 3664 (2009)

[PICK2006] J. E. Pickard, J. A. Hossack, S. T. Acton, "Shape model segmentation of Long –axis contrast enhanced echocardiography", ISBI 2006, pp. 1112-1115 (2006)

[PIZ1987] S. M. Pizer, E. P. Amburn, J.D. Austin, R. Cromartie, A.Geselowitz, T. Greer, B.H. Romeny, J. B. Zimmerman and K. Zuiderveld, "Adaptive histogram equalization and its variations", Computer Graphics Image Processing, Vol.39 (3), pp. 355-368, (1987)

[PETER 1996] Peter Toft, "The Radon Transform - Theory and Implementation, PhD Thesis, IMM, Technical University of Denmark, 1996

[POTTER2001] M. Potter, W. Kinsner, "Competing ICA techniques in biomedical signal analysis", Canadian Conference on Electrical and Computer Engineering, Vol. 2, pp. 987 – 992, (2001)

[PPSR2005] S. Petersen, V. Peto, P. Scarborough and M. Rayner, "Coronary heart disease Statistics – 2005 edition", British Heart Foundation: London (2005)

Q

[QAZI2005] M. Qazi, G. Fung, S. Krishnan, J. Bi, R. B. Rao, and A. Katz, "Automated Heart Wall Motion Abnormality Detection using Sparse Linear Classifiers", ICMLA05 special edition journal

[QAZI2007] M. Qazi, G. Fung, S. Krishnan, R. Rosales, H. Steck, R. B. Rao, D. Poldermans and D. Chandrasekaran, "Automated Heart Wall Motion Abnormality Detection From Ultrasound Images using Bayesian Networks" Proceedings of the 20th international joint conference on Artifical intelligence, pp. 519-525 (2007)

R

[RADON1917] J. Radon," Über die Bestimmung von Funktionen durch ihre Integralwerte längs gewisser Mannigfaltigkeiten. Berichte Sächsische Akademie der Wissenschaften, Leipzig" , Mathematisch-Physikalische Klasse, 69:262–277, 1917.

[RAJ2006] J.Rajan, http://www.mathworks.cn/matlabcentral/fileexchange/11432-frost-filter-for-speckle-noise-reduction

[RAN1998] T. S. Ranganathan, " A text book of human anatomy", S. Chand & company Ltd. (1998)

[RG1979] J. L. Rose, B. B. Goldberg, "Basic Physics in Daignostic ultrasound", John Wiley & sons, Inc (1979)

[RGR1987] M.H. Repacoholi, M. Grandolfo and A. Rindi, "Ultrasound", Plenum press, New York (1987)

[RMLVAB2009] S. D. Roes, S. A. Mollema, H. J. Lamb, E. E. Van der Wall, Albert de Roos, and J. J. Bax, "Validation of Echocardiographic Two-Dimensional Speckle Tracking Longitudinal Strain Imaging for Viability Assessment in Patients With Chronic Ischemic Left Ventricular Dysfunction and Comparison With Contrast-Enhanced Magnetic Resonance Imaging", The American Journal of Cardiology, Vol. 104(3), pp. 312-317 (August 2009)

[ROUL1997] Roulston, M. S. and Muhleman, D. O. "Synthesizing Radar Maps of Polar Regions with a Doppler-Only Method." Applied Optics, Vol. 36, pp. 3912-3919, (1997)

[RRV2008] M. C. dos Reis, A. F. da Rocha, D. F. Vasconcelos, B. L. M. Espinoza, F. A. de O. Nascimento, J. L. A. de Carvalho, S. Salomoni and J. F. Camapum, "Semi-Automatic Detection of the Left Ventricular Border", International IEEE EMBS Conference, pp. 218-221 (2008)

[RWC1998] C. M. Rumack, S.R. Wilson and J. W. Charboneau, "Diagnostic ultrasound", Mosby – Year Book, Inc (1998)

S

[SAIM2000] H. B. Saim, S. C. Fhong; N. B. M. Noor, , J. B. A. Wahab, "Contrast resolution enhancement based on wavelet shrinkage and gray level mapping technique", TENCON 2000. Proceedings, Vol. 2, pp. 165 - 170 (2000)

[SAL] E. Salcedo, "Atlas of Echocardiography (2nd Edition)", chapter 11. The Left

Ventricle, pages 197—215.

[SAPR1998] R. Sapraa, B. Singha, D. Thataia, D. Prabhakarana, A. Malhotrab, S. C. Manchanda, "Critical appraisal of left ventricular function assessment by the automated border detection method on echocardiography. Is it good enough?", International Journal of Cardiology, Vol. 65, pp. 193–199 (1998)

[SET1998] S. K. Setarehdan, "Echocardiographical cardiac function assessment and wall motion visualisation using fuzzy logic and the wavelet transform, Thesis, (1998)

[SCK1986] D. J. Skorton, S. M. Collins, and R. E.Kerber, " Cardiac Imaging and image processing, pages171-205, McGrw-Hill,(1986)

[SDS2005] V. N. Singh, P. Deedwania, R. K. Sharma, "Coronary Artery Atherosclerosis", http://www.emedicine.com/med/topic446.htm , (2005)

[SHAH2000] A. I. Shahib, "Fuzzy clustering algorithms and their applications to medical image analysis", PhD Thesis, Imperial college of Science, Technology and Medicine (2000)

[SHB1993] M.Sonka, V. Hlavac, and R. Boyle, "Image Processing Analysis and Machine Vision", Chapman and Hall Computing, (1993)

[SHEW1999] J. R. Shewchuk, Lectures Notes on Delaunay Mesh Generation, University of California at Berkeley, (1999).

[SIEP2003] G. Serpen, R. Iyer, H. M. Elsamaloty and E. I. Parsai. "Automated lung outline reconstruction in ventilation -perfusion scans using principal component analysis techniques", Computers in Biology and Medicine, 33, pp. 119-142, (2003)

[SING2002] P. K. Singh, S. J. Simoff, L. Holley, L. Thomas, D. Richards, "Computer assisted detection of ischemia utilizing echocardiograms before and after stress", Computers in Cardiology, Vol. 29, pp. 355-358 (2002) [SK2006] M Span¡el and P. Kr¡sek, "Vector based medical image segmentation using adaptive Delaunay triangulation", Proceedings of the Sixth IASTED International Conference on Visualization, Imaging, and Image Procesing (2006)

[SK2007]M.Span.el, P. Kr.sek, M .Svub, V.Stancl, and O.Siler, "Delaunay-Based Vector Segmentation of Volumetric Medical Images", CAIP 2007, LNCS 4673, Springer-Verlag Berlin Heidelberg , pp. 261–269, (2007)

[SIL2005] L Silva, J. Scharcanski"A lossless compression approach for mammographic digitalimages based on the Delaunay triangulation" IEEE International Conference on Image Processing, ICIP 2005

[SMITH2002] L. I. Smith. "A tutorial on Principal Component Analysis" http://www.cs.otago.ac.nz/cosc453/student_tutorials/principal_component.pdf,(2002)

[SMN2007] M. L. de Siqueira, D. N. Muller, P. O. A. Navaux , "Cardiac Structure Recognition in Ultrasound Images", Systems, Signals and Image Processing 6th EURASIP Conference, pp. 463-466 (2007)

[SS1996] S. K. Setarehdan, J. J. Soraghan, Automatic left ventricular feature extraction and visualisation from echocardiographic images, Computers in Cardiology, 23, pp. 9-12 (1996)

[SS1996-2] S. K. Setarehdan, J J Soraghan, "Fully Automatic Echocardiographical Feature Extract ion Applied to Left Ventricular Wall Motion and Volume Changes Visualisation", 18th Annual International Conference of the IEEE Engineering in Medicine and Biology Society, pp. 877-878 (1996)

[SS1997] S. K. Setarehdan, J. J. Soraghan, Automatic left ventricular Center point extraction in echocardiographic images, Signal Processing, 61, pp. 275 -288 (1997)

[SS1999] S. K. Setarehdan, J. J. Soraghan, Automatic cardiac LV boundary detection and tracking using hybrid fuzzytemporal and fuzzy multiscale edge detection", IEEE transaction on Biomedical Engineering, Vol. 46 (11), pp. 1364-1378 (1999)

[SUIN2009] A. Suinesiaputra, A. F. Frangi, T. A. M. Kaandorp, H. J. Lamb, J. J. Bax, J. H. C. Reiber, and B. P. F. Lelieveldt , "Automated Detection of Regional Wall Motion Abnormalities Based on a Statistical Model Applied to Multislice Short-Axis Cardiac MR Images", IEEE Transactions on Medical Imaging, Vol. 28(4), pp. 595-607 (2009)

[SUK1995] M. Sukumar, "Quantification of cardiac wall motion abnormalities using cardiac displacement plot", Proceedings of IEEE conference of Engineering in Medicine and Biology, pp. 2.105-2.106 (1995)

[SUT1993] D. Sutton, "A textbook of radiology and imaging", Fifth edition, Churchill Livingstone (1993)

T

[TANG2009] J. Tang, X. Liu, Q. Sun,"A Direct Image Contrast Enhancement Algorithm in the Wavelet Domain for Screening Mammograms", IEEE Journal of Selected Topics in Signal Processing, Vol. 3 (1), pp. 74 – 80 (2009)

[TAS1986] G. E. Trahey, J. W. Allison, S. W. Smith, and O. T. von Ramm, A quantitative approach to speckle reduction via frequency compounding, Ultrason. Imag., 8 (3), (1986) 151–164.

[TAXT2004] T. Taxt, and R. Jirik, “Super resolution of Ultrasound Images Using the First and Second Harmonic Signal”, IEEE Transactions on Ultrasonics, Ferroelectrics, and Frequency Control, Vol. 51 (2), pp. 163 – 175 (2004)

[TDB2009] A. K. Talukdar, B. Deka, P. K. Bora, “Wavelet based adaptive Bayesian despeckling for medical ultrasound images”, IEEE Conference TENCON 2009 , pp. 1 – 6 (2009)

[TG2004] I. E. Timor-Tritsch, S. R. Goldstein, “Ultrasound in Gynecology”, pages: 9-44, Churchill Livingstone (2004)

[TG1999] Y.Tao and W. I. Grosky, “Delaunay triangulation for image object indexing: a novel method for shape representation”, Proceedings of the Seventh SPIE Symposium on Storage and Retrieval for Image and Video Databases (1999)

[TIM2006] J. Timperley , A.R.J. Mitchell, D.J. Blackman, C. Shirodaria, J. Eichhofer, M. Mulet-Parada, H. Becher, “Semi-automatic boundary detection to improve reporting of regional left ventricular function”, Eur J Echocardiography , Vol. 7, 209-216 (2006)

[TP2006] J. D. Thomas, Z. B. Popovic, “Assessment of left ventricular function by cardiac ultrasound”, Journal of the American College of Cardiology, Vol.48 (10), pp. 2012 -2025 (2006)

[TP11991] M. A. Turk and A. P. Pentland. “Eigenfaces for recognition”, Journal of Cognitive Neuroscience, 3, pp. 71-86, (1991)

[TP21991] M. A. Turk and A. P. Pentland. “Face recognition using eigenfaces”, Proceedings of the IEEE Computer Society Conf. On Computer Vision and Pattern Recognition, pp. 586-591, (1991)

[TTI2000] M. Tsubai, A. Takemura,M. Ito, “Morphological operations for ultrasound images by locally variable structuring elements and their analysis of effective parameters”, IEEE Engineering in Medicine and Biology Society, 2000. Proceedings, Vol. 4, pp. 2526 - 2528 (2000)

V

[VASAN1999] R. S Vasan, M. G. Larson, E. J. Benjamin, J. C. Evans, C. K. Reiss and D. Levy, “Congestive Heart Failure in Subjects With Normal Versus Reduced Left Ventricular Ejection FractionPrevalence and Mortality in a Population-Based Cohort”, Journal of the American College of Cardiology, Vol. 33 (7), pp. 1948-1955 (1999).

[VENKAT2006] P. Venkatesan and S. Anitha, “Application of a radial basis function neural network for diagnosis of diabetes mellitus”, Current Science, Vol. 91 (9), (2006)

W

[WEBB1988] Steve Webb, “The physics of medical imaging”, IOP Publishing Ltd, (1988)

[WEL1989] P.N.T. Wells, “Technical introduction to echocardiography”, British Medical Bulletin, 45(4), pp. 829—837 (1989)

[WEL1993] P.N.T. Wells, ”Advances in ultrasound techniques and instrumentation”, Churchill Livingston Inc. NewYork, N.Y., USA. (1993)

[WEISSTEIN] E.W. Weisstein, "Radon Transform." From MathWorld--A Wolfram Web Resource. http://mathworld.wolfram.com/RadonTransform.html

[WGL1992] D. C. Wilson, E. A. Geiser and J. H. Li, The use of matched filters for extraction of left ventricular features in 2- dimensional short-axis echocardiographic images., Mathematical methods in Medical Imaging, Vol. 1768, pp 37-49, SPIE, (1992)

X

[XIA2005] Xianju Wang and C.H. Chen, “Ultrasound image restoration using spatially adaptive filter for independent component analysis”, Machine Learning for Signal Processing IEEE Workshop, pp. 195-199 (2005)

[XIA2007] X. Li; D. C. Liu, “Ultrasound Image Enhancement using Dynamic Filtering”, Image and Graphics Fourth International Conference, ICIG 2007, pp. 106 – 109 (2007)

[XY2003]Y. Xiao, H. Yan “Text region extraction in a document image based on the Delaunay tessellation”, Pattern Recognition, 36, pp.799 – 809, (2003)

[XY2004]Y. Xiao, H. Yan “Location of title and author regions in document images based on the Delaunay triangulation”, Image and Vision Computing 22, pp. 319–329, (2004)

Y

[YAN2003] J.Y. Yan, T. Zhuang, “Applying improved fast marching method to endocardial boundary detection in echocardiographic images”, Pattern Recognition Letters, Vol. 24, pp. 2777–2784 (2003)

[YAO2004] W. Yao, J. Tian, B. Zhao, N. Chen, G. Qian, “Star algorithm: detecting the ultrasonic endocardial boundary Automatically” MEDINFO 2004, Amsterdam: IOS Press, pp.1919 (2004)

[YE2007] Z. Ye, H. Mohamadian, S. PANG, S. Iyengar, “Image Contrast Enhancement and Quantitative Measuring of Information Flow”, 6th WSEAS International Conference on Information Security and Privacy, pp.172-177 (2007)

[YOO2008] B.C. Yoo, J.G. Ryu, H. K. Park, T. Nishimura, “Multi-scale Based Adaptive SRAD for Ultrasound Images Enhancement”, World Congress on

Engineering and Computer Science, WCECS '08, Advances in Electrical and Electronics Engineering, pp. 258 – 266 (2008)

[YOO2009] B. Yoo, T. Nishimura, "A study of ultrasound images enhancement using adaptive speckle reducing anisotropic diffusion", IEEE International Symposium on Industrial Electronics, ISIE 2009, pp. 581 – 585 (2009)

Z

[ZA2004] G. Zwim, S. Akselrod, "A Histogram-Based Technique for Echocardiographic Image Enhancement", Computers in Cardiology, Vol. 31, pp. 81-84 (2004)

[ZEV2005] M. E. Zevitz, "Heart Failure",

http://www.emedicine.com/med/topic3552.htm, (2005).

[ZEV2006] M. E. Zevitz, V. N. Singh, "Myocardial Ischemia", http://www.emedicine.com/med/topic1568.htm , (2006)

[ZHANG2008] X. Zhang, L. Ge, T. Wang, "Entropy-Based Local Histogram Equalization for Medical Ultrasound Image Enhancement", International Conference on Bioinformatics and Biomedical Engineering, ICBBE 2008, pp. 2427 – 2429 (2008)

[ZHANG2009] D. Zhang and T. H. Nishimutra "Medical Image Noise Reduction Using Radon Transform and Walsh List in Laplacian Pyramid Domain", Proceedings of the 13th IEEE International Symposium on Consumer Electronics, pp. 756-760 (2009)

[ZHANS2005] H. Zhang, L. Zhang, "ECG analysis based on PCA and Support Vector Machines", International Conference on Neural Networks and Brain, ICNN&B '05, Vol. 2, pp. 743 – 747 (2005)

[ZHENG2006] W. Zeng, XX Meng, C L. Yang, L. Huang "Feature extraction for online handwritten characters using Delaunay triangulation", Computers & Graphics 30, pp. 779–786, (2006)

[ZHOU2008] X. Zhou and D. C. Liu, "Interactive Frequency Compounding to Medical Ultrasound Images", Proceedings of Asian-Pacific Conference on Medical and Biological Engineering IFMBE, pp. 286-289 (2008)

[ZHUANG2005] L. Zhuang, H. Liu, X. Liang, H. Bao, H. Hu, and P. Shi, "A Simultaneous Framework for Recovering Three Dimensional Shape and Nonrigid Motion from Cardiac Image Sequences", Proceedings of the IEEE Engineering in Medicine and Biology, pp. 5731-5734 (2005)

[ZLG1998] X. Zong, A. F. Laine, E. A. Geiser, Speckle reduction and contrast enhancement of echocardiograms via multi scale nonlinear processing, IEEE Transaction on Medical Imaging, 17 (4), (1998) 532 – 540.

[ZP1996] M. S. Zua and J. Potts, "Prevalence of myocardial ischemia as depicted by regional wall motion abnormality in blacks", Journal of the National Medical Association, 88(7), pp. 444–448, (1996)

[ZYKK2007] F. Zhang, Y. M. Yoo, L. M. Koh, Y.Kim, Nonlinear diffusion in Laplacian pyramid domain for ultrasonic speckle reduction, IEEE Transactions on Medical Imaging, 6 (2), (2007) 200-211.

APPENDIX A
FRACTIONAL MYOCARDIAL WALL THICKENING

Normal heart has systolic wall thickening while the diseased heart has decreased systolic wall thickening. Fractional Myocardial Wall Thickening (FMWT) is used to measure this thickening. The difference between the wall thickness at ES and ED is normalised by ED wall thickness to obtain the FMWT. The table below provides the six segment FMWT measure of SA view obtained for 8 normal and 8 abnormal hearts. The positive FMWT value for the segments suggests that the myocardial segment is normal and the negative FMWT value for the segments suggests the presence of abnormality in the segment.

Images	Seg 7	Seg 8	Seg 9	Seg 10	Seg 11	Seg 12
Normal	0.363104	0.519287	0.417361	0.485519	0.037499	0.341102
Normal	0.581593	0.1341	0.227104	0.276342	0.073957	0.402921
Normal	0.875822	0.513536	0.551549	0.433186	0.44473	0.169793
Normal	0.941637	0.625689	0.396471	0.660435	0.328444	0.292339
Normal	0.501983	0.408966	0.071989	0.449213	0.384657	0.56399
Normal	0.417529	0.568418	0.439151	0.557752	0.930576	0.762851
Normal	0.139949	0.164668	0.165665	0.352867	0.266923	0.122022
Normal	0.221468	0.101362	0.136814	0.037795	0.338267	0.849583
Abnormal	0.839712	0.64574	0.533323	0.491526	0.312754	0.303364
Abnormal	**-0.15571**	**-0.2471**	0.047841	0.114954	0.231369	0.044253
Abnormal	0.515186	0.742739	0.468053	0.827364	0.282678	0.468776
Abnormal	0.137581	**-0.00616**	0.105807	**-0.05697**	0.117144	0.316078
Abnormal	0.089489	0.030772	0.16487	**-0.12167**	**-0.21044**	0.131401
Abnormal	0.117076	**-0.07387**	**-0.17348**	0.436934	0.339821	0.083147
Abnormal	**-0.15479**	0.200188	0.008248	0.377593	**-0.18794**	0.186849

APPENDIX B
LEFT VENTRICLE FEATURES (GLOBAL AND SEGMENTAL)

The features which are extracted from the Left ventricle (LV) boundaries for few sample normal and abnormal heart images are shown here.

Global features: LV Ejection Fraction and systolic cavity area

- The global features of LV such as volume and systolic cavity area have a maximum value at the end- diastole and a minimum value at the end systole.
- The LV Ejection fraction (LVEF) is also determined from the end-diastole and end-systole volume. LVEF is greater than 0.5 (50%) in healthy individuals

Segmental features: segmental cavity area, segmental wall thickness and wall displacement

- The local cavity area varies with a minimum value at the end-systole and maximum value at the end-diastole for a normal heart
- Systolic wall thickening is present in a normal heart, where the wall thickness at the end-systole is greater than the wall thickness at the end-diastole.
- A wall displacement or maximal endocardial wall excursion measure is the difference between the maximum displacement of the wall edge and the minimum displacement of the wall edge.

Normal heart 1

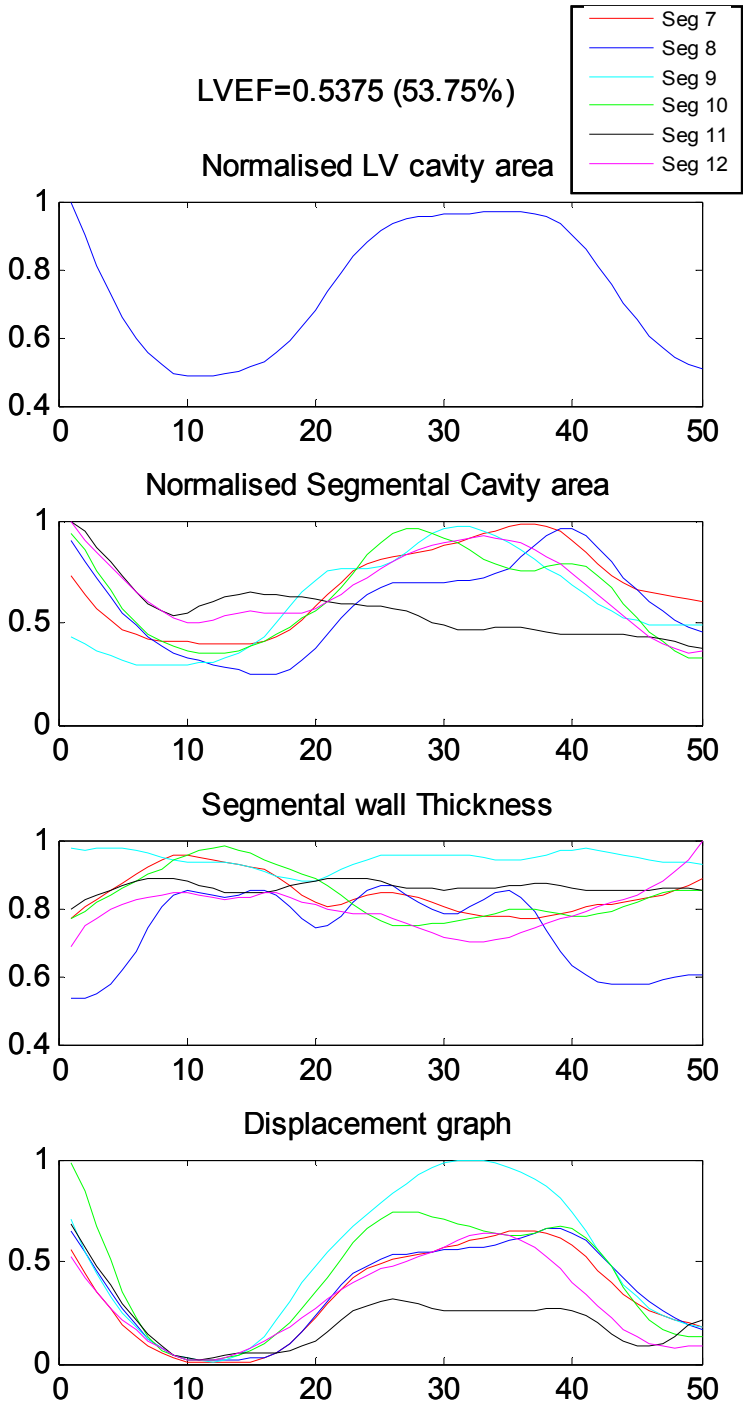

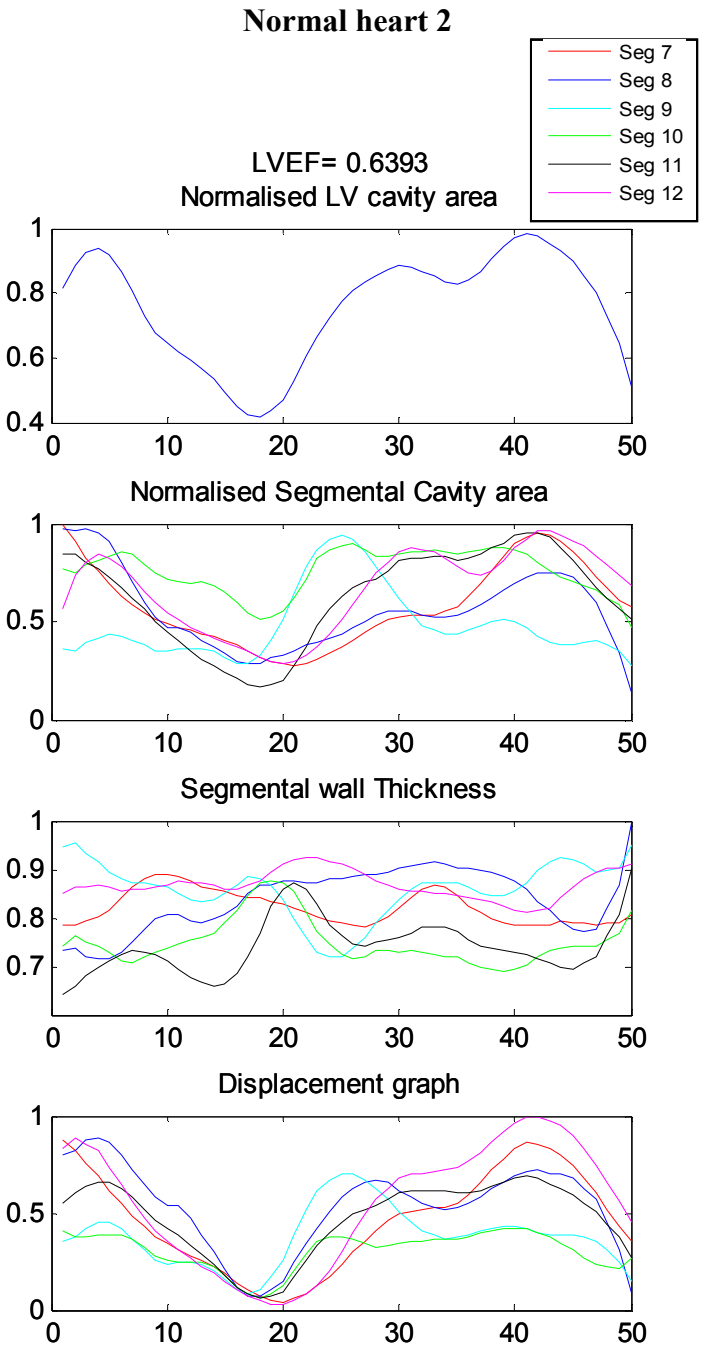
Normal heart 2
Seg 7
Seg 8
Seg 9
Seg 10
Seg 11
Seg 12
LVEF= 0.6393
Normalised LV cavity area
Normalised Segmental Cavity area
Segmental wall Thickness
Displacement graph

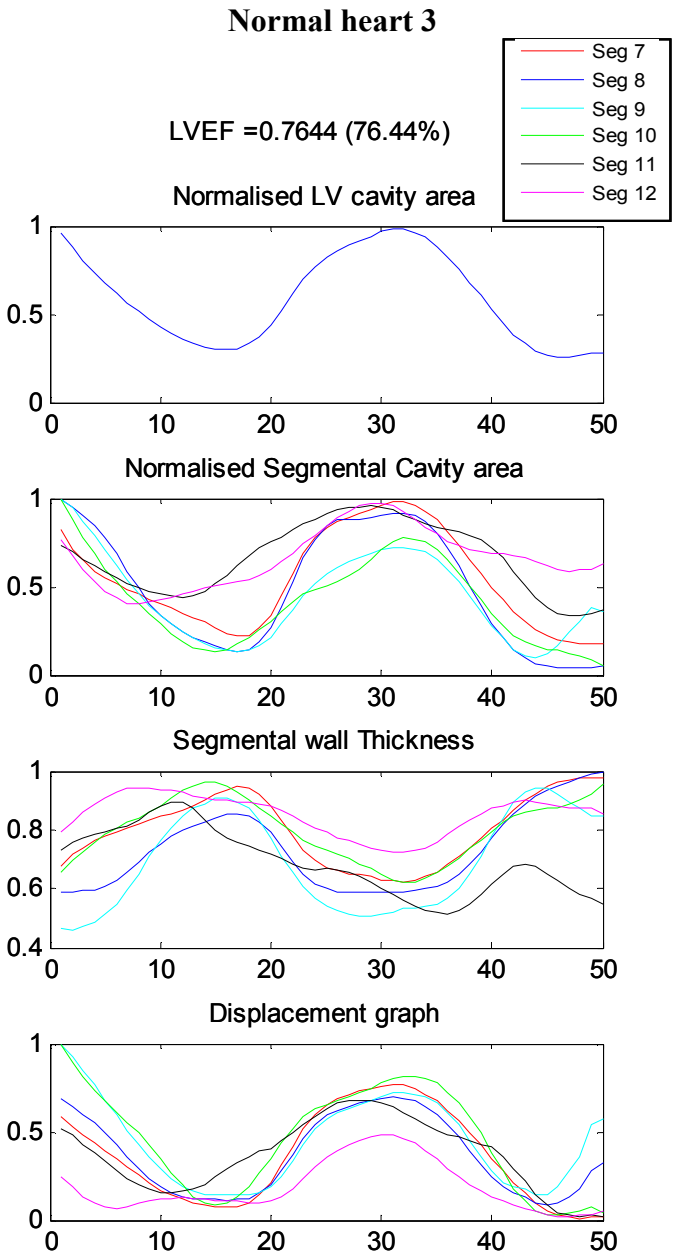
Normal heart 3
Seg 7
Seg 8
Seg 9
Seg 10
Seg 11
Seg 12
LVEF =0.7644 (76.44%)
Normalised LV cavity area
Normalised Segmental Cavity area
Segmental wall Thickness
Displacement graph

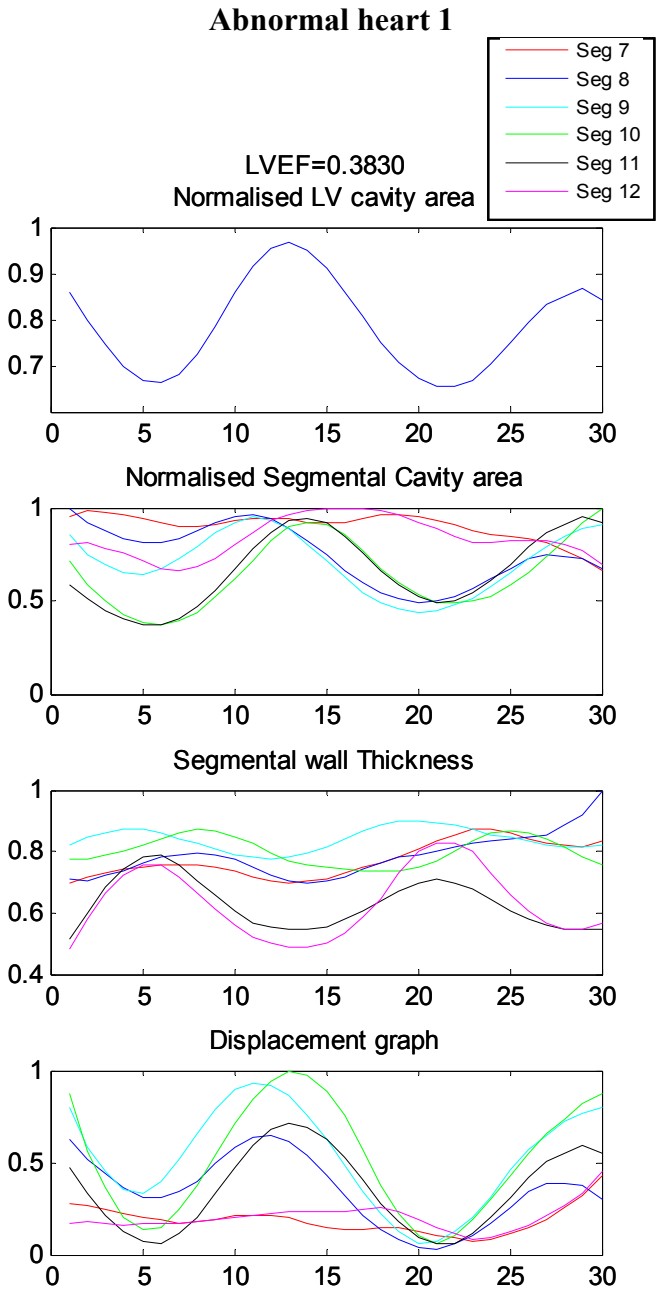
Abnormal heart 1
Seg 7
Seg 8
Seg 9
Seg 10
Seg 11
Seg 12
LVEF=0.3830
Normalised LV cavity area
Normalised Segmental Cavity area
Segmental wall Thickness
Displacement graph

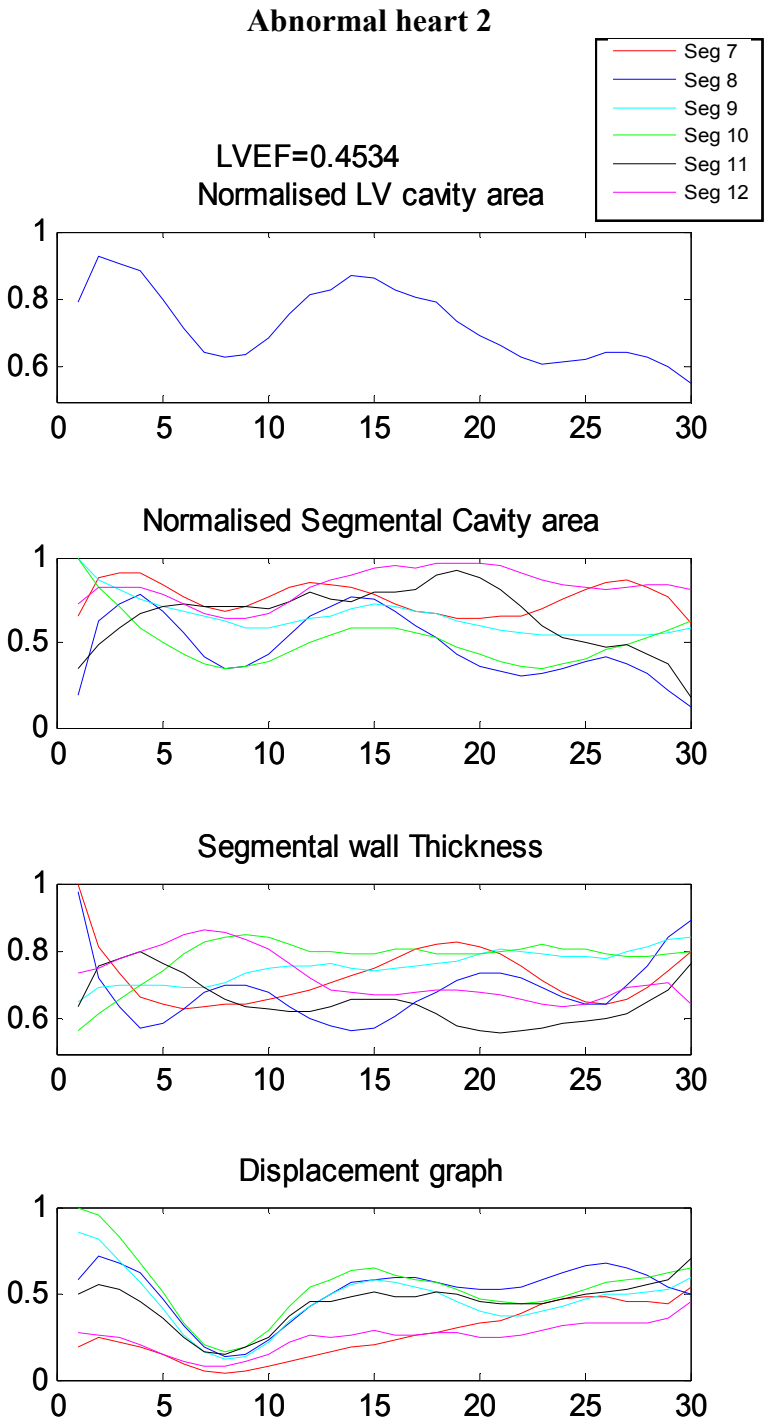
Abnormal heart 2
Seg 7
Seg 8
Seg 9
Seg 10
Seg 11
Seg 12
LVEF=0.4534
Normalised LV cavity area
Normalised Segmental Cavity area
Segmental wall Thickness
Displacement graph

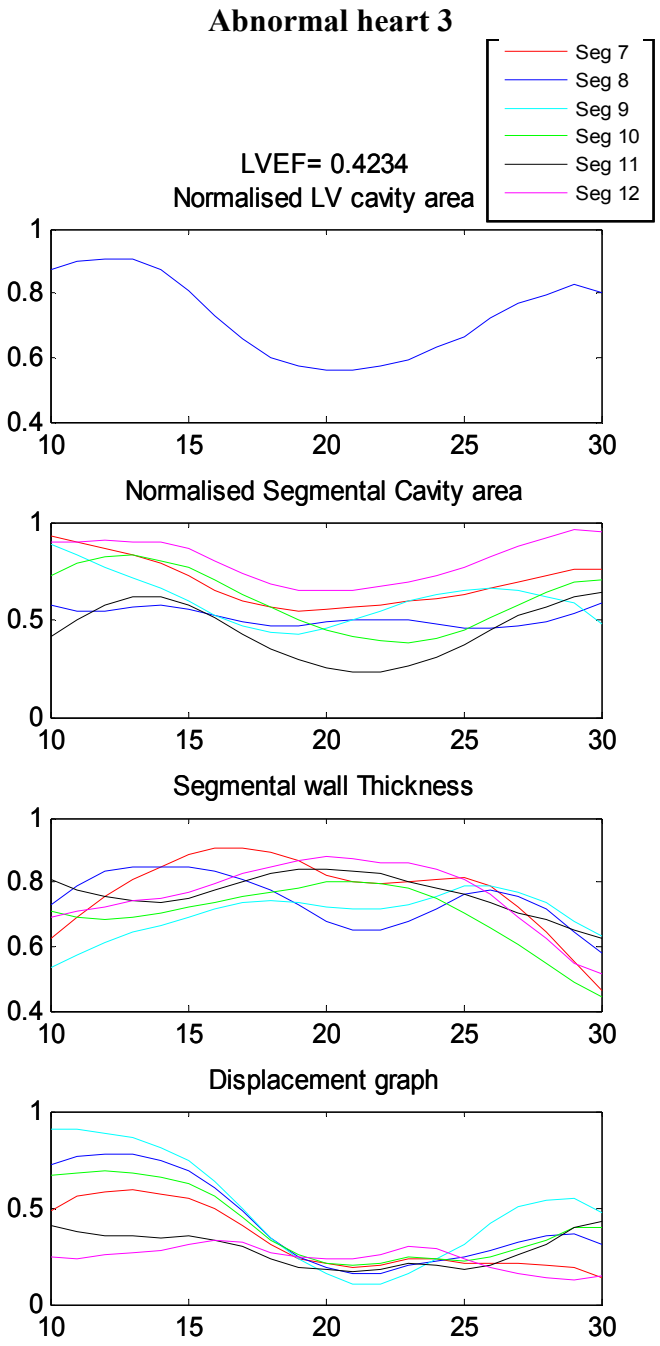
Abnormal heart 3
Seg 7
Seg 8
Seg 9
Seg 10
Seg 11
Seg 12
LVEF= 0.4234
Normalised LV cavity area
Normalised Segmental Cavity area
Segmental wall Thickness
Displacement graph